SYSTEM DESIGN FOR QCM BASED BIOSENSOR

by

Saibe Demir

B.S., Electrical and Electronics Engineering, İstanbul University, 2020

Submitted to the Institute for Graduate Studies in
Science and Engineering in partial fulfillment of
the requirements for the degree of
Master of Science

Graduate Program in Electrical and Electronics Engineering
Boğaziçi University

2023

ACKNOWLEDGEMENTS

I would like to express my deepest gratitude and appreciation to Professor Günhan Dündar, my supervisor, for his continuous support, motivation, and remarkable knowledge. Without his guidance, I would not be able to continue my master's program. I hope that throughout my life, I will be enlightened by his wisdom.

I want to express my sincere gratitude to Assistant Professor Okan Zafer Batur for his assistance with every aspect of my thesis. Also, I want to thank Buğra Selim Bulut and Can Ervakit for their help with this thesis.

Finally, I want to give my special thanks to my dear sister for her tremendous support and understanding and I want to thank my family for their love and support.

This thesis is supported partly by the research grant of the Scientific and Technological Research Council of Turkey (TUBITAK) project under project number 122E166.

ABSTRACT

SYSTEM DESIGN FOR QCM BASED BIOSENSOR

QCM (quartz crystal microbalance) measures the mass change per unit area by measuring the frequency change of a quartz crystal. The resonance is changed by adding or removing a small mass due to oxide growth, decay, or film deposition on the surface of the acoustic resonator. QCMs can be used in vacuum, gas phase, or in liquid. Since the early 1980s QCMs have been used as sensors, and they are the popular choice for biosensing nowadays. Early detection of viruses or genetically modified organism detection are some examples that QCM is used as a biosensor.

In this thesis, a system is designed for QCM-based biosensor. The method that is used in the designed system is explained. Then the measurements of suitable components for this system are presented. System measurements and VNA measurements are compared with each other to verify the operation of the designed system.

Also, an alternative system design is explained. The same steps are followed for the alternative system. Finally, the conclusion is drawn, and future work is presented.

ÖZET

QCM TABANLI BİOSENSÖR İÇİN SİSTEM TASARIMI

QCM (kuvars kristal mikro terazi) birim alandaki kütle değişimini kuvars kristalin frekans değişimini ölçerek belirler. Rezonans, akustik rezonatörün yüzeyinde oksit büyümesi, bozulması veya film birikmesi nedeniyle küçük bir kütlenin eklenmesi veya çıkarılmasıyla değiştirilir. Qcmler vakumda, gaz fazında ya da sıvıda kullanılabilir. 1980'lerin başından beri QCM'ler sensöre olarak kullanılmıştır, günümüzde bioalgılama için popular bir seçimdir. Virüslerin erken tespiti veya genetiği değiştirilmiş organizma tespiti, QCM'nin bir biyosensör olarak kullanıldığı bazı örneklerdir.

Bu tezde QCM tabanlı biosensor için bir sistem tasarlanmıştır. Tasarlanan sistemdeki method açıklanmıştır. Daha sonra bu sistem için uygun bulunan elemanların ölçümleri sunulmuştur. Sistem ölçümleri ve VNA ölçümleri, tasarlanan sistemin çalıştığını doğrulamak için birbiri ile karşılaştırılmıştır.

Ayrıca alternatif bir sistem tasarımı daha açıklanmıştır. Aynı adımlar bu system için de izlenmiştir. Son olarak sonuç çıkarılmış ve gelecek çalışmalar sunulmuştur.

TABLE OF CONTENTS

ACKNOWLEDGEMENTS . . . iii
ABSTRACT . . . iv
ÖZET . . . v
LIST OF FIGURES . . . ix
LIST OF TABLES . . . xx
LIST OF SYMBOLS . . . xxii
LIST OF ACRONYMS/ABBREVIATIONS . . . xxiii
1. INTRODUCTION . . . 1
2. BACKGROUND . . . 3
2.1. Principles of A QCM Sensor . . . 4
2.1.1. The Piezoelectric Effect . . . 4
2.1.2. Physical Structure of QCM . . . 4
2.1.3. Operation Principle of QCM Sensor . . . 5
2.2. QCM Behavior . . . 6
2.2.1. QCM's Behavior in Gas Environment . . . 6
2.2.2. QCM's Behavior in Liquid Environment . . . 7
2.3. QCM Measurement Methods . . . 7
2.3.1. Oscillator Circuit . . . 7
2.3.2. Dedicated Circuits . . . 8
2.3.3. Vector Network Analyzer (VNA) . . . 9
3. SYSTEM DESIGN FOR QCM BASED BIOSENSOR . . . 12
3.1. Frequency Synthesizer . . . 13
3.1.1. ADF4351 . . . 13
3.2. Gain/Phase Detector . . . 16
3.3. Directional Couplers . . . 18
3.4. MCU . . . 21
4. MEASUREMENTS . . . 23
4.1. ADF4351 Frequency Synthesizer Measurements . . . 23

4.2. AD8302 Gain Phase Detector Measurements 27
4.3. Couplers (ADC-15-4+) Measurements 30
4.4. MCU (ARDUINO DUE) Tests 33
4.4.1. Configuration of ADF4351 with Arduino Due 33
4.4.2. Controlling Evaluation Board of AD8302 with Arduino Due . . 35
4.5. Measurements of QCMs using a VNA 36
4.5.1. Measurements of a Packed QCM 36
4.5.2. Measurements of an Open QCM 37
4.6. QCM Measurements with The System 39
4.6.1. Packed QCM Measurements using The System 39
4.6.2. Open QCM Measurements using The Designed Circuit 43
4.6.3. System Measurements using an Open QCM in Water 44
4.6.4. System Measurements using an Open QCM in a Flow Cell . . . 46
4.6.5. System Measurements and Impedance Analyzer Measurements using an Open QCM in a Flow Cell 49
5. ALTERNATIVE SYSTEM DESIGN 55
5.1. DDS-PLL Components and Methods 55
5.1.1. DDS (Direct Digital Synthesizer) 56
5.1.2. AD9850 57
5.1.3. ADF4351 58
5.1.4. Controlling The Alternative System Design with Arduino DUE 58
5.2. Measurements of QCM's with Alternative System Design 59
5.2.1. Measurements of an Open QCM with Alternative System Design in Water 62
5.2.2. Alternative System Measurements using an Open QCM in a Flow Cell 64
5.2.3. Measurements of Alternative System and Impedance Analyzer using an Open QCM in a Flow Cell 66
6. CONCLUSION 70
REFERENCES 72
APPENDIX A: REGISTER MAPS OF ADF4351 76

APPENDIX B: ARDUINO DUE CODE 80
APPENDIX C: DETAILED ANLY. OF ADF435'S LP. FL. USING ADISIMPLL 84
APPENDIX D: MATLAB CODE 86
APPENDIX E: MATLAB CODE 87
APPENDIX F: MATLAB CODE 89
APPENDIX G: IMPEDANCE ANALYZER MEASUREMENT RESULTS . . 90
APPENDIX H: DESIGNED SYSTEM MEASUREMENT RESULTS 92
APPENDIX I: ARDUINO DUE CODE FOR DDS-PLL SYSTEM 99
APPENDIX J: MATLAB CODE FOR DDS-PLL SYSTEM 103
APPENDIX K: DDS-PLL SYSTEM MEASUREMENT RESULTS 105

LIST OF FIGURES

Figure 1.1. Major areas of biosensor usage. 1

Figure 2.1. Measured parameters for QCM sensing applications. 3

Figure 2.2. Structure of a QCM sensor. 4

Figure 2.3. Pierce Oscillator. 8

Figure 2.4. Circuit block diagram. 9

Figure 2.5. VNA with two ports. 10

Figure 3.1. VNA block diagram [25]. 12

Figure 3.2. Functional block diagram of ADF4351 [26]. 15

Figure 3.3. Functional block diagram of AD8302. 18

Figure 3.4. Directional coupler schematic. 19

Figure 3.5. Arduino Due. 21

Figure 3.6. Designed system schematic. 22

Figure 4.1. Measurement of ADF4351 output with signal analyzer at 35 MHz. 23

Figure 4.2. Measurement of ADF4351 output with signal analyzer at 500 MHz. 24

Figure 4.3. Measurement of ADF4351 output with signal analyzer at 2.5 GHz. 24

Figure 4.4. Evaluation board schematic of ADF4351. 25

Figure 4.5. Measurement of ADF4351 evaluation board with an oscilloscope at 35 MHz after modification. 26

Figure 4.6. Measurement of ADF4351 evaluation board with an oscilloscope at 100 MHz after modification. 26

Figure 4.7. Expected values of AD8302's outputs according to its datasheet. . 27

Figure 4.8. Measurement values of phase and gain outputs of AD8302 evaluation board (without attenuation and peak to peak is 200 mV). . . 28

Figure 4.9. Measurement values of phase and gain outputs of AD8302 evaluation board with 10 dB attenuation to input a (peak to peak is 200mV). 28

Figure 4.10. Set-up for measurements of AD8302 using ADF4351 (Arduino Uno used as a power supply for AD8302). 29

Figure 4.11. Measurement values of phase and gain outputs of AD8302 evaluation board using ADF4351 evaluation board as a signal generator. 29

Figure 4.12. Schematic of ADC-15-4+ [29]. 30

Figure 4.13. ADC-15-4+ on a PCB with SMA connectors. 30

Figure 4.14. ADC-15-4+ properties as given in the datasheet. 30

Figure 4.15. VNA measurement of ADC-15-4+ on a PCB when VNA cables connected to its input and coupled ports. 31

Figure 4.16. VNA measurement of ADC-15-4+ on a PCB when VNA cables connected to its input and output ports. 31

Figure 4.17. VNA measurement of ADC-15-4+ on a PCB when VNA cables are connected to its output and coupled ports. 32

Figure 4.18. RF output frequency schematic of ADF4351 (when the loop is closed before output divider) [26]. 33

Figure 4.19. Loop filter's circuit [26]. 34

Figure 4.20. Packed QCM. 36

Figure 4.21. Packed QCM VNA result. 37

Figure 4.22. Open QCM. 37

Figure 4.23. Open QCM VNA measurement result for 10 MHz center frequency. 38

Figure 4.24. Open QCM VNA measurement result for 50.2 MHz center frequency. 39

Figure 4.25. Set-up for measurements of the whole circuit with packed QCM. . 40

Figure 4.26. One sweep result of the gain output of AD8302. 40

Figure 4.27. 10 sweeps result of gain output of AD8302. 41

Figure 4.28. Raw data graphs of a sweep that takes eleven measurements at the same frequency. 41

Figure 4.29. After the data of a sweep is processed (It is the same measurement in Figure 4.28. But this measurement is done after a few days). . 42

Figure 4.30. Designed system measurement set-up for measuring an open QCM. 43

Figure 4.31. Open QCM designed system measurement results. 44

Figure 4.32. Open QCM is in the water. 44

Figure 4.33. Designed system measurement set-up for measuring an open QCM when QCM is in the water. 45

Figure 4.34. Open QCM designed system measurement results in the air. . . . 45

Figure 4.35. Designed system measurement results using an open QCM when it is in the water. 46

Figure 4.36. VNA measurement results for an open QCM in flow cell without water. 46

Figure 4.37. Designed system measurement results for an open QCM in flow cell without water. 47

Figure 4.38. An open QCM in flow cell after a few drops of water added. . . . 47

Figure 4.39. VNA measurement results for an open QCM in flow cell after water was added. 48

Figure 4.40. Designed system measurement results for an open QCM in flow cell after water was added. 48

Figure 4.41. Flow Cell. 49

Figure 4.42. Measurement set-up. 50

Figure 4.43. Designed system measurement results when QCM was in the air-resonance frequency. 51

Figure 4.44. Designed system measurement results when QCM was in the air - dip magnitude. 52

Figure 4.45. Designed system measurement results - resonance frequency. . . . 52

Figure 4.46. Designed system measurement results - dip magnitude. 53

Figure 5.1. Block diagram of alternative system. 55

Figure 5.2. Simplified block diagram of the direct digital synthesizer [33]. . . . 56

Figure 5.3. Pin diagram of AD9850. 57

Figure 5.4. Arduino Due connections that are being used in DDS-PLL system. 59

Figure 5.5. Set-up for measurement of alternative system design with packed QCM. 60

Figure 5.6. Measurement result of alternative system design with packed QCM. 60

Figure 5.7. Set-up for measurement of alternative system design with an open QCM. 61

Figure 5.8. Measurement result of alternative system design for an open QCM. 62

Figure 5.9. Measurement result of alternative system design with an open QCM in the air. 63

Figure 5.10. Measurement result of alternative system design with an open QCM when it is in the water. 63

Figure 5.11. Alternative system design measurement results for an open QCM in flow cell before water was added. 64

Figure 5.12. Alternative system design measurement results for an open QCM in flow cell after water was added. 65

Figure 5.13. DDS-PLL system measurement results when QCM was in the air-resonance frequency. 67

Figure 5.14. DDS-PLL system measurement results when QCM was in the air - dip magnitude. 67

Figure 5.15. DDS-PLL system measurement results - resonance frequency. . . . 68

Figure 5.16. DDS-PLL system measurement results - dip magnitude. 68

Figure 6.1. Schematic of system design for wireless and electrodeless QCM based biosensor. 71

Figure A.1. Register maps. 76

Figure A.2. Register 0. 77

Figure A.3. Register 1. 77

Figure A.4. Register 2. 78

Figure A.5. Register 3. 78

Figure A.6. Register 4. 79

Figure A.7. Register 5. 79

Figure C.1. Detailed Analysis Of ADF435's Loop Filter Using ADISIMPLL . . 84

Figure C.2. ADF435's Loop Filter Analysis Graphs 85

Figure G.1. Impedance analyzer measurement results when open QCM was in the air. 90

Figure G.2. Impedance analyzer measurement results when open QCM was in water. 90

Figure G.3. Impedance analyzer measurement results when open QCM was in 100 ml water after 1ml glycerol was added. 91

Figure G.4. Impedance analyzer measurement results when open QCM was in 100 ml water after 3ml glycerol was added. 91

Figure H.1. Designed system measurement results-1 when open QCM was in the air. 92

Figure H.2. Designed system measurement results-2 when open QCM was in the air. 92

Figure H.3. Designed system measurement results-3 when open QCM was in the air. 93

Figure H.4. Designed system measurement results-4 when open QCM was in the air. 93

Figure H.5. Designed system measurement results-5 when open QCM was in the air. 93

Figure H.6. Designed system measurement results-1 when open QCM was in water. 94

Figure H.7. Designed system measurement results-2 when open QCM was in water. 94

Figure H.8. Designed system measurement results-3 when open QCM was in water. 94

Figure H.9. Designed system measurement results-4 when open QCM was in water. 95

Figure H.10. Designed system measurement results-5 when open QCM was in water. 95

Figure H.11. Designed system measurement results-1 when open QCM was in 100 ml water after 1ml glycerol was added. 95

Figure H.12. Designed system measurement results-2 when open QCM was in 100 ml water after 1ml glycerol was added. 96

Figure H.13. Designed system measurement results-3 when open QCM was in 100 ml water after 1ml glycerol was added. 96

Figure H.14. Designed system measurement results-4 when open QCM was in 100 ml water after 1ml glycerol was added. 96

Figure H.15. Designed system measurement results-5 when open QCM was in 100 ml water after 1ml glycerol was added. 97

Figure H.16. Designed system measurement results-1 when open QCM was in 100 ml water after 3ml glycerol was added. 97

Figure H.17. Designed system measurement results-2 when open QCM was in 100 ml water after 3ml glycerol was added. 97

Figure H.18. Designed system measurement results-3 when open QCM was in 100 ml water after 3ml glycerol was added. 98

Figure H.19. Designed system measurement results-4 when open QCM was in 100 ml water after 3ml glycerol was added. 98

Figure H.20. Designed system measurement results-5 when open QCM was in 100 ml water after 3ml glycerol was added. 98

Figure K.1. DDS-PLL system measurement results-1 when open QCM was in the air. 105

Figure K.2. DDS-PLL system measurement results-2 when open QCM was in the air. 105

Figure K.3. DDS-PLL system measurement results-3 when open QCM was in the air. 106

Figure K.4. DDS-PLL system measurement results-4 when open QCM was in the air. 106

Figure K.5. DDS-PLL system measurement results-5 when open QCM was in the air. 106

Figure K.6. DDS-PLL system measurement results-1 when open QCM was in water. 107

Figure K.7. DDS-PLL system measurement results-2 when open QCM was in water. 107

Figure K.8. DDS-PLL system measurement results-3 when open QCM was in water. 107

Figure K.9. DDS-PLL system measurement results-4 when open QCM was in water. 108

Figure K.10. DDS-PLL system measurement results-5 when open QCM was in water. 108

Figure K.11. DDS-PLL system measurement results-1 when open QCM was in 100 ml water after 1ml glycerol was added. 108

Figure K.12. DDS-PLL system measurement results-2 when open QCM was in 100 ml water after 1ml glycerol was added. 109

Figure K.13. DDS-PLL system measurement results-3 when open QCM was in 100 ml water after 1ml glycerol was added. 109

Figure K.14. DDS-PLL system measurement results-4 when open QCM was in 100 ml water after 1ml glycerol was added. 109

Figure K.15. DDS-PLL system measurement results-5 when open QCM was in 100 ml water after 1ml glycerol was added. 110

Figure K.16. DDS-PLL system measurement results-1 when open QCM was in 100 ml water after 3ml glycerol was added. 110

Figure K.17. DDS-PLL system measurement results-2 when open QCM was in 100 ml water after 3ml glycerol was added. 110

Figure K.18. DDS-PLL system measurement results-3 when open QCM was in 100 ml water after 3ml glycerol was added. 111

Figure K.19. DDS-PLL system measurement results-4 when open QCM was in 100 ml water after 3ml glycerol was added. 111

Figure K.20. DDS-PLL system measurement results-5 when open QCM was in 100 ml water after 3ml glycerol was added. 111

LIST OF TABLES

Table 3.1. Comparison of different frequency synthesizers. 14

Table 3.2. Values of each bit at register 5. 17

Table 3.3. Comparison of RF Couplers. 20

Table 4.1. Comparison of measurement results and datasheet properties of ADC-15-4+ with frequency range of 0 - 100 MHz. 32

Table 4.2. Results of VNA measurements for packed QCM. 37

Table 4.3. Properties of impedance analyzer measurements. 50

Table 4.4. Impedance analyzer measurements results. 51

Table 4.5. Frequency shift according to air. 53

Table 4.6. Frequency shift according to water. 53

Table 5.1. Measurement results for packed QCM. 61

Table 5.2. Measurement results for the open QCM. 61

Table 5.3. Measurement results for the open QCM in the water. 63

Table 5.4. Measurement results for the open QCM in a flow cell. 65

Table 5.5. Measurement results for the open QCM in a flow cell after water added. 65

Table 5.6. Frequency shift according to air. 69

Table 5.7. Frequency shift according to water. 69

LIST OF SYMBOLS

C	Crytal constant
d	Thickness of the quartz
f	Frequency
f_0	Resonant Frequency of QCM
m	Mass
n	Overtone Number
n_l	Liquid Viscosity
S_A	Electrode Area
v	Velocity
V_{INA}	Voltage of Input A
V_{INB}	Voltage of Input B
V_{MAG}	The output voltage corresponding to the magnitude of the signal level difference
V_{PHS}	The output voltage corresponding to the phase difference of signals
V_Φ	Phase slope in mV/degrees
Δ	Change
Φ	Each signal's relative phase in degrees
λ	Wavelength
μ_q	Shear modulus of quartz for AT-cut crsytal
ρ_l	Liquid Density
ρ_q	Density of Quartz

LIST OF ACRONYMS/ABBREVIATIONS

ADC	Analog to Digital Converter
Anly.	Analysis
DAC	Digital to Analog Converter
DDS	Direct Digital Synthesizer
FL.	Filter
LP.	Loop
PLL	Phase Lock Loop
QCM	Quartz Crystal Microbalance
VNA	Vector Network Analyzer

1. INTRODUCTION

Biosensors measure biological or chemical responses, and they transform these responses into electrical signals. They are analytical tools. A biosensor should be extremely precise, unaffected by physical factors like temperature, and reusable [1]. The first biosensor was created by the American biochemist "Leland C. Clark" in 1956. The Clark electrode, also known as the oxygen electrode, was used to measure blood oxygen levels [2].

Enzyme-based, tissue-based, immunosensor, DNA-based, thermal, and piezoelectric biosensors are some of the biosensors being used today. They are used in various applications such as drug discovery, disease detection, and soil and water quality management. Figure 1.1 shows the major areas of biosensor usage [3].

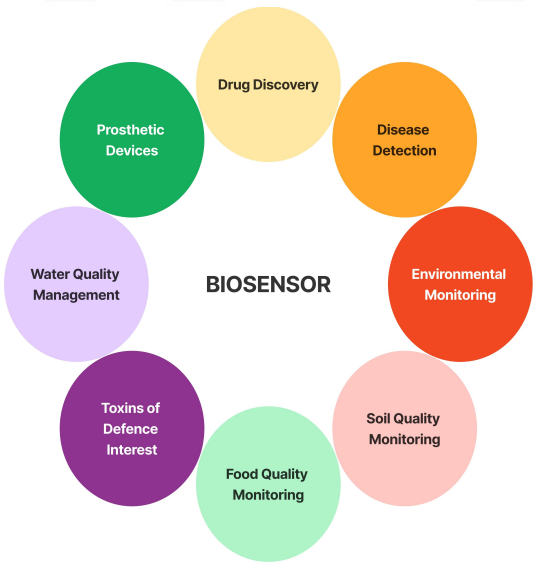

Figure 1.1. Major areas of biosensor usage.

The surface acoustic wave resonators and the bulk acoustic wave resonators such as quartz crystal microbalance (QCM) are two different types of piezoelectric biosensors. They are based on the detection of the piezoelectric crystal's resonance frequency shift caused by changes in the mass of the crystal.

For sensor applications, QCM is the most popular and commonly utilized acoustic transducer. Due to its high sensitivity, durability, compact design, and ease of integration with electronic measurement systems, it has a wide range of applications in chemical and biosensing. Early detection of viruses [4], genetically modified organism detection [5] and an immunosensor [6] are some examples of QCM-based biosensors.

This thesis aims to design a system that can measure the resonance frequency change of a QCM that is to be used later on for cancer diagnosis in blood.

The organization of the thesis is as follows: Chapter 2 presents background principles, theory, and measurement methods of the QCM. Chapter 3 explains the system design for QCM-based biosensor. Chapter 4 gives the measurements for each suitable component of the system and measurement results of the designed system including the VNA measurements. Chapter 5 explains an alternative system design and presents the measurements of this system. Finally, Chapter 6 draws a general conclusion of the thesis and explains the future work.

2. BACKGROUND

The main advantages of QCM such as simplicity and versatility for various applications were found over 60 years ago [7]. But it was not used as a sensor until the early 1980s. Due to its sensitivity, it has been the popular choice for many applications since then. A summary of the most used measurement parameters in different applications is given in Figure 2.1 (Δf is the QCM resonant frequency shift, and ΔR is the QCM equivalent resistance change) [8].

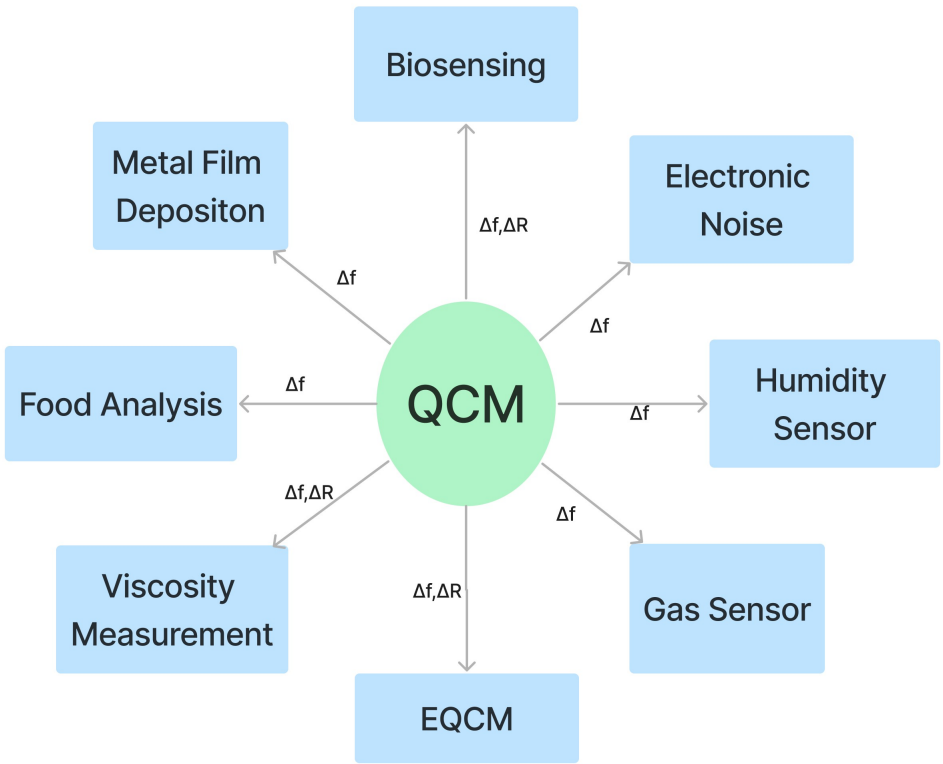

Figure 2.1. Measured parameters for QCM sensing applications.

In this chapter, the fundamentals, theory, and measurement methods of the QCM will be explained in order to give a better understanding of this thesis.

2.1. Principles of A QCM Sensor

2.1.1. The Piezoelectric Effect

Piezoelectricity means the production of electricity in response to mechanical deformation caused by mechanical stress. French physicists Pierre Curie and Jacques Curie discovered this effect in 1880.

A year later, they showed that the opposite effect is also possible. When voltage is applied, the crystal deforms along the crystal direction [9, 10]. The opposite effect is the working principle of the QCM. Internal mechanical strain is generated when an electrical field is applied to the crystal.

2.1.2. Physical Structure of QCM

A pair of gold electrodes which is coupled with a piezoelectric crystal make up the physical structure of the QCM [11]. The quartz crystal is made of SiO2. When the measurement of the resonance frequency of an open QCM is desired, it is placed between wire holders as in Figure 2.2.

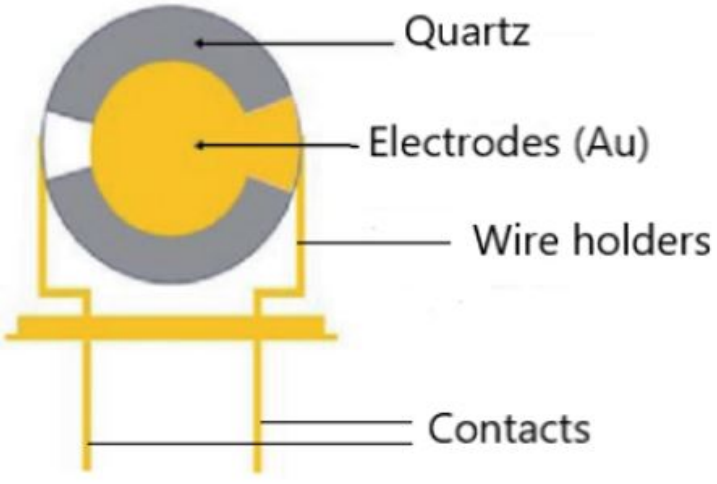

Figure 2.2. Structure of a QCM sensor.

Wafers from which crystals are made for electronics applications are cut from quartz stones. The crystal's vibration mode is determined by the cut direction. So-called AT-cut crystals make up 90 percent of all crystals utilized in electronics applications. This indicates that the stones are cut 35° 15' away from the Z-axis. The thermal properties of the generated crystals are what make the AT-cut so popular. They have a useful temperature range from -40°C to + 125°C and a 25°C inflection point, which is the symmetry point at which the frequency changes depending on the temperature [12].

2.1.3. Operation Principle of QCM Sensor

Depending on the cutting angle and quartz crystal thickness, QCM has a unique associated frequency. The thickness-shear mode of the QCM is also called QCM's oscillation mode. It oscillates with maximum amplitude at the surface of the quartz plate and a displacement direction perpendicular to the thickness of the quartz.

QCM can determine the accumulated mass on the surface of the electrode. For the thickness-shear mode, d is crystal thickness, and it is half of the wavelength of the shear mode. It is given by

$$d = \frac{\lambda}{2}. \tag{2.1}$$

Since frequency times wavelength equals the velocity of the sound wave, the equivalent equation can be obtained as

$$f = \frac{v}{2d}. \tag{2.2}$$

There will be a corresponding shift in resonant frequency (Δf) if the additional mass works as a thickness increase in the quartz per unit area, increasing it by Δd. The resonance frequency is decreased as a result of this mass addition. The equivalent equation can be obtained as

$$(f + \Delta f) = \frac{v}{2(d + \Delta d)}. \tag{2.3}$$

It was discovered that the QCM's mass sensitivity is most vital at the center and gradually decreases away from the center. A Gaussian curve can be utilized for representing the sensitivity curve [13, 14].

2.2. QCM Behavior

Understanding QCM behavior in the open air is crucial for using QCM effectively. In this section, QCM's behavior in gas environment and liquid environment will be analyzed.

2.2.1. QCM's Behavior in Gas Environment

In 1959, Sauerbrey was the first to describe how mass deposition caused a decrease in frequency. Using the crystal as the oscillator circuit's frequency-identifying element, he simultaneously created a technique for determining the characteristic frequency and its variations. His approach, which is still used as the primary measurement tool in research using quartz crystal microbalances (QCMs) to convert the frequency to mass.

The equation is created by treating the mass that has been deposited as if it were an addition to the thickness of the quartz underneath it [15]. As a result, electrode geometry has little effect on the mass-to-frequency correlation (as established by Sauerbrey's equation). The setup is beneficial from a cost and time investment perspective because it enables mass determination without calibration. The Sauerbrey Equation is defined as

$$\Delta f = -\frac{2f_0^2}{S_A\sqrt{\rho_q\mu_q}}\Delta m, \tag{2.4}$$

where f_0 is the resonant frequency of the fundamental mode (Hz), Δf is frequency change (Hz), Δm is mass change (g), S_A is electrode area (cm^2), ρ_q is density of quartz (g/cm^3), and μ_q is shear modulus of quartz for AT-cut crystal (g/cms^2).

Also, Sauerbrey showed that the mass change (Δm) and frequency change (Δf) of oscillating quartz could be linearly related. Mass change (Δm) can be expressed as

$$\Delta m = -C * (1/n) * \Delta f, \tag{2.5}$$

where n is the overtone number and C is a constant that depends on the property of the crystal used and Δf is the frequency change.

For a 5 MHz AT-cut quartz crystal at room temperature, C is approximately equal to 17.7 $ng/(cm^2Hz)$. This means that the addition of 17.7 $ng/(cm^2)$ of mass on a 5 MHz quartz crystal causes a frequency change of 1 Hz [16]. The precision of this method makes it very useful for biomedical applications such as the mass measurements of small molecules or organisms like proteins, simple polymers and monomers, viruses, and bacteria.

Even though Sauerbrey explains the response to mass change explicitly, when the QCM is utilized in a liquid environment, it does not consider the viscosity of the solution.

2.2.2. QCM's Behavior in Liquid Environment

In 1985, Kanazawa and Gordon derived an equation [17, 18], which explains the frequency variation of a quartz crystal in contact with a liquid using the material characteristics of the fluid and the quartz. The equation is given below:

$$\Delta f = -{f_0}^{3/2}\sqrt{\frac{n_l\rho_l}{\pi\rho_q\mu_q}}, \tag{2.6}$$

where f_0 is the resonant frequency of the fundamental mode (Hz), n_l is liquid viscosity (cP), ρ_l is liquid density (g/cm^3), ρ_q is density of quartz (g/cm^3), and μ_q is shear modulus of quartz for AT-cut crystal (g/cms^2) .

2.3. QCM Measurement Methods

In this section, three QCM measurement methods will be discussed in detail.

2.3.1. Oscillator Circuit

The Pierce oscillator, as depicted in Figure 2.3, is the most basic QCM circuit. It has two capacitors, a digital inverter, and a feedback resistor. This design is widely used in microcomputer technology because of its simple structure and stable clock-

generating function. A readout circuit using a Pierce Oscillator with the QCM fully immersed in liquid was examined in [19], and the results were not satisfactory.

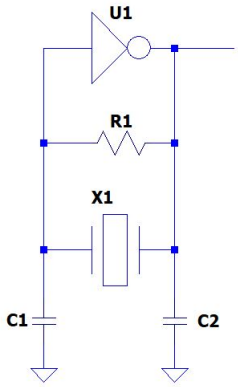

Figure 2.3. Pierce Oscillator.

In 2011, Satoh proposed double resonance using the Pierce oscillator topology [20]. This design works in full water immersion. Then in 2012, it was stated that a design with a variable-capacitance diode could make it easier to adjust oscillation frequency [21].

However, as the use of QCM has been extended to various sensing methods, the need for a coating to increase QCM sensitivity is inevitable, and sadly, these coatings tend to be viscous. The standard oscillator circuit becomes inaccurate due to this loading.

2.3.2. Dedicated Circuits

We can utilize the motional admittance property of the QCM with the dedicated circuits. Numerous methods have been provided, primarily focusing on obtaining the Q-factor, series resistance, and resonant frequency. The exponentially decayed technique and the phased-locked technique will be discussed in this section.

The exponential decay should be the most popular method for finding out the QCM's resonant frequency and dissipation because it yields sufficient data. Figure 2.4

illustrates how to isolate the QCM from the oscillator circuit by using a relay switch. The dissipation factor has a negative relationship with the decay rate of the oscillation signal over time. A droplet of aqueous glycerol solution was used to evaluate the system's performance [22].

In order to make it easy to comprehend the QCM response, the phased-locked technique seeks to lock the oscillation frequency to that of the motional series resonance frequency, which directly represents the QCM behavior. Zero-phase and maximum conductance are the two different types of these approaches. Both of them provide the driving frequency to QCM using a Phase Lock Loop (PLL) oscillator.

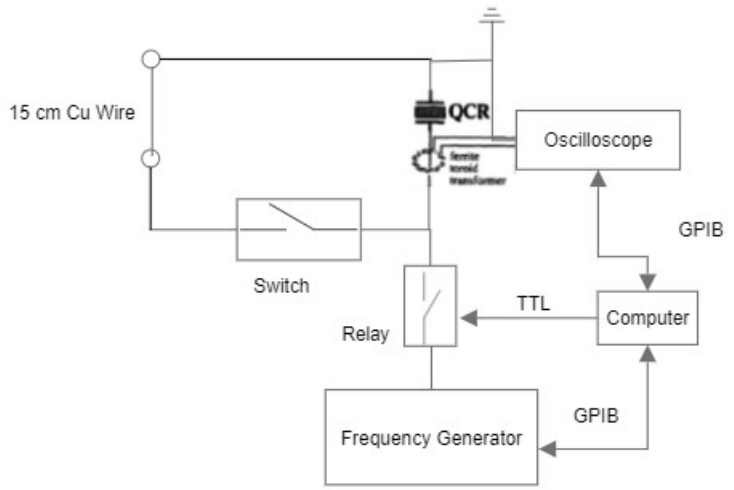

Figure 2.4. Circuit block diagram.

2.3.3. Vector Network Analyzer (VNA)

Network analysis is one of the most popular and essential activities in radio frequency (RF) engineering. A network analyzer is a tool that is commonly utilized for this purpose and that measures RF network components very effectively and precisely.

The network analyzer's sinusoidal signal is applied to the device under test (DUT). The instrument then measures the response of the DUT. The amplitude and phase of the signal from the DUT to the network analyzer are different from the sig-

nal sent to the DUT. These signals are utilized to characterize the DUTs. There are two types of network analyzers: scalar network analyzer and vector network analyzer (VNA).

Only the amplitude difference between the wave incident on the DUT and the wave reflected off the DUT is measured by the scalar network analyzer. The VNA, on the other hand, measures the amplitude and phase of both the incident and the reflected waves. VNA has more accuracy and precision but requires a more complex implementation [23]. The data collected from the VNA in the frequency domain can be converted to the time domain for additional analysis. Also, VNA can be used to characterize one-, two- or multi-port networks.



Figure 2.5. VNA with two ports.

In a two-port network analyzer, as depicted in Figure 2.5, there are also forward and reverse transmissions besides the reflections. These quantities can be expressed in terms of scattering parameters (s-parameters).

The ratios of the incident and reflected wave quantities are known as the S-parameters. The four s-parameters s_{11}, s_{21}, s_{12}, and s_{22} are necessary to fully characterize the network in the case of a two-port network.

The input and output reflection coefficients at ports 1 and 2, respectively, are s_{11} and s_{22}. While s_{21} and s_{12}, respectively, indicate the forward and reverse transmission coefficients.

The s_{11} parameter can be used for QCM measurements. It represents the ratio of the reflected signal to the incident signal from port 1. In this thesis, s_{11} is used to characterize the QCMs.

The ability to quickly derive the QCM's resonant frequency from the measurement is one of the significant benefits of the Vector Network Analyzer. Furthermore, QCM sensors can also be characterized regardless of external electronics. When compared to other measurement techniques, this methodology is thought to offer the most precise measurement. Therefore, this measurement method was chosen for this thesis.

3. SYSTEM DESIGN FOR QCM BASED BIOSENSOR

Measuring QCM with a Vector Network Analyzer has a big advantage that the resonance frequency of the QCM can be directly known as soon as the measurement is done. Also, this method is considered as the most accurate way to measure a QCM. This chapter will explain how a system is designed to measure QCM and how suitable components are selected for this system.

A VNA has one (or more) signal sources that can generate a signal and receivers that can determine the change in the given signal caused by the device under test (DUT) [24]. VNA measures the amplitude and phase of both incident and reflected waves of DUT ports. The measurement results are processed digitally and sent to display. Figure 3.1 shows the block diagram of a Vector Network Analyzer.

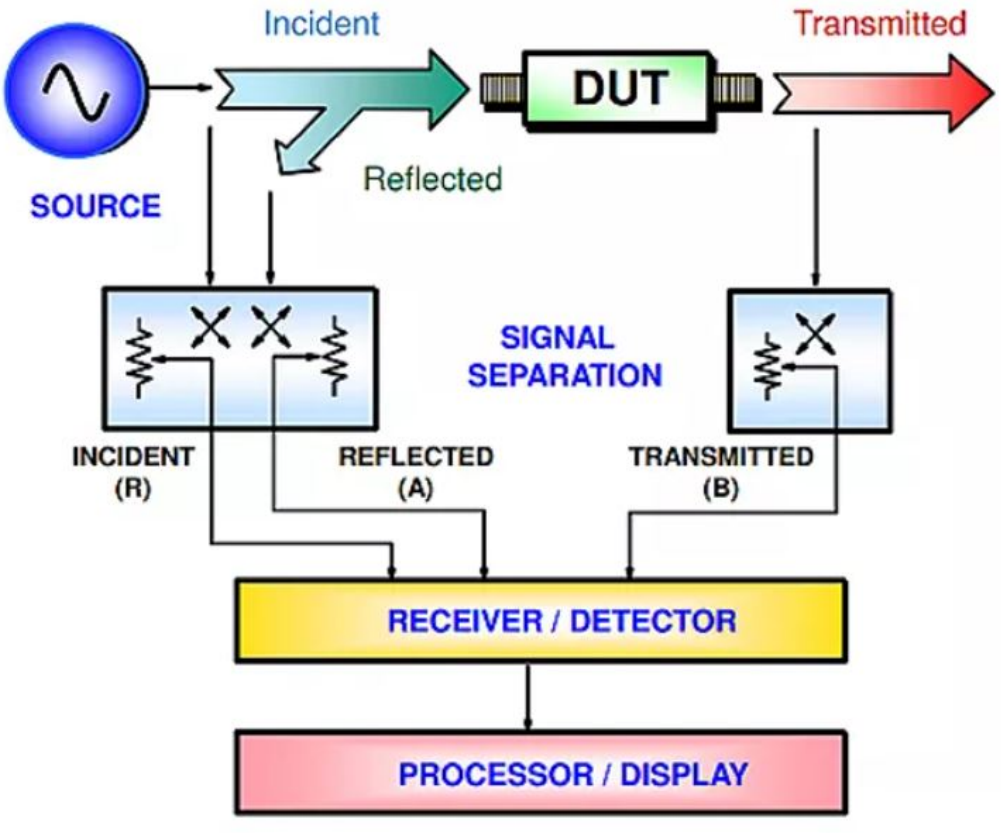

Figure 3.1. VNA block diagram [25].

VNA measurements are based on S (scattering) parameters. The s-parameters are defined as the ratio of the reflected wave to incident wave quantities. s-parameters are s_{11}, s_{21}, s_{12}, and s_{22}. The s_{11} parameter is used for QCM's phase and resonance frequency measurements in this thesis. It represents the ratio of the reflected signal to the incident signal from port 1 which is connected to QCM.

In order to design a system that can measure s_{11}, a RF source that can generate a signal with a controllable frequency, directional couplers, a gain/phase detector to compare the reflected signal to the incident signal, and a MCU that will control the system are required.

3.1. Frequency Synthesizer

Frequency synthesizer is a unit that can generate frequencies from a reference frequency generated by a stable frequency source such as a crystal oscillator. As a source of this system, a frequency synthesizer with at least a range of 50 MHz to 1 GHz is needed. Table 3.1 shows different frequency synthesizer aspects that are considered for this system.

After comparison, ADF4351 is chosen as this system's frequency synthesizer due to its low 1/f noise and low price. Even though its starting frequency is 35 MHz, its frequency range is enough for this system. If necessary, a frequency divider can be employed to reduce the lower frequency further.

3.1.1. ADF4351

ADF4351 is a wideband synthesizer with an integrated VCO (Voltage Controlled Oscillator). It can be used as a fractional-N or integer-N phase-locked loop (PLL) frequency synthesizer.

Table 3.1. Comparison of different frequency synthesizers.

Frequency Synthesizers	**RF Output Frequency**	**RF Input Frequency**	**1/f Noise (dBc/Hz)**	**Normalized Phase Noise**	**Is**	**Vs**	**Price (Dollar)**
ADF4150HV	10 MHz-3 GHz	10 MHz -300 MHz	-113	-213	50-60 mA	3-3.6	3.04
HMC703LP4E	10 KHz- 8 GHz	50 MHz -350 MHz	-130	-230	34-90mA	2.7-3.6	18.52
HMC704LP4E	10 KHz- 8 GHz	DC-350 MHz	-128	-230	38-58 mA	3-3.5	18.52
HMC701LP6CE	10 KHz- 8 GHz	100 KHz - 250 MHz	—	-221	90 mA	3-3.45	14.82
HMC702LP6CE	10 KHz- 14 GHz	100 KHz - 250 MHz	—	-221	135 mA	3-3.45	18.52
ADF4360-9	2-200 MHz	10 MHz -250 MHz	-110 (at 1 kHz offset)	-218	23mA	3-3.6	3.31
HMC1031	100 KHz - 500 MHz	140 MHz	-112	-208	1.95 mA	2.7-3.5	7.55
LTC6950	1 MHz - 1.4GHz	2 MHz -250 MHz	-134	-226	500 mA	3.15-3.45	12.08
HMC4069LP4E	10 MHz -2.9 GHz	10 MHz -1.3 GHz	-144	-233	295 mA	4.75-5.5	59.68
HMC700LP4	100 KHz - 8 GHz	200 KHz - 200 MHz	—	-221	90-110 mA	3-3.45	14.82
ADF4351	35 MHz - 4.4 GHz	10 MHz - 250 MHz	-118	-221	110 mA	3-3.6	8.25
ADF4355	54MHz - 6.8 GHz	10 MHz - 600 MHz	-116	-223	140 mA	3.15-3.45	27.87
ADF4355-2	54MHz - 4.4 GHz	10 MHz - 600 MHz	-116	-223	140 mA	3.15-3.45	19.75
ADF4355-3	51.56MHz - 6.6 GHz	10 MHz - 600 MHz	-116	-223	146 mA	3.15-3.448	27.87
ADF4356	53.125MHz-6.8 GHz	10 MHz - 600 MHz	-121	-227	166 mA	3.15-3.45	27.66
ADF4360-8	65 MHz - 400 MHz	10 MHz - 250 MHz	—	-216	35 mA	3-3.6	3.31
ADF4371	62.5 MHz - 32 GHz	10 MHz - 600 MHz	-127	-234	260 mA	3.15-3.45	275
ADF4372	62 MHz - 16 GHz	10 MHz - 600 MHz	-127	-234	270 mA	3.15-3.45	71.50

It has a VCO with a fundamental output frequency range from 2200 MHz to 4400 MHz. Its divide by-1/-2/-4/-8/-16/-32/-64 circuits allow the user to generate RF output frequencies as low as 35 MHz. It also has an auxiliary RF output that can be used if it is necessary.

It is configured through its chip registers with 3 I/O pins. It can operate with a power supply range of 3 to 3.6 volts. Figure 3.2 shows its functional diagram.

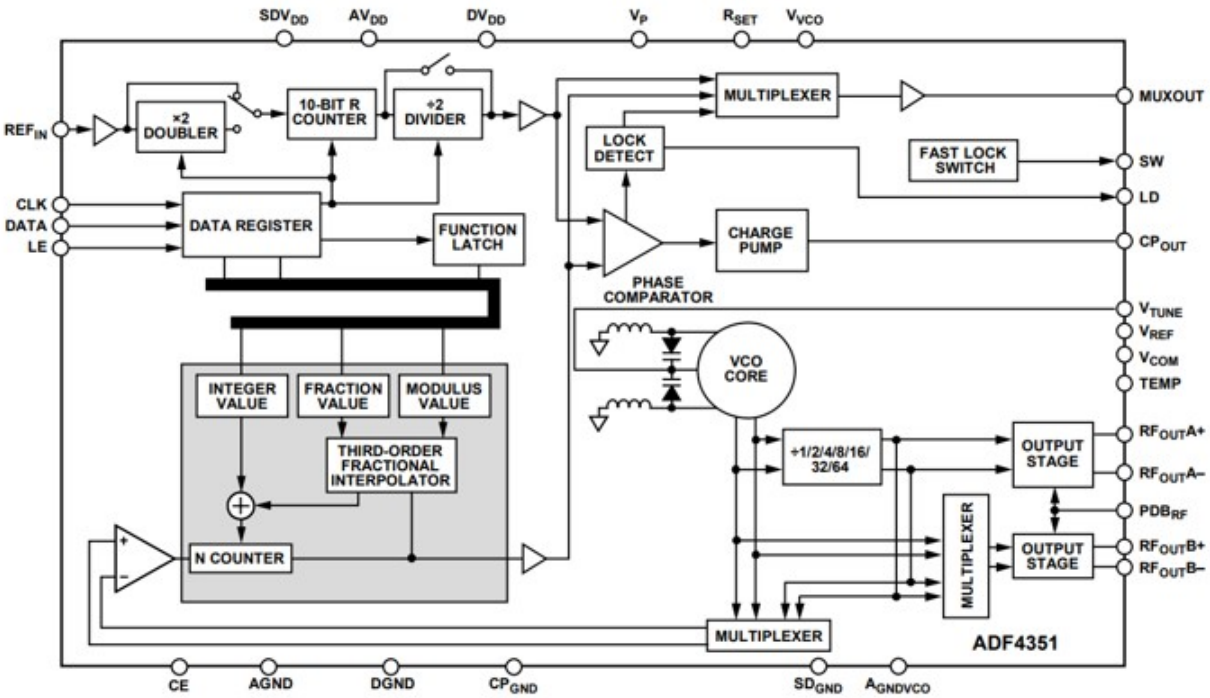

Figure 3.2. Functional block diagram of ADF4351 [26].

In this thesis, ADF4351 is controlled by Arduino Due using SPI. CLK, DATA, CE, LD, LE pins of the ADF4351 evaluation board are used to program its RF output frequencies with an Arduino.

ADF4351 has six registers numbered from 0 to 5. Each register controls different aspects of the synthesizer and has 32 bits. The first 3 bits are control bits for each register, but there are also various reserved bits in each register. Register 0 controls the INT and FRAC values of ADF4351's evaluation board. Register 1 controls the MOD,

Phase value, Prescaler and Phase adjust. Register 2 controls R counter value, Muxout, Low noise low spur mode, CP three state, Charge Pump current state, LDF, LDP, RDiv2, Double Buffer, PD Polarity and Power Down. Register 3 controls Clock divider value, CLK divider mode, Band Select CLK Mode, CSR, ABP and Charge cancel. Register 4 controls RF Divider select, Feedback divider select, MTLD, AUX Output Select, AUX Output Enable, AUX Output Power, RF Output Enable, Output Power and VCO Power Down. Register 5 controls LD Pin Mode. A detailed explanation is given in Appendix A. Table 3.2 shows the values of each bit for Register 5 as an example. C2, C1, and C0 are control bits. D15,D14 chose as 0,1 for digital lock detect. Rest of the bits are reserved.

3.2. Gain/Phase Detector

In this system, the gain/phase detector compares the incident signal's gain and phase features with the reflected signal's gain and phase features.

AD8302 is chosen for this system as a gain/phase detector. The functional block diagram of AD8302 can be seen in Figure 3.3 [27]. AD8302 is an integrated system for measuring gain/loss and phase. It requires a single supply of 2.5 Volt to 5.5 Volt. It has two inputs, called Input A and Input B. Its input signals are ac-coupled, and they have a range of -60 dBm to 0 dBm in a 50 Ω system from low frequencies to 2.7 GHz. Also, its signal inputs are single-ended, and this allows the signal inputs to be matched and connected directly to directional couplers.

AD8302's phase and gain outputs provide an accurate measurement. The range of the phase output is scaled between 0°–180° with 10 mV/degree. Its gain output range is scaled between ±30 dB with 30 mV/dB. AD8302's phase and gain behaviors can be written as

$$\begin{aligned} V_{PHS} &= V_{\Phi}[\Phi(V_{INA}) - \Phi(V_{INB})], \\ V_{MAG} &= V_{SLP} \log(V_{INA}/V_{INB}). \end{aligned} \tag{3.1}$$

Table 3.2. Values of each bit at register 5.

R31	**R30**	**R29**	**R28**	**R27**	**R26**	**R25**	**R24**	**R23**	**R22**	**R21**	**R20**	**R19**	**R18**	**R17**	**R16**	**R15**	**R14**	**R13**	**R12**	**R11**	**R10**	**R9**	**R8**	**R7**	**R6**	**R5**	**R4**	**R3**	**R2**	**R1**	**R0**
X	X	X	X	X	X	X	X	D15	D14	X	X	X	X	X	X	X	X	X	X	X	X	X	X	X	X	X	X	X	C2	C1	C0
0	0	0	0	0	0	0	0	0	1	0	1	1	0	0	0	0	0	0	0	0	0	0	0	0	0	0	0	0	1	0	1

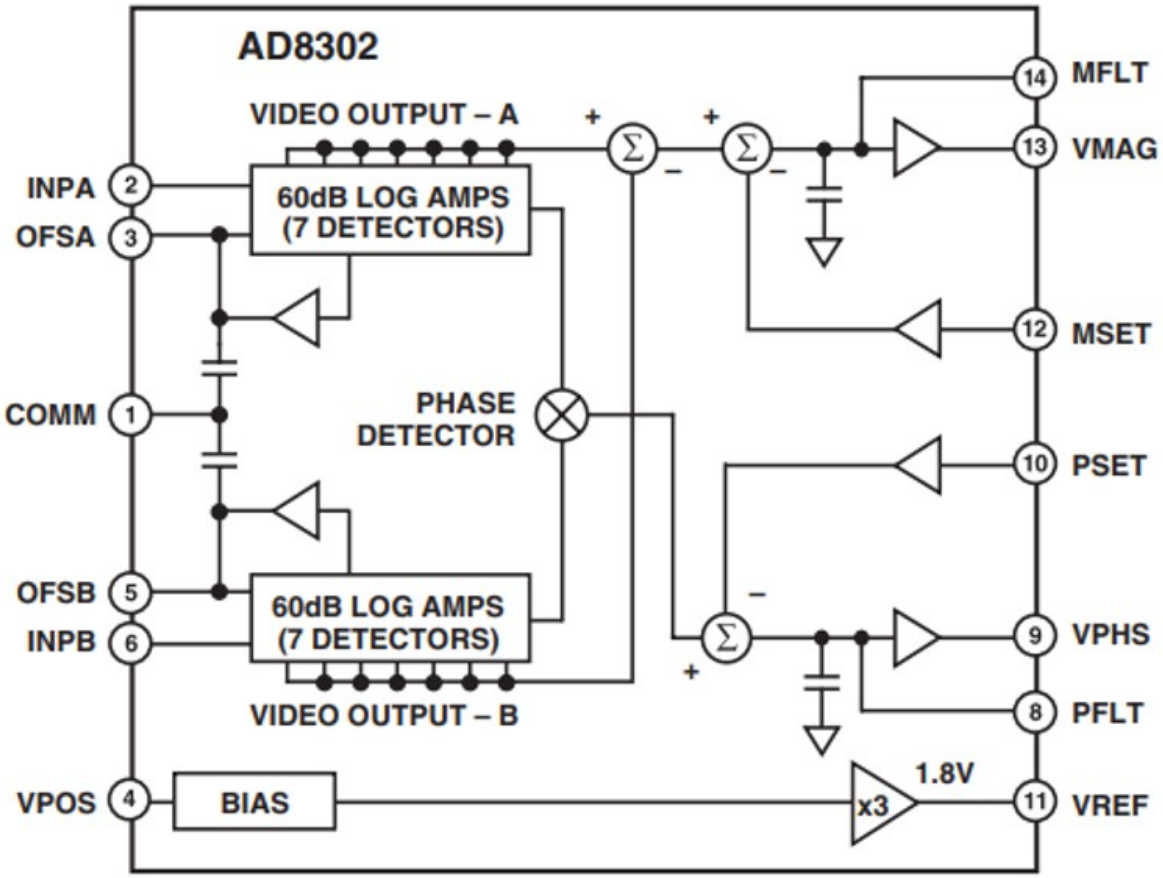

Figure 3.3. Functional block diagram of AD8302.

3.3. Directional Couplers

The function of the directional coupler is to sample the isolated (reflected) signal. Directional couplers have three ports. Their fourth port is internally terminated as in Figure 3.4 [16] to increase directivity. Since one of the coupled ports is terminated, only one coupled signal and this coupled port samples the reverse wave. This sampling can be changed simply by changing the positions of the connections.

Directional coupler is chosen to be used in this system due to its high directivity, performance, and isolation.

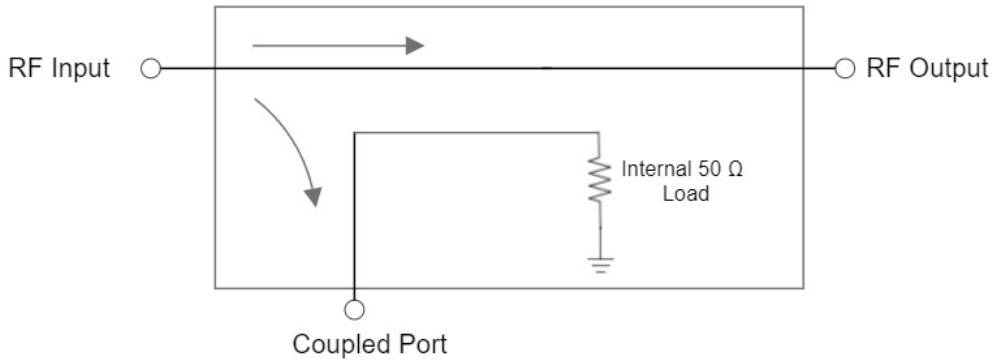

Figure 3.4. Directional coupler schematic.

When choosing a directional coupler for this system, coupler's frequency range, its coupling, main loss, directivity, and its impedance were the main criteria. Table 3.3 shows the aspects of different couplers.

A Coupler's frequency range should be at least between 10 MHz to 1 GHz and its impedance has to be 50 Ohm. According to these standards, ADC-15-4+ is chosen for this system.

Table 3.3. Comparison of RF Couplers.

RF Couplers	**Frequency (min.)**	**Frequency (max.)**	**Coupling (dB)**	**Main Loss (dB)**	**Directivity (dB)**	**VSWR**	**Power Input**	**Impedance**	**Price (Dollar)**
ADC-6-10-75+ (+)	20 MHz	1 GHz	6.6	2.1-2.8	9-15	1.33	0.5	75 Ohm	6.95(10)
ADC-10-4+ (+)	5 MHz	1 GHz	10.5	0.8-1.5	13-40	1.2	1	50 Ohm	6.95(10)
ADCB-20-82+ (+)	1 MHz	800 MHz	20	0.1-0.57	15-20		0.5-1	50 Ohm	7.95(10)
RBDC-20-63+	DC	6 GHz	20	0.98-1.35	20	1.3	0.25	50 Ohm	
ZDC-20-3	0.2 MHz	250 MHz	19.5	0.24-0.6	20-36	1.2	1.5-4	50 Ohm	
RDC-20-232-75X+	5 MHz	2.35 GHz	20	0.85-1.1	7-22		1	75 Ohm	
ZFDC-20-33+	20 MHz	3 GHz	19-22.8	0.4-1.8	10-25		0.5-1	50 Ohm	
SYD-20-33+	30 MHz	3 GHz	20.8-21.5	1.1-2.5	9-20	1.1-1.2	1	50 Ohm	
ADC-15-4+	5 MHz	1 GHz	15.5	0.6	24	1.2	1	50 Ohm	8.79(10)

3.4. MCU

An MCU is a semiconductor IC that has a memory module(s), a processor unit, communication interfaces and peripherals. Its history goes back to the invention of MOSFET Technology. Today ARM architecture dominates the market for 32-bit MCU's.

For this system, Arduino DUE depicted in Figure 3.5 is chosen because it is easy to code, and is open source. Also, its sample rate and flash memory were found to be sufficient for this system. It has 12 Analog input pins and 2 Analog output pins. Its operating voltage is 3.3 V. It has 512 KB Flash memory, and its sample rate is up to 1 MHz per second.

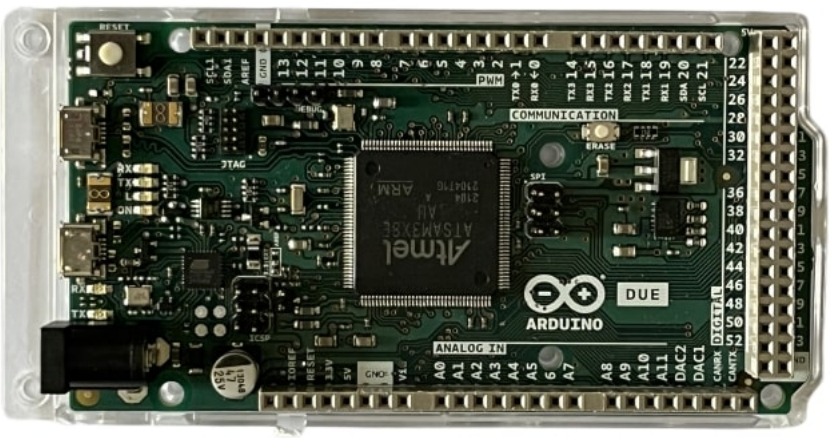

Figure 3.5. Arduino Due.

This system's code is written in ARDUİNO IDE. 2 Analog input pins, 2 digital pins, 2 SPI pins, and Ground pins are used (A2 and A3). Also, its 5V and 3.3-volt pins are used to supply ADF4351's chip and the evaluation board of ADF4351.

Figure 3.6 shows the schematic of the designed system after all the suitable components are selected.

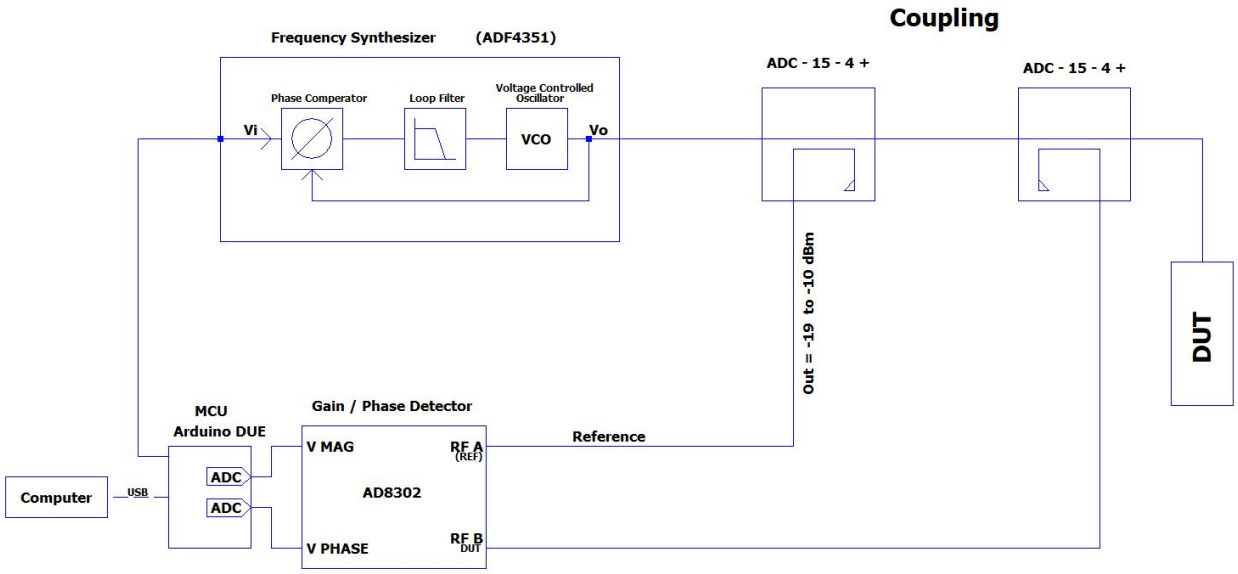

Figure 3.6. Designed system schematic.

The ADF4351 generates the signal at the desired frequency. Directional couplers are used to replicate the incident signal and transmit the reflected signal from the QCM and the incident signal to the AD8302. Then the AD8302 compares these signals and outputs two different outputs for gain and phase comparison of these signals. The MCU controls the ADF4351 so that it generates the desired signal(s) for the scans and reads the outputs of the AD8302.

4. MEASUREMENTS

After selecting suitable components for the system described in this thesis, each system board was tested individually to ensure proper operation.

4.1. ADF4351 Frequency Synthesizer Measurements

Initially, the aim was to verify that the evaluation board of the ADF4351 could generate signals with frequencies between 35 MHz and 4.4 GHz. The evaluation software of ADF4351 was downloaded from the website of Analog Devices and the software was used to generate signals from the evaluation board. Some example results are provided in Figures 4.1, 4.2, and 4.3.

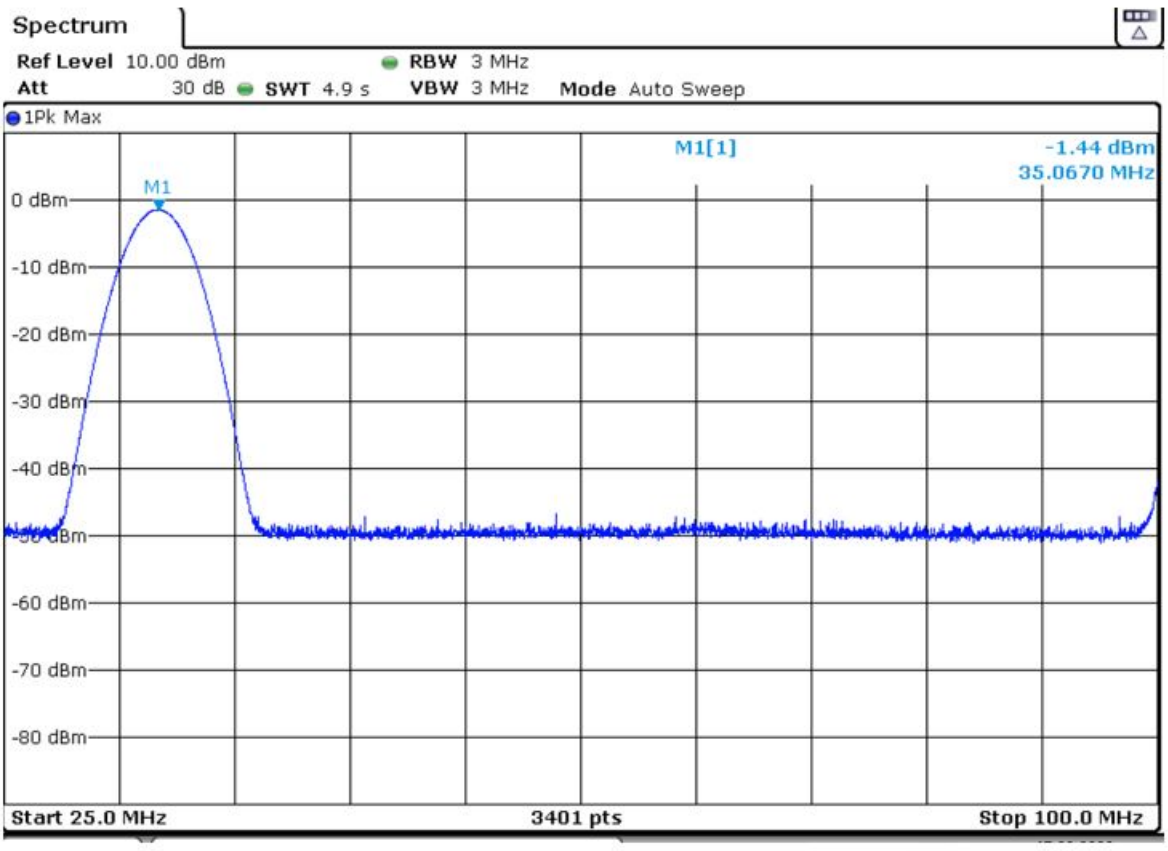

Figure 4.1. Measurement of ADF4351 output with signal analyzer at 35 MHz.

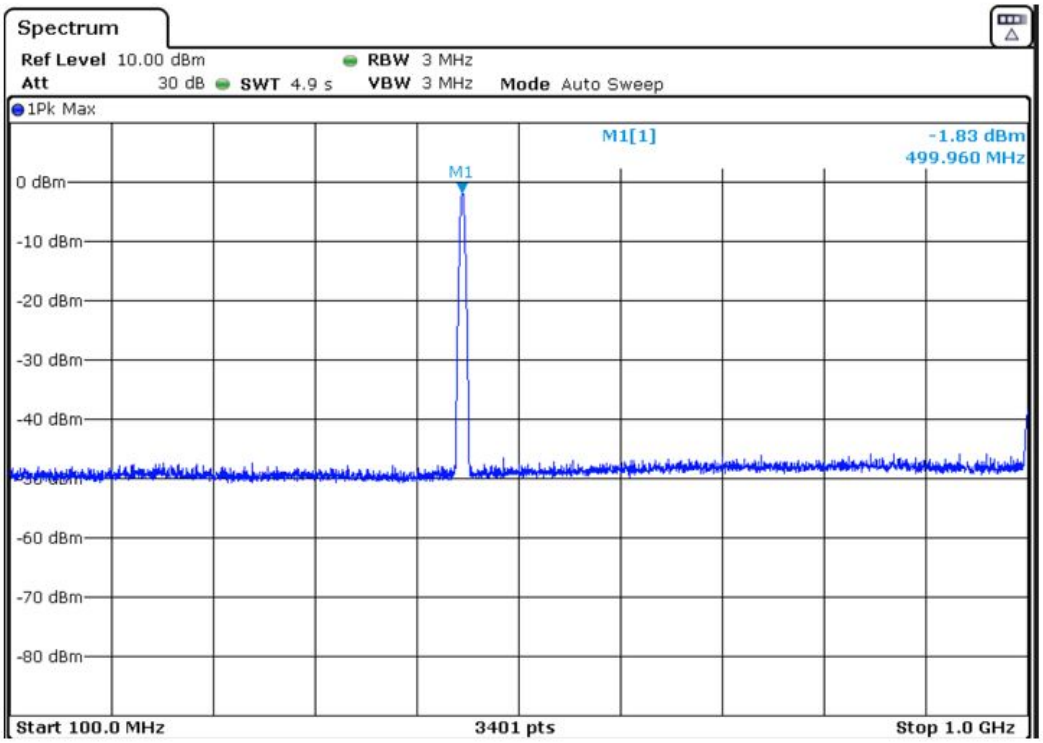

Figure 4.2. Measurement of ADF4351 output with signal analyzer at 500 MHz.

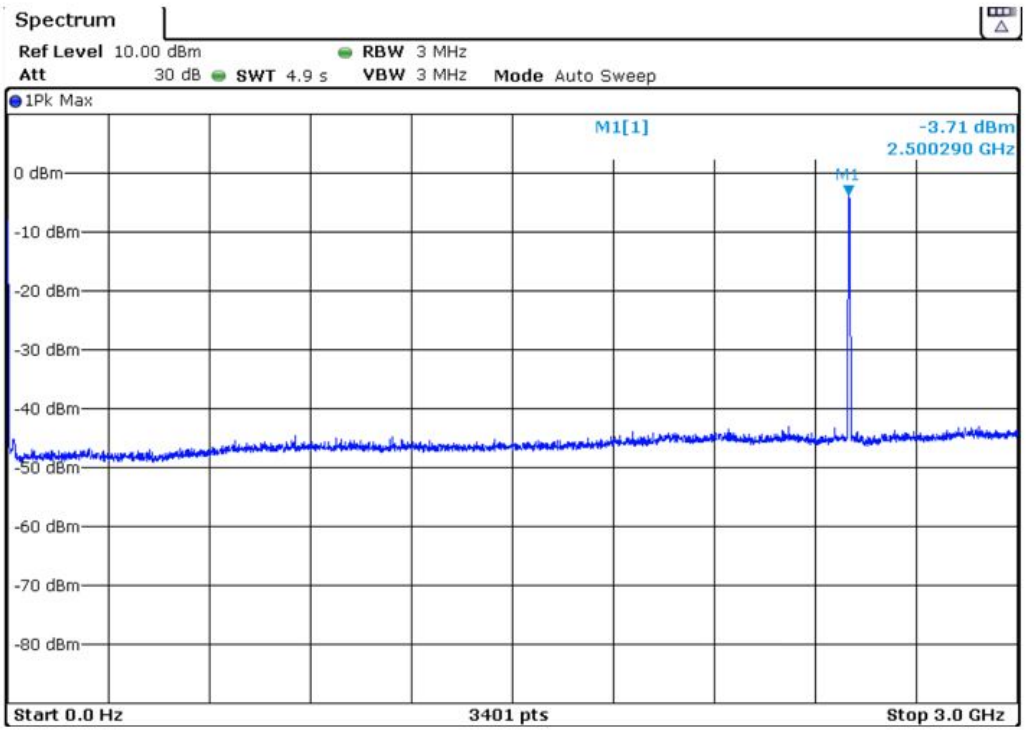

Figure 4.3. Measurement of ADF4351 output with signal analyzer at 2.5 GHz.

The RFout A+ channel of the ADF4351 was monitored with an oscilloscope. The board generates square wave signals without any problem at higher frequencies.

For optimum operation with a good broadband match, the output of the ADF4351 is modified. The L1, L2, L3, and L4 inductors whose values are 1.9 nH, 7.5 nH, 7.5 nH, and 1.9 nH respectively were replaced by a short circuit, 50 Ohm resistor, 50 Ohm resistor, and a short circuit in this order. The evaluation board's schematic is in Figure 4.4 [28]. The new results are depicted in Figures 4.5 and 4.6.

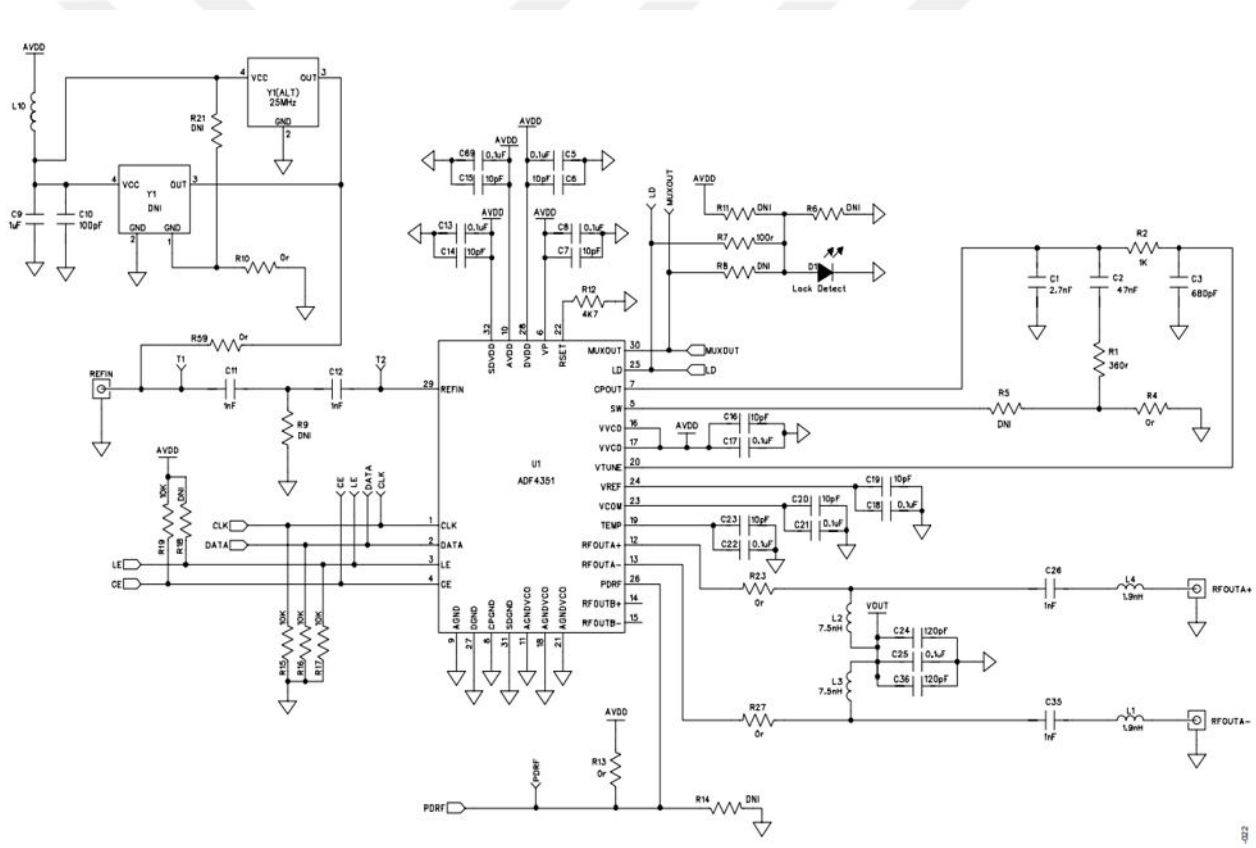

Figure 4.4. Evaluation board schematic of ADF4351.

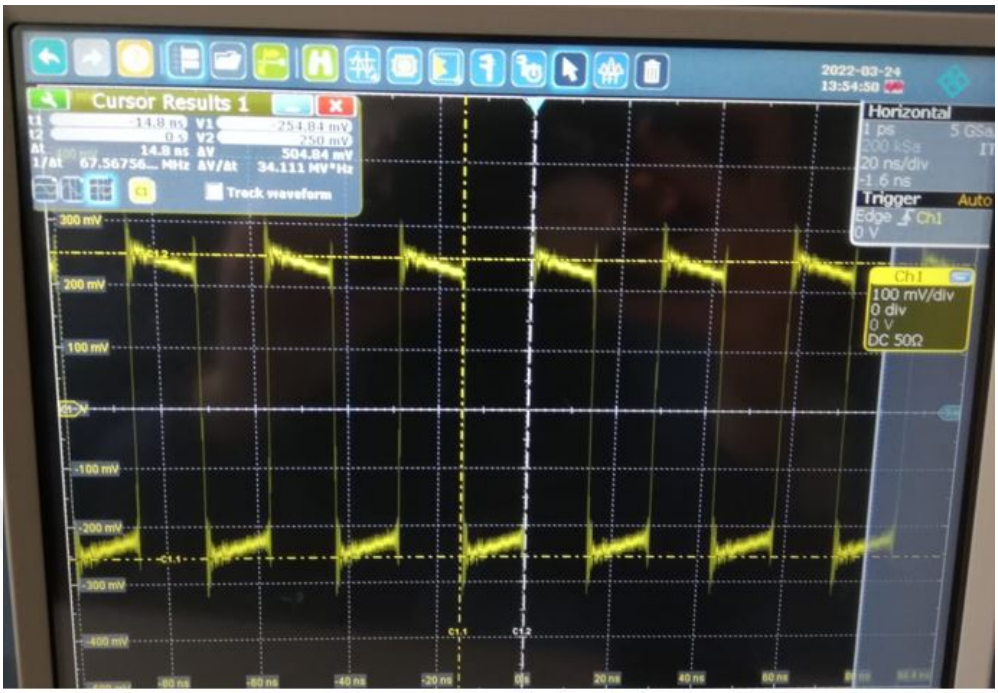

Figure 4.5. Measurement of ADF4351 evaluation board with an oscilloscope at 35 MHz after modification.

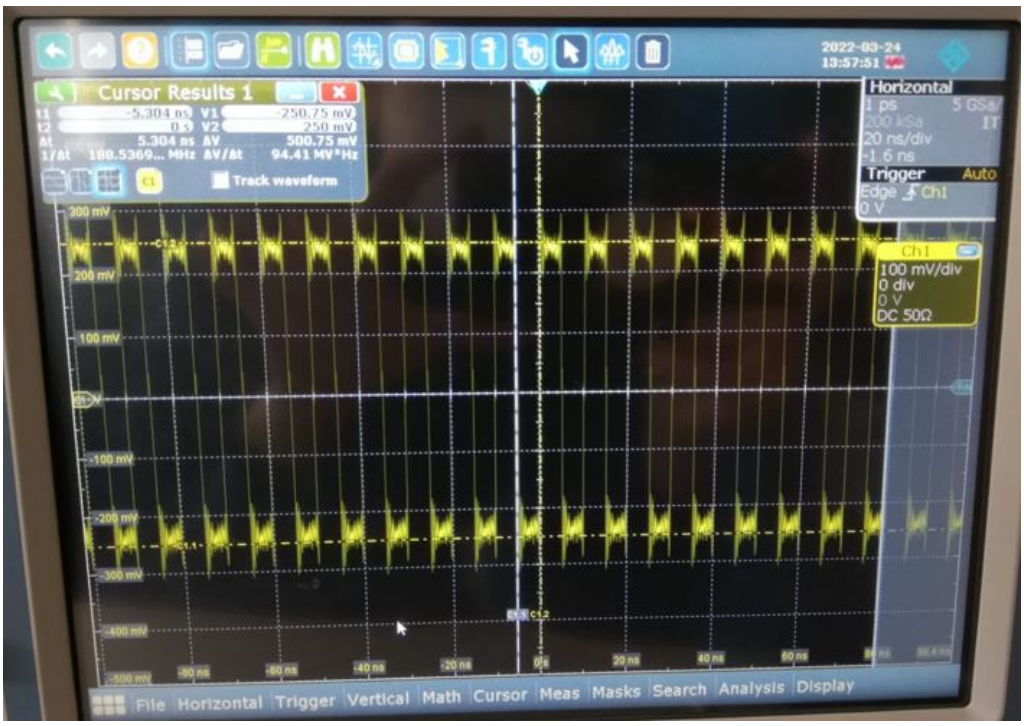

Figure 4.6. Measurement of ADF4351 evaluation board with an oscilloscope at 100 MHz after modification.

4.2. AD8302 Gain Phase Detector Measurements

First, a signal that has a 200-mV peak-to-peak amplitude was obtained with a signal generator and this signal was replicated using a sma female T adaptor. Then, these identical signals were connected to input a and input b of the AD8302 Evaluation board using cables of different lengths. The phase, gain, and Vref outputs of the AD8302 evaluation board were measured with a multimeter to verify the operation of the evaluation board against its datasheet. These measurements were repeated for different frequencies. Expected values of AD8302 outputs according to its datasheet are depicted in Figure 4.7 [27] and the measurement results are depicted in Figures 4.8 and 4.9.

The results of the measurements were as expected. So, a 10dB attenuator was added to input a in order to create a difference of magnitude between signals, and the outputs of the AD8302 evaluation board were measured again.

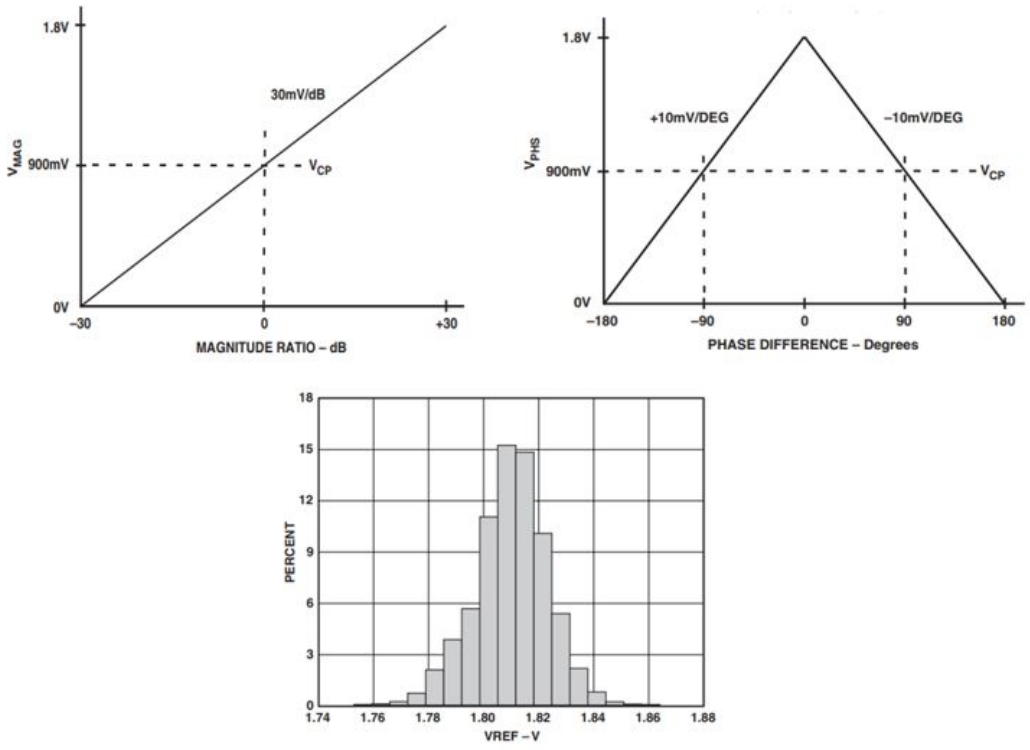

Figure 4.7. Expected values of AD8302's outputs according to its datasheet.

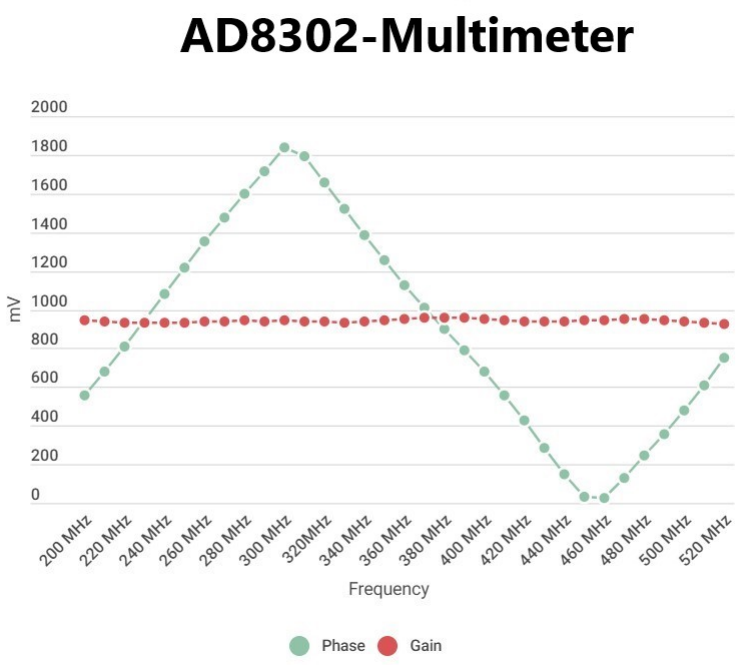

Figure 4.8. Measurement values of phase and gain outputs of AD8302 evaluation board (without attenuation and peak to peak is 200 mV).

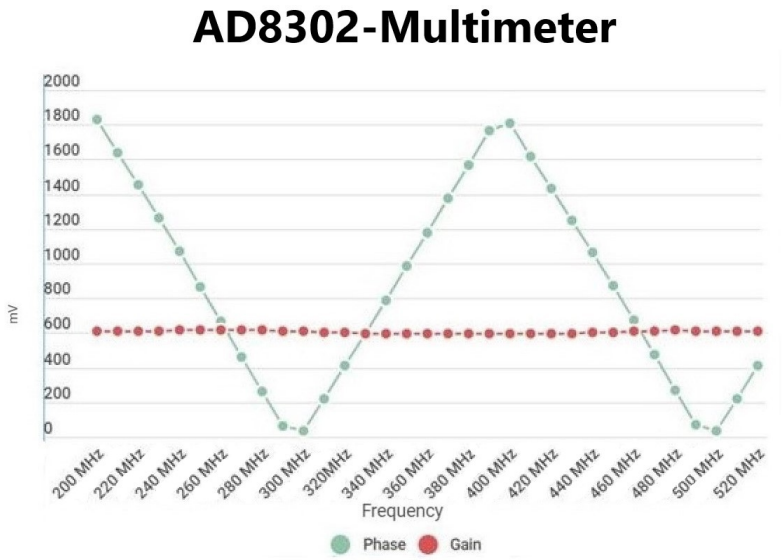

Figure 4.9. Measurement values of phase and gain outputs of AD8302 evaluation board with 10 dB attenuation to input a (peak to peak is 200mV).

After having verified the operation of the AD8302 evaluation board, one last measurement was carried out using the ADF4351 evaluation board instead of the signal generator to observe the effect on the phase and gain outputs of the AD8302 evaluation board as in Figure 4.10. The phase and gain outputs are shown in Figure 4.11.

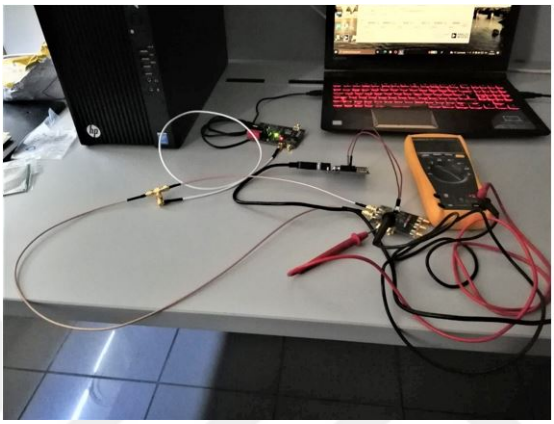

Figure 4.10. Set-up for measurements of AD8302 using ADF4351 (Arduino Uno used as a power supply for AD8302).

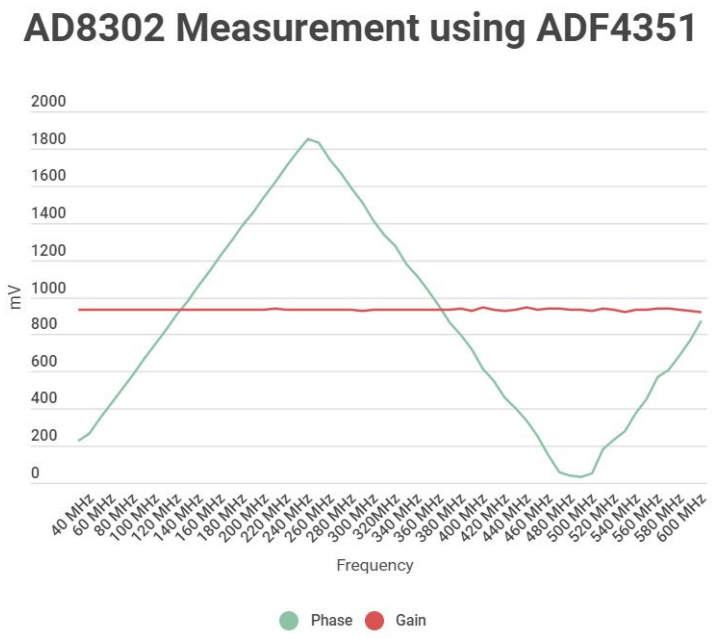

Figure 4.11. Measurement values of phase and gain outputs of AD8302 evaluation board using ADF4351 evaluation board as a signal generator.

4.3. Couplers (ADC-15-4+) Measurements

ADC-15-4+ was selected as the coupler in the system design. After it was soldered on a PCB as in Figure 4.13 and a 50 Ohm resistor was added as termination as shown in Figure 4.12, it has been measured with a VNA to check its operation. Figure 4.14 [29] shows properties of ADC-15-4+ as given in the datasheet.

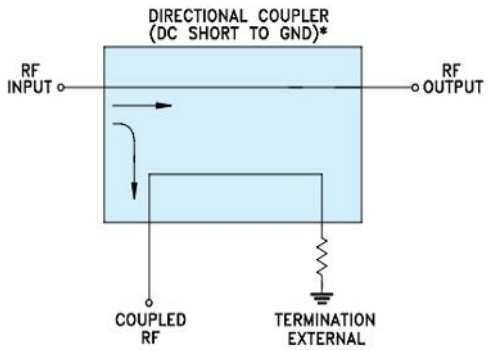

Figure 4.12. Schematic of ADC-15-4+ [29].



Figure 4.13. ADC-15-4+ on a PCB with SMA connectors.

Directional Coupler Electrical Specifications

FREQ. (MHz)	COUPLING (dB)		MAINLINE LOSS[1] (dB)			DIRECTIVITY (dB)			VSWR (:1)	POWER INPUT, W	
			L	M	U	L	M	U		L	MU
f_L-f_U	Nom.	Flatness	Typ. Max.	Typ. Max.	Typ. Max.	Typ. Min.	Typ. Min.	Typ. Min.	Typ.	Max.	Max.
5-1000	15.5±0.5	±0.5	0.6 1.0	0.6 1.0	0.8 1.2	23 20	24 20	28 17	1.20	1.0	1.0

L= 5-50 MHz M= 50-500 MHz U= 500-1000 MHz
1. Mainline loss includes theoretical power loss at coupled port.

Figure 4.14. ADC-15-4+ properties as given in the datasheet.

Initially, the input and the coupled ports of the coupler were connected to the VNA to measure the coupling. The results are shown in Figure 4.15. Then, the input and the output ports were measured, and the mainline loss was observed as in Figure 4.16. Finally, the isolation between the coupled port and the output port was measured as in Figure 4.17.

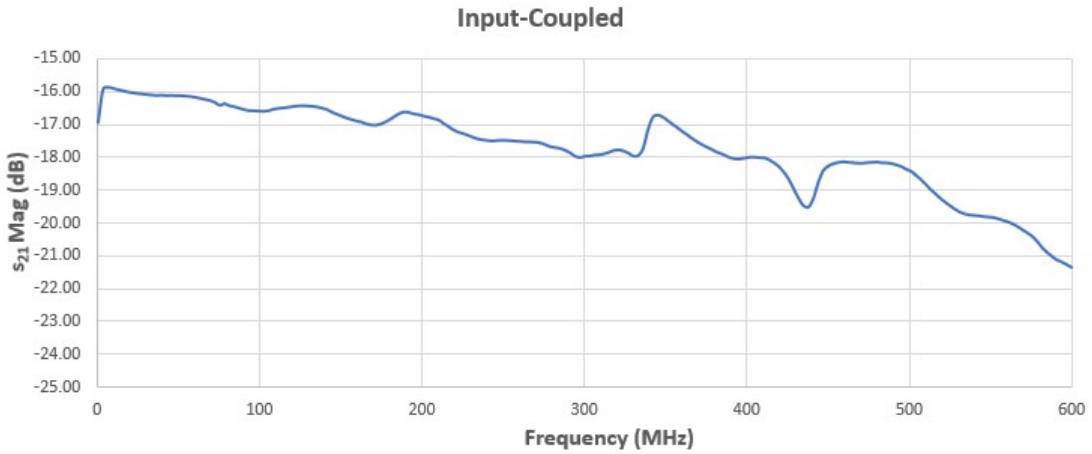

Figure 4.15. VNA measurement of ADC-15-4+ on a PCB when VNA cables connected to its input and coupled ports.

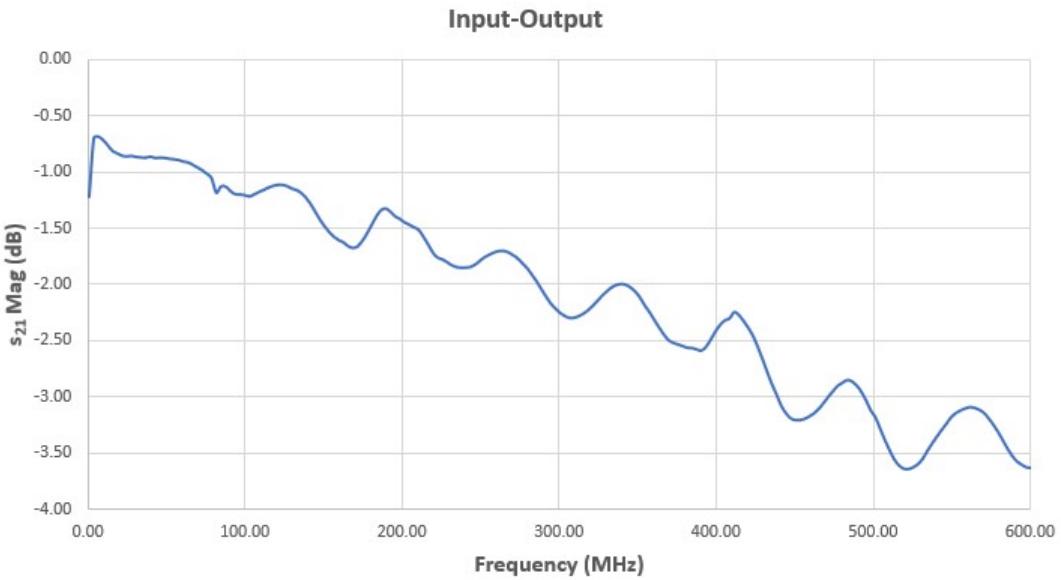

Figure 4.16. VNA measurement of ADC-15-4+ on a PCB when VNA cables connected to its input and output ports.

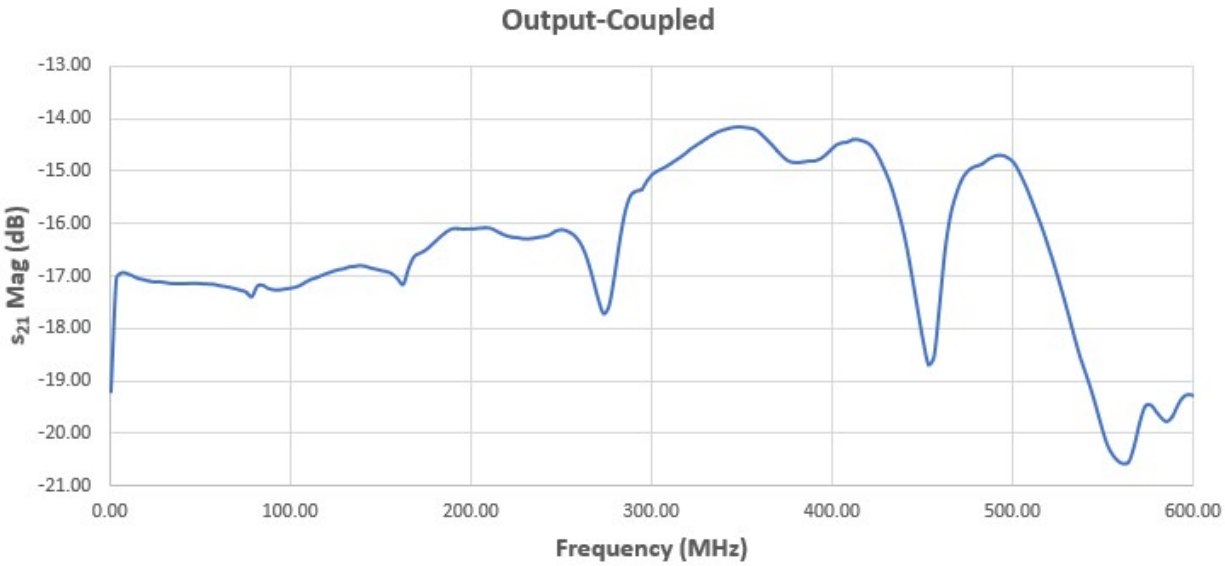

Figure 4.17. VNA measurement of ADC-15-4+ on a PCB when VNA cables are connected to its output and coupled ports.

The measurements demonstrate satisfactory operation although one-to-one correspondence with the curves in the datasheet was not obtained as shown in Table 4.1. The reason may be losses in the PCB and the connecting cables.

Table 4.1. Comparison of measurement results and datasheet properties of ADC-15-4+ with frequency range of 0 - 100 MHz.

	Coupling (dB)	**Mainline Loss (dB)**	**Directivity (dB)**
Datasheet	15.5 ± 0.5	0.6 - 1	20 - 24
Measurement Results	16 - 17	1 - 1.5	17 - 17.5

4.4. MCU (ARDUINO DUE) Tests

4.4.1. Configuration of ADF4351 with Arduino Due

The ADF4351 IC has six registers labeled 0 to 5. (See Appendix A for ADF4351's Register Maps) Most features of the ADF4351 can be controlled by the registers. All register values are sent to ADF4351 using SPI (Serial Peripheral Interface). As a first step, the baud rate of the interface was set as 9600. Then, the baud rate is selected as 115200 bps to achieve a fast configuration of ADF4351. This will allow us to increase the scan rate of the system.

The main focus was on the register bits that are controlling FRAC, INT, MOD, and R values (See Figure 4.18) because these determine the frequency to be generated. These equations can be written as

$$RF_{OUT} = [INT + (FRAC/MOD)] * (f_{PFD}/RFDivider), \quad (4.1)$$

$$(f_{PFD} = REF_{IN} * [(1 + D)/(R * (1 + T))]. \quad (4.2)$$

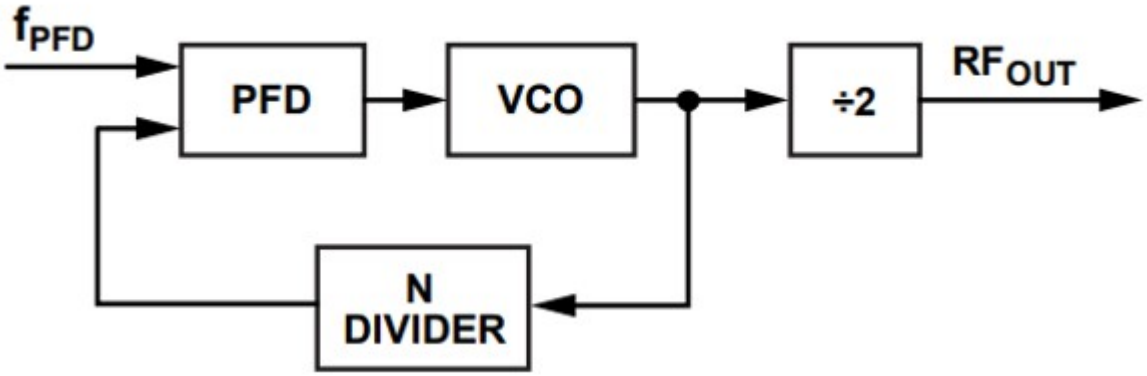

Figure 4.18. RF output frequency schematic of ADF4351 (when the loop is closed before output divider) [26].

The dual-modulus prescaler (P/P + 1), along with the INT, FRAC, and MOD values, determines the overall division ratio from the VCO output to the PFD input. The PR1 bit (DB27) in Register 1 sets the prescaler value.

Operating at CML levels, the prescaler takes the clock from the VCO output and divides it down for the counters. The prescaler is based on a synchronous 4/5 core. When the prescaler is set to 4/5, the maximum RF frequency allowed is 3.6 GHz. The prescaler value was chosen as 4/5 since this system doesn't need to generate frequencies over 3.6 GHz. Also, digital lock detect was chosen as the detection mode and the output frequency divider was disabled.

After writing a code that makes ADF4351 generate a signal at the desired frequency, two loops were included in the code to make a sweep between desired frequencies. Because generating a signal at one frequency is not enough to find the resonance frequency of the QCM. In order to find it, a sweep between frequencies close to its center frequency is required. (See Appendix B for the complete code that is used to control ADF4351 and read AD8302's phase and gain outputs.)

The first loop starts when FRAC is equal to 0 and continues until MOD-1 to generate signals according to equation 4.1. In the second loop,the only difference is that INT value is increased by 1. So, the frequency sweep continues until the frequency is higher than the resonance frequency of the QCM. (So, one sweep has 8190 data points since each loop has 4095 data points.) Also, ADF4351 uses digital lock detect as well. It waits for the lock signal to generate the next output at higher frequency until the previous signal has settled.

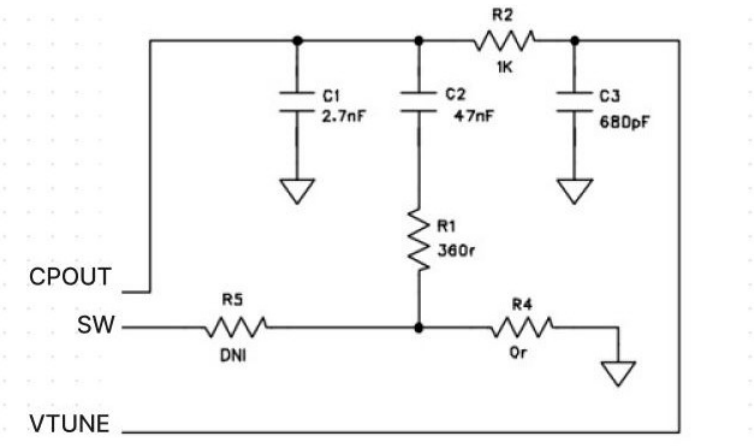

Figure 4.19. Loop filter's circuit [26].

Lock detect occurs when the absolute frequency error is 1000 Hz, and the output phase error is close to 0°. Usually, lock detect takes microseconds but it changes according to loop bandwidth, phase margin, channel resolution, MOD and REFIN values of the PLL. Loop bandwidth and phase margin are calculated from the loop filter on the Evaluation Board. Also, REFIN is 25 MHz, and it is a constant created by crystal. MOD is 4095 and channel resolution is 19 Hz. (See Appendix C for a detailed analysis of ADF4351's Loop Filter using ADIsimPLL (Analog Devices Software).). ADF4351's Loop Filter is shown in Figure 4.19. In the designed system, lock detect takes almost 70 microseconds on average.

4.4.2. Controlling Evaluation Board of AD8302 with Arduino Due

To test the analog input ports of the Arduino DUE board and the ADC present in the board, a DC voltage was applied first. The digital value corresponding to the DC input was observed on the Arduino IDE's serial monitor. Then a ramp signal at 10 Hz with 1V peak to peak amplitude was applied to the board from a signal generator. The Cool Term software was utilized to read the serial port and simultaneously save the data in a text file. Finally, a small code was developed in MATLAB to plot the data. (See Appendix D)

When this test was repeated at higher frequencies, the board's sample rate was not enough. In order to determine the maximum sample rate, timing flags were added before and after the measurements. The first measurement yielded a sample rate of 227 Ksamples/sec, whereas changing the mode to free running mode increased the rate to 370 Ksamples/sec.

After the operation of Arduino's ADC was verified, analog input ports were selected, and the code described above was used to measure AD8302's gain and phase outputs.

A ramp signal with a one-volt peak to peak amplitude was applied and the gain and phase outputs of the ADC8302 board were measured with a multimeter and the built in ADC of the Arduino board simultaneously. When the results were compared, only 5mV difference between the two results was observed.

4.5. Measurements of QCMs using a VNA

In this thesis, a packed QCM and an open QCM were used. Before measuring these QCMs with the designed system, both QCMs have been measured using a VNA in order to compare the results with each other and evaluate the accuracy of the results of the designed system.

4.5.1. Measurements of a Packed QCM

The Packed QCM in Figure 4.20 has a 50 MHz resonance frequency. For this QCM, a VNA measurement was made. The properties and results of this measurement are shown in Table 4.2, and Figure 4.21.

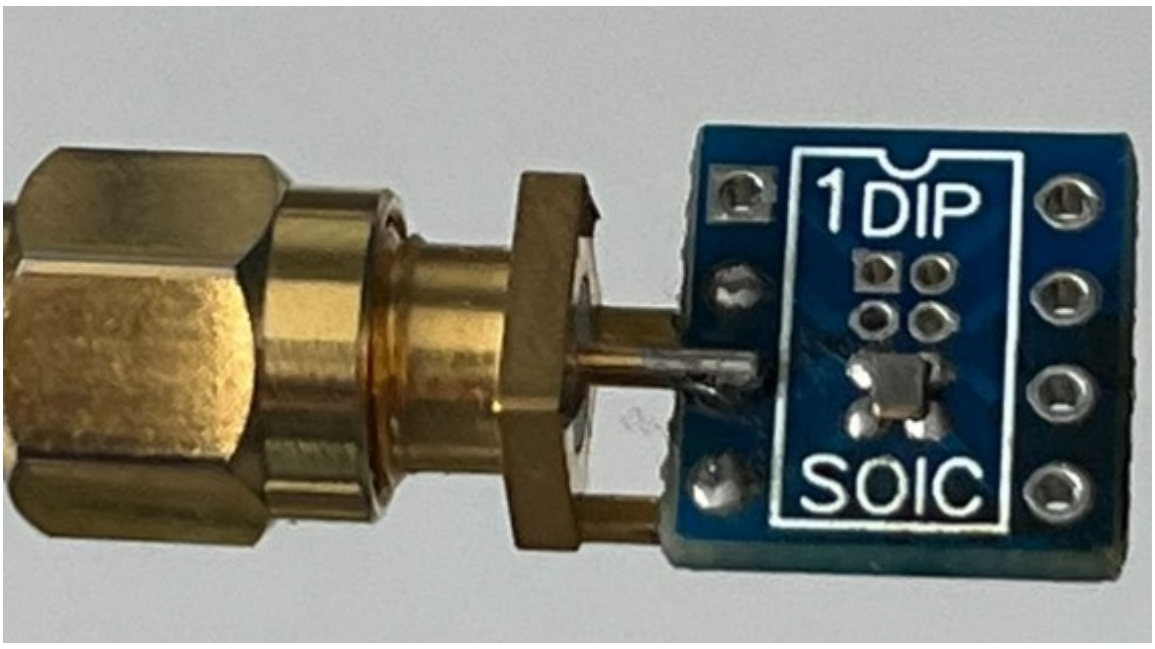

Figure 4.20. Packed QCM.

Table 4.2. Results of VNA measurements for packed QCM.

Start Frequency	Stop Frequency	Number of Points	Resonance Frequency	Dip Magnitude
49.8 MHz	50.2 MHz	5000	49.994519 MHz	13.1263 dB

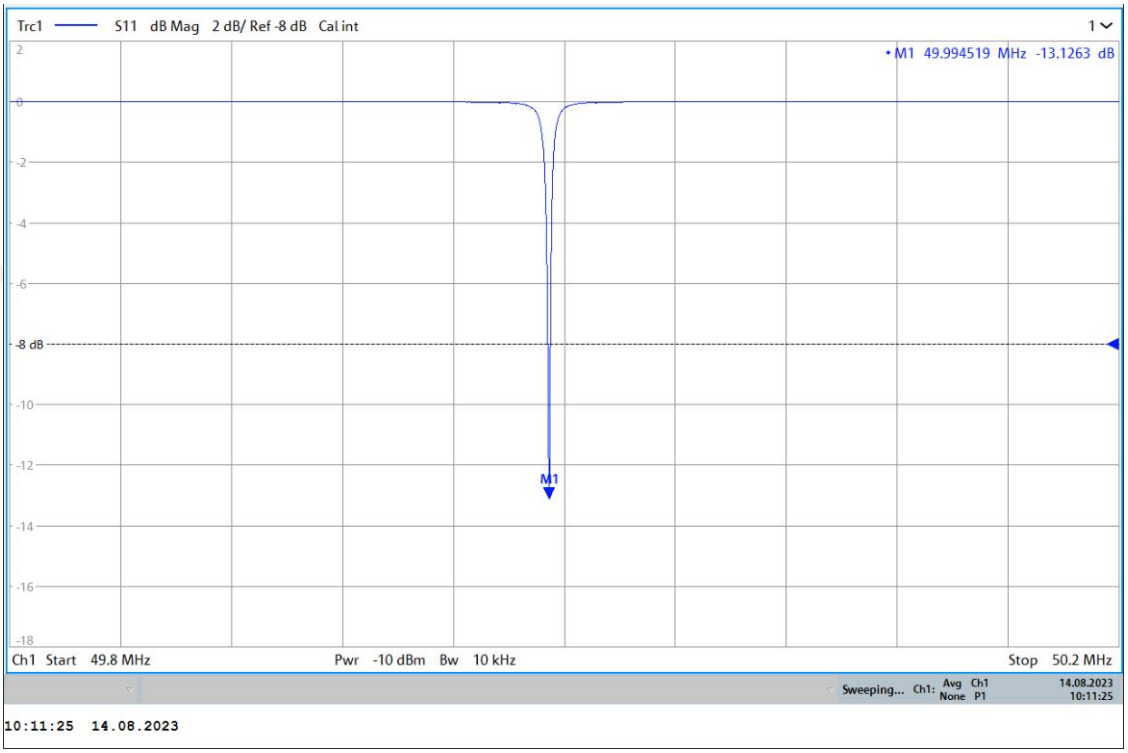

Figure 4.21. Packed QCM VNA result.

4.5.2. Measurements of an Open QCM

Five different open QCMs as in Figure 4.22 were used in this thesis. They all have a resonance frequency of approximately 10 MHz.

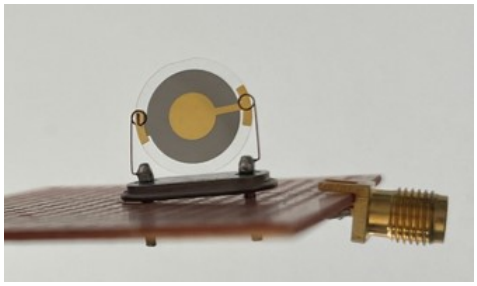

Figure 4.22. Open QCM.

However, the precise value of their resonance frequency and their dip magnitude are all different. The results in this chapter belong to an open QCM that has larger dip magnitude at its resonance frequency, and it is also used for the measurements of the designed system.

More than one open QCM was utilized because they are fragile. During measurements, two of them broke accidentally. Whenever an open QCM is broken, the replacement QCM was first measured using a VNA and then used in all circuit measurements in order to have VNA measurements for comparison with system measurements.

Due to the limitations of the ADF4351 chip, system measurements can only start at 35MHz. But the resonance frequency of the available open QCM was at 10 MHz. For this reason, two measurements were performed for one open QCM at two different frequencies. The first one had a 10 MHz center frequency and the second one had a 50.075 MHz center frequency so that third harmonic response is observed. The measurement results are depicted in Figures 4.23 and 4.24. The number of points was 5000 for all the measurements using VNA.

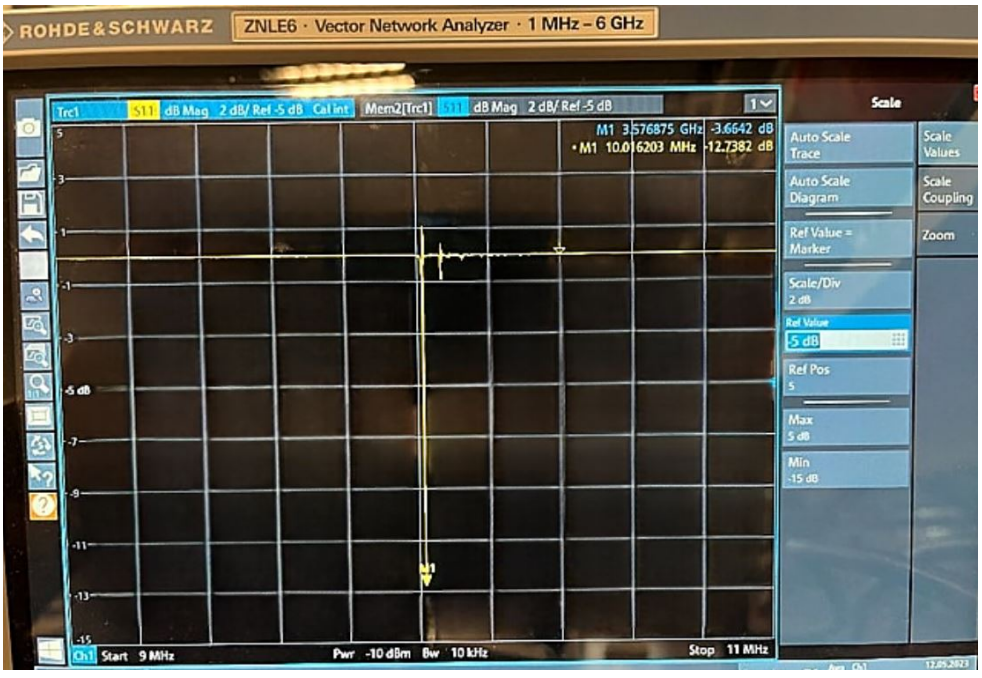

Figure 4.23. Open QCM VNA measurement result for 10 MHz center frequency.

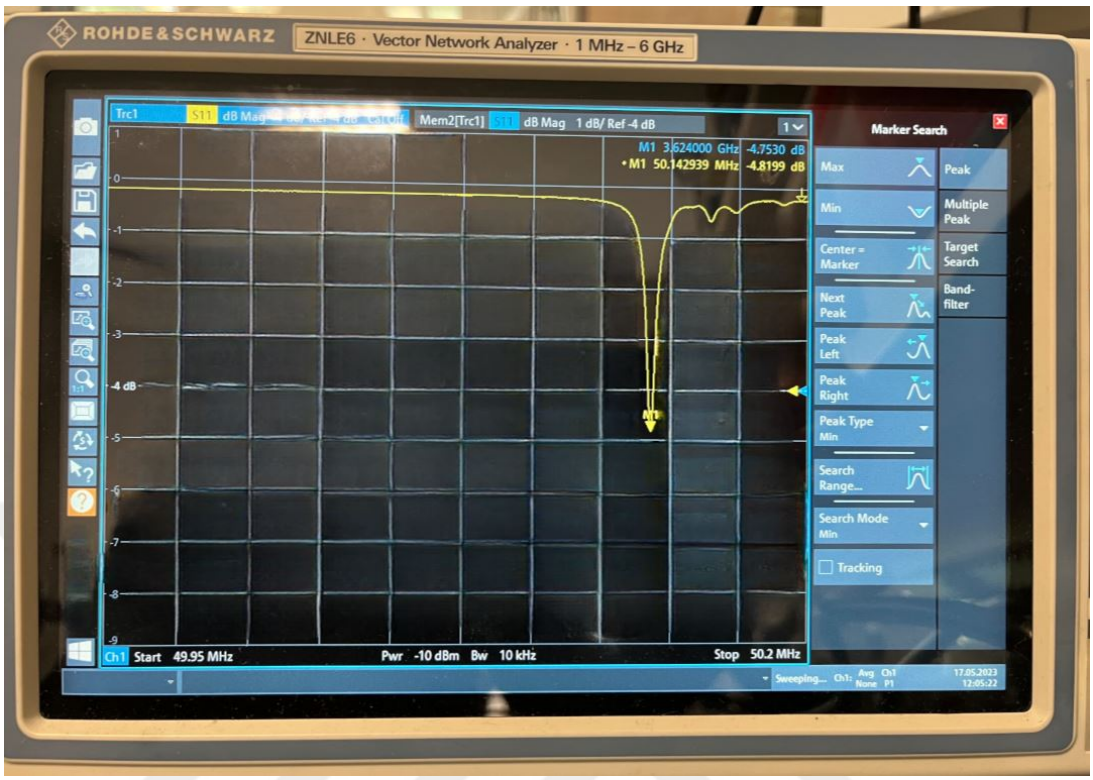

Figure 4.24. Open QCM VNA measurement result for 50.2 MHz center frequency.

4.6. QCM Measurements with The System

4.6.1. Packed QCM Measurements using The System

After testing all the components and making sure they were all working properly, the system was assembled as in Figure 4.25 and used to measure the resonance frequency of the QCM.

In the beginning of the system measurements, the frequency sweep was done just once, and the data were evaluated. For these measurements a packed QCM was used, the AD8302 board was supplied via an independent power supply of 5V, and the ADF4351 RFout was connected to a signal analyzer to ensure the signal generation at the desired frequencies.

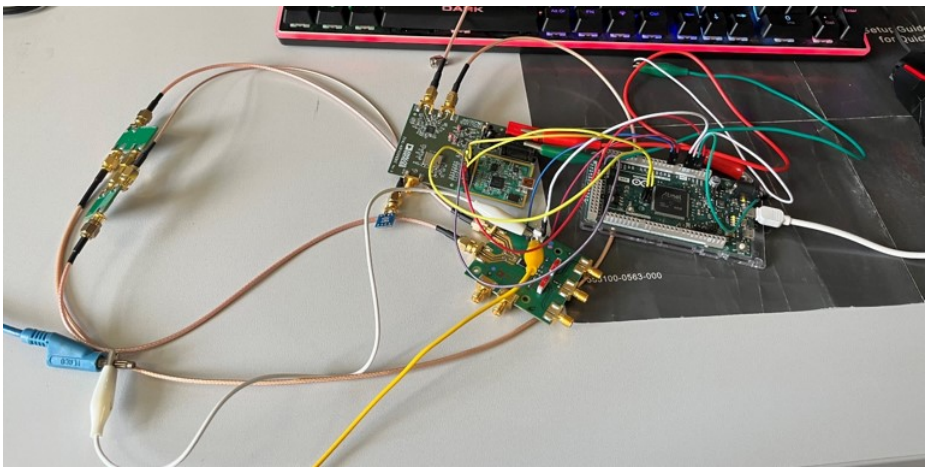

Figure 4.25. Set-up for measurements of the whole circuit with packed QCM.

The sweep took 35 seconds for one channel (only gain output or only phase output), and it has 8190 data points. Data were obtained through the serial port using Cool Term program in a text file. The data in the text file was graphed by MATLAB with a simple code as in Figure 4.26. (See Appendix D)

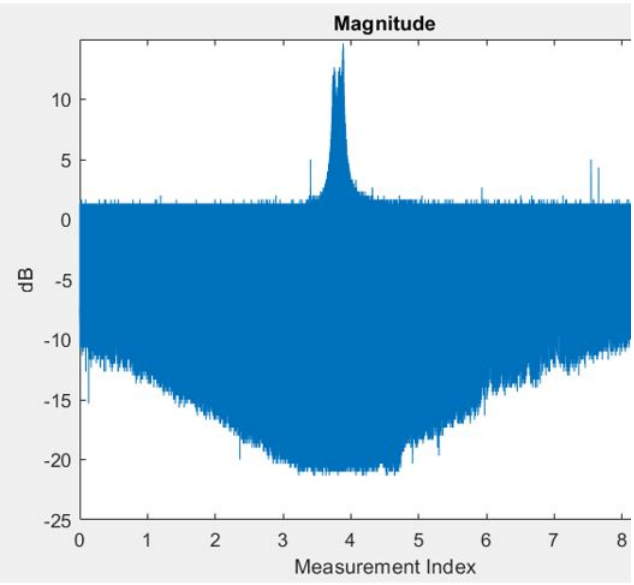

Figure 4.26. One sweep result of the gain output of AD8302.

Next, 10 sweeps were performed back-to-back, and the data from these sweeps were drawn over each other as in Figure 4.27.

In order to make ten back-to-back sweeps, the sweep loop of the Arduino code was set to 10 times and the MATLAB code was changed as well. (See Appendix E for MATLAB Code.) The total sweep took almost three and half minutes and it had 81900 data points.

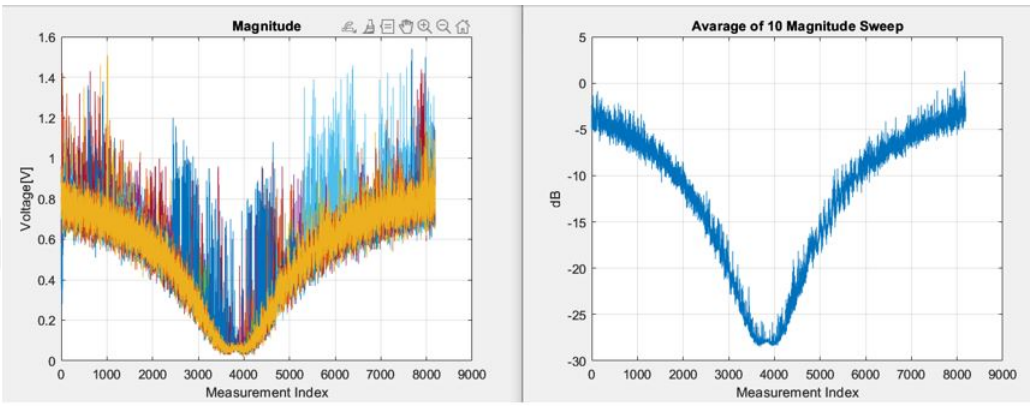

Figure 4.27. 10 sweeps result of gain output of AD8302.

After the results were evaluated, it was seen that doing ten sweeps back-to-back is better than making just one sweep. But comparing these ten sweeps with each other may not give us the perfect results due to the possibility of Arduino Due's ADC not measuring the output of the AD8302 exactly. (It can be seen on the left side of Figure 4.28.) Also, generating a different frequency for every point takes time. Taking multiple measurements at the same frequency is faster.

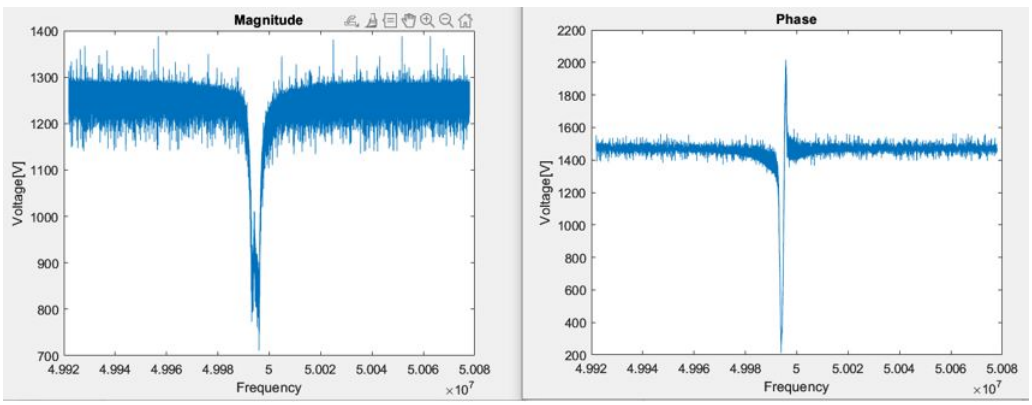

Figure 4.28. Raw data graphs of a sweep that takes eleven measurements at the same frequency.

In order to make more accurate measurements, it was decided to perform measurements 10 or 11 times without changing the frequency, then continue to the subsequent frequency, and do the sweep, in this manner.

To make this kind of a sweep, a few minor changes have been made in the Arduino code, and the MATLAB code was changed completely (See Appendix F). Arduino sends the data without converting it to voltage values and MATLAB draws magnitude and phase values at different graphs after converting it to voltage. Also, the MATLAB code takes the median of eleven values for magnitude and phase after discarding the first value of each eleven measurement because it is seen that ADC of Arduino Due does not measure correctly at the first of each measurement and this repeats itself with every new frequency. The frequency values are plotted on the x-axis.

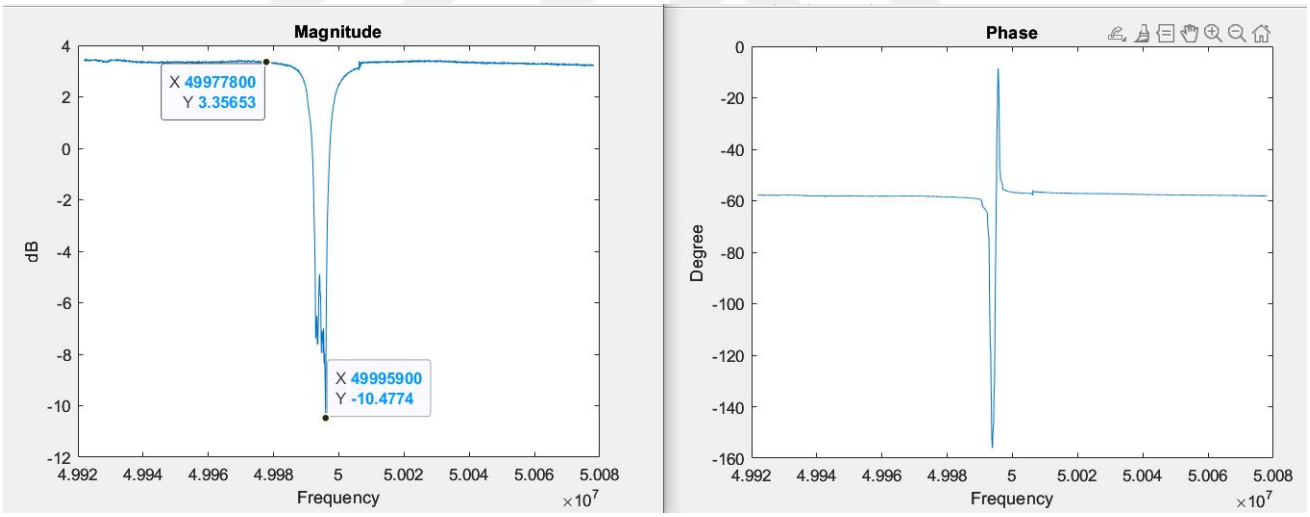

Figure 4.29. After the data of a sweep is processed (It is the same measurement in Figure 4.28. But this measurement is done after a few days).

This sweep took 3 minutes and 25 seconds and it has 90090 data points because eleven measurements of the same frequency were taken.

As can be seen from the results that are shown in Figures 4.28 and 4.29, taking eleven measurements at the same frequency, and getting the median of these values gives more accurate results and it makes the results less affected by noise.

Also packed QCM's dip magnitude was measured as 13.8339 dB at 49.995900 with the designed system. The VNA result was 13.1263 dB at 49.994519 MHz. QCM's resonance frequencies are not the same but they are remarkably close.

These differences can be due to the fact that the designed system has a 19 Hz resolution whereas the VNA resolution is 80 Hz for these sweeps.

4.6.2. Open QCM Measurements using The Designed Circuit

After observing good performance from the system, an open QCM has been measured with the same designed system (See Figure 4.31). The dip magnitude of the QCM was 10.69 dB at 50.1498 MHz. As seen in Figure 4.24, the measured dip magnitude was -4.8199 dB at 50.142939 with VNA.VNA measurement has a 50 Hz resolution, and the designed system has 19 Hz. The designed system was placed in a box to make sure the measurement was not affected by the environment. Any activity around the system was causing changes and noise in the data. The overall system with the box is depicted in Figure 4.30.

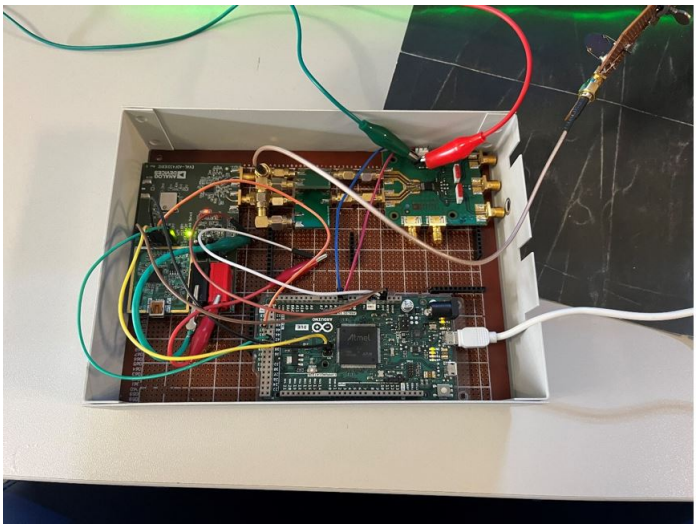

Figure 4.30. Designed system measurement set-up for measuring an open QCM.

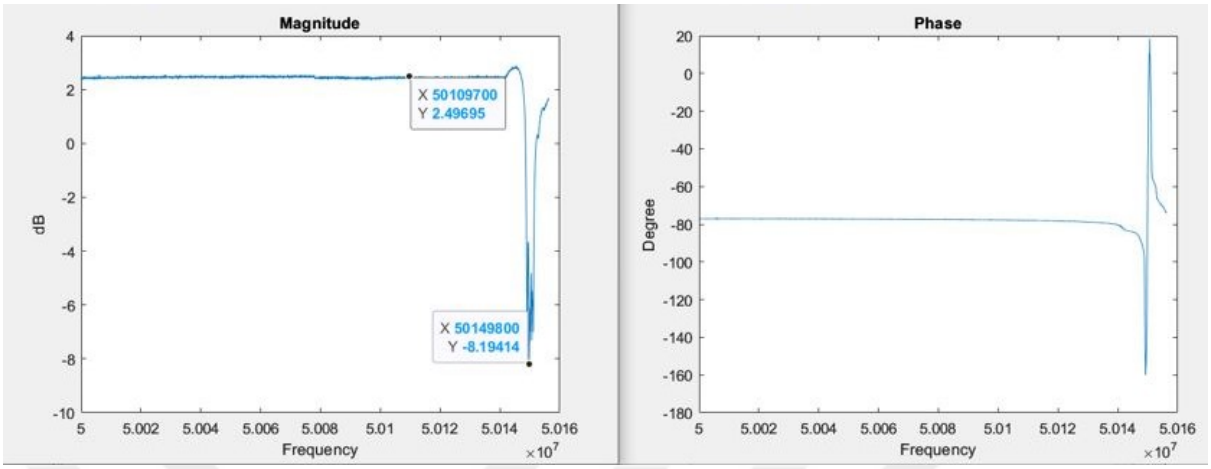

Figure 4.31. Open QCM designed system measurement results.

4.6.3. System Measurements using an Open QCM in Water

After getting reliable results, for the QCM in air, the performance of the open QCM in water was investigated. Only the open QCM was in water not the designed system. The AD8302 board was supplied with a 3.5V battery that has 900 mAh capacity. Figures 4.32 and Figure 4.33 depict the system.

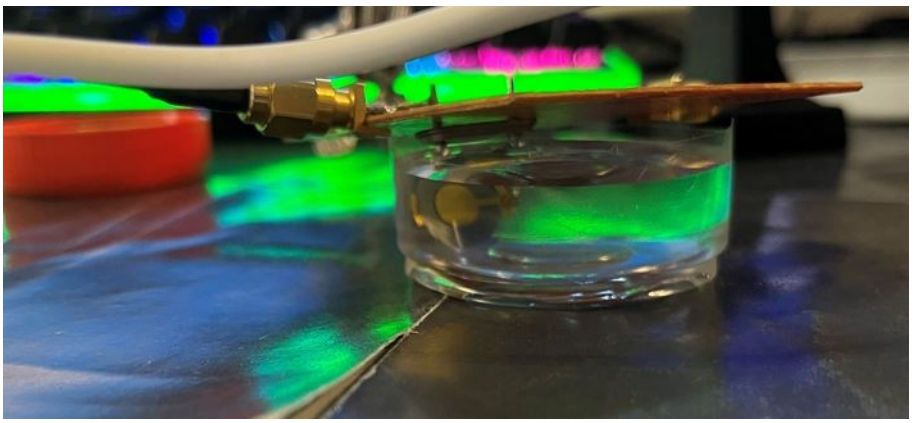

Figure 4.32. Open QCM is in the water.

In order to make a comparison with the performance of the QCM in air and in water, consecutive measurements were taken. Figure 4.34 shows the result in the air and Figure 4.35 shows the result in the water. Since the QCM was broken in the process, the measurements in the air and in the water correspond to different QCMs.

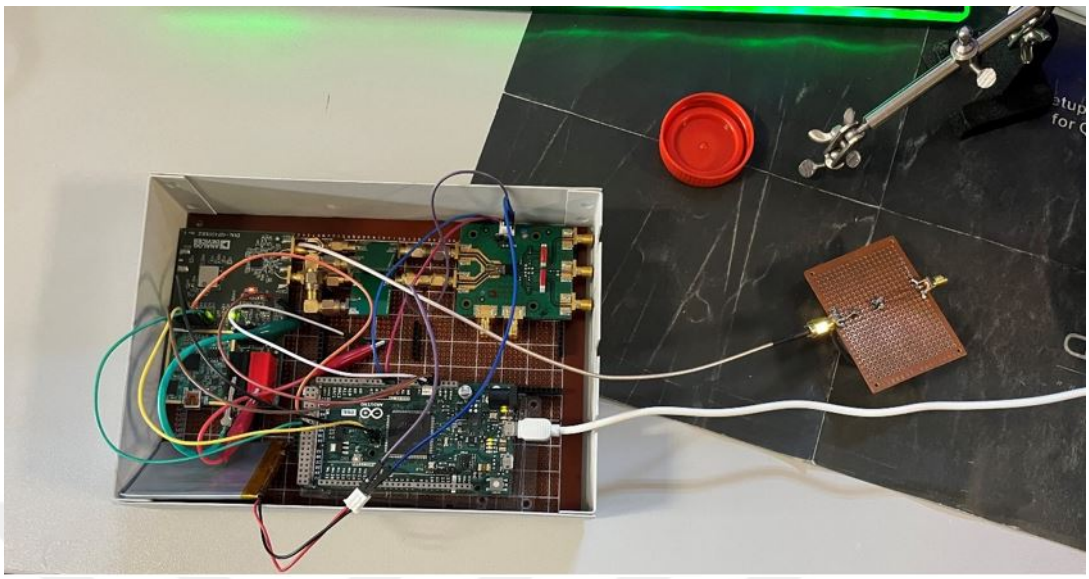

Figure 4.33. Designed system measurement set-up for measuring an open QCM when QCM is in the water.

Therefore, the resonance frequency and the dip magnitude are slightly different. Furthermore, VNA results are not available due to the accident with the QCM.

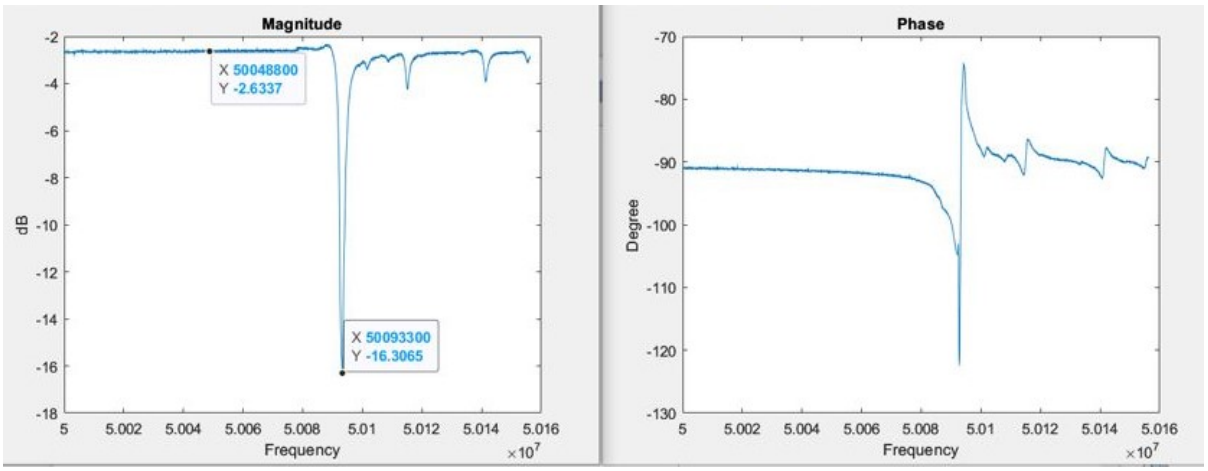

Figure 4.34. Open QCM designed system measurement results in the air.

As can be seen from the results, the designed system successfully measured the QCM's resonance frequency when it is in the water. It was expected to see a decrease in the resonance frequency since the QCM has different behavior in liquid. Results show that the frequency shift was 7.8 kHz.

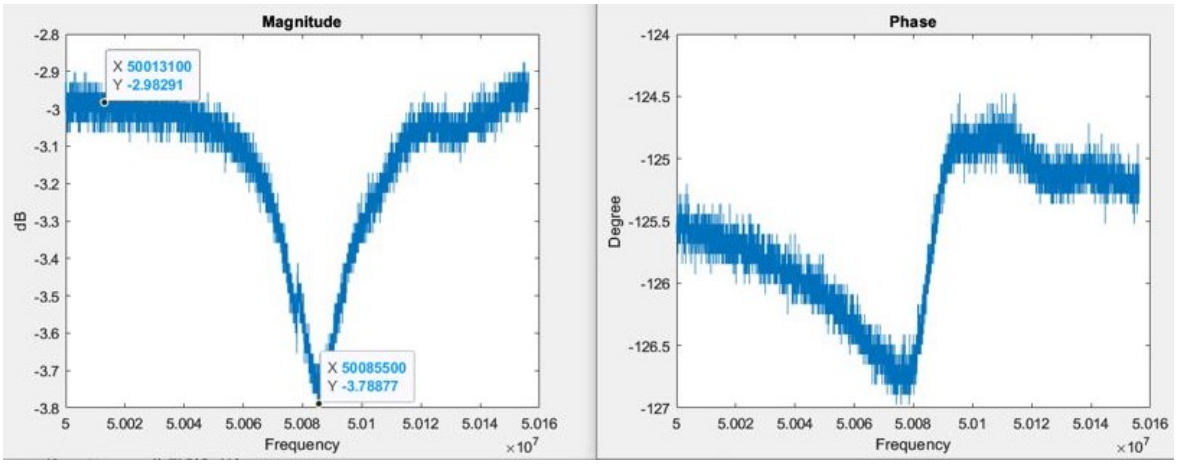

Figure 4.35. Designed system measurement results using an open QCM when it is in the water.

4.6.4. System Measurements using an Open QCM in a Flow Cell

After verifying that the designed system can measure QCM's behavior in liquid, an open QCM was measured without water and with water in a Flow cell. Then, the results were compared with each other. The results are provided in Figures 4.36 and 4.37.

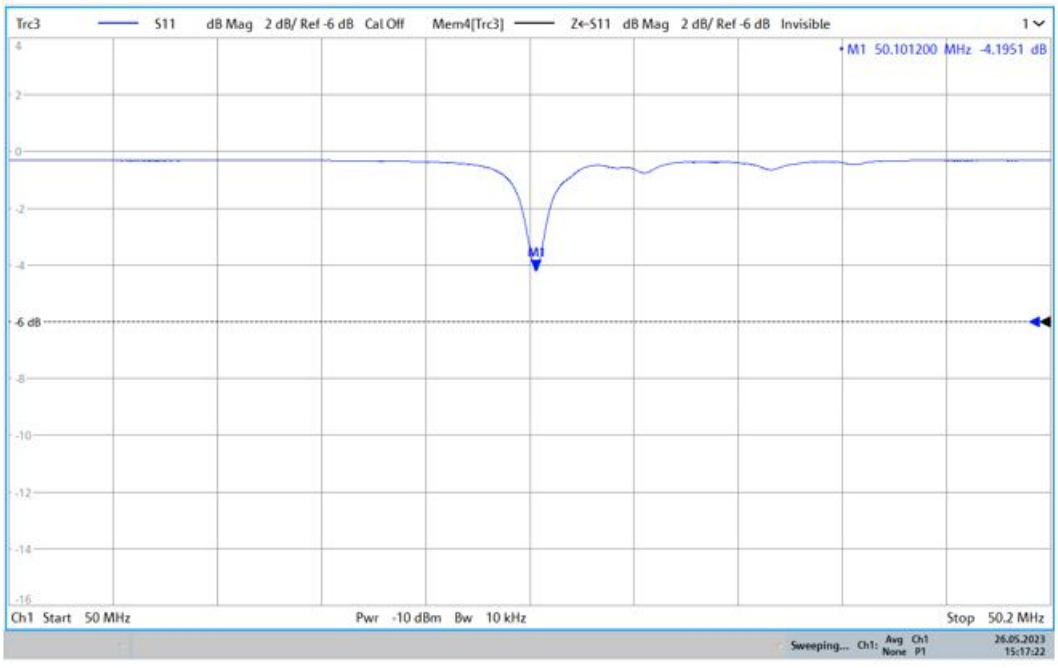

Figure 4.36. VNA measurement results for an open QCM in flow cell without water.

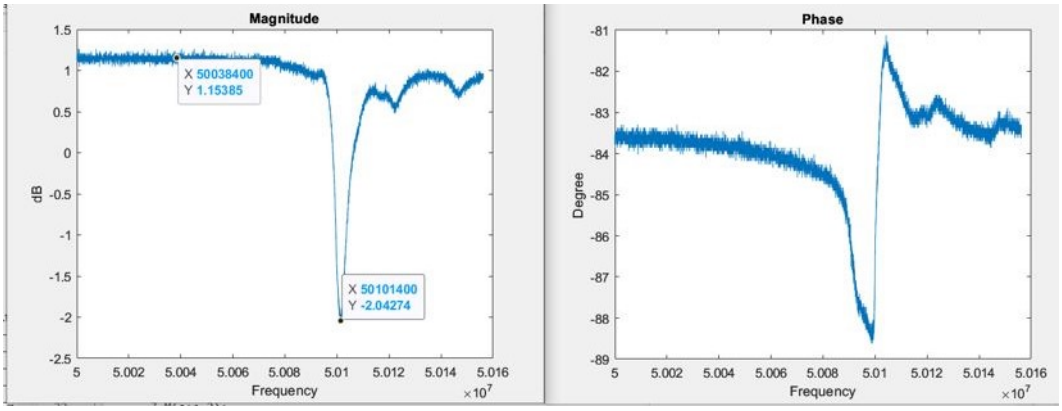

Figure 4.37. Designed system measurement results for an open QCM in flow cell without water.

Without adding any water to the flow cell, open QCM was measured with a VNA and the designed system. The results are remarkably similar. VNA measurement result shows that QCM's resonance frequency is at 50.101200 MHz, and it has 4.1951 dB of dip. The designed system measurement result shows that QCM's resonance frequency is at 50.101400 MHz and its dip magnitude is 3.19 dB. VNA measurement had a 40 Hz resolution, designed system measurement had a 19 Hz resolution. Measured resonance frequencies are almost the same, but magnitudes are different. The reason could be due to the resolution and impedance mismatches.

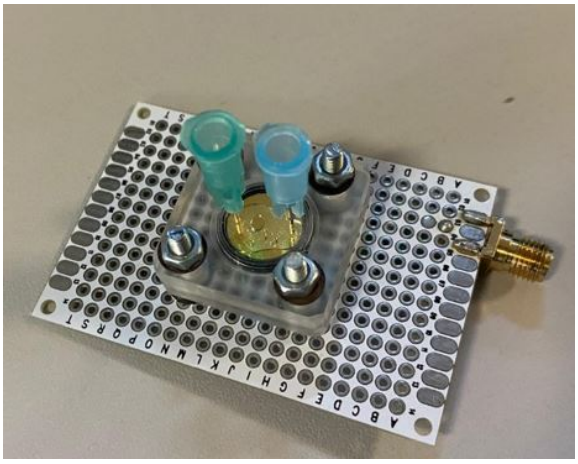

Figure 4.38. An open QCM in flow cell after a few drops of water added.

After a comparison of these measurement results, a few drops of water were added to the flow cell (Figure 4.38).

The measurements were repeated, and the results of these measurements are shown in Figure 4.39 and Figure 4.40.

As can be seen from the results, after adding water to the flow cell, the resonance frequency of the QCM shifted. According to the VNA measurements, the shift is 680 Hz, and the dip magnitude of the QCM is 1.9583 dB. According to the designed system, the frequency shift is 1 kHz, and the dip magnitude is 1.61 dB.

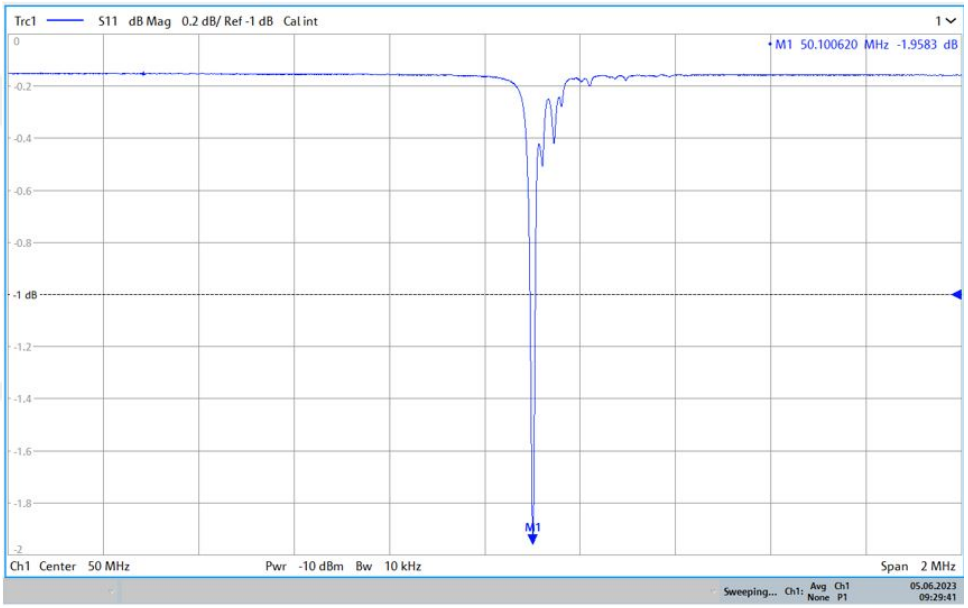

Figure 4.39. VNA measurement results for an open QCM in flow cell after water was added.

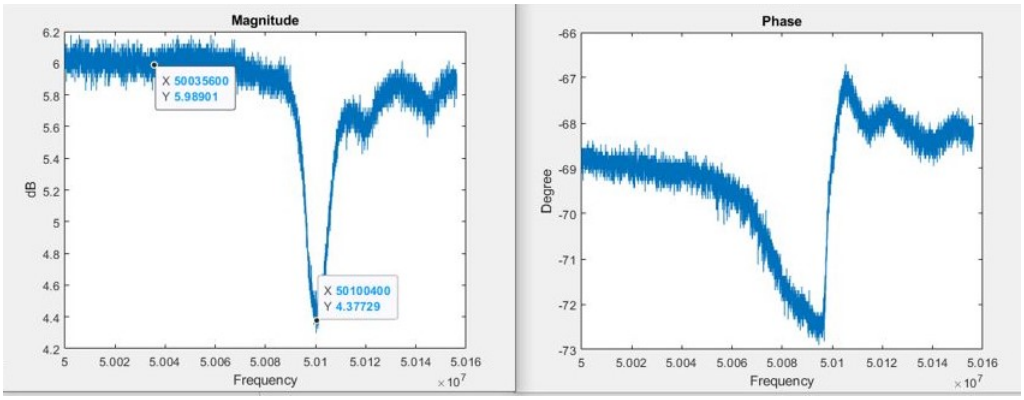

Figure 4.40. Designed system measurement results for an open QCM in flow cell after water was added.

4.6.5. System Measurements and Impedance Analyzer Measurements using an Open QCM in a Flow Cell

After verifying that the designed system can measure QCM's behavior in air and in water, a preliminary measurement was made to verify the system again when two sugar cubes were added to 100 ml of water. At the end of this measurement, the designed system is verified and another measurement was performed at Acıbadem University using an Impedance Analyzer.

An impedance analyzer is utilized for accurate impedance measurement of electronic components and circuits at a test frequency [30]. For this measurement, KEYSIGHT E4990A - Impedance Analyzer [31] was used with a MATLAB code. The flow cell in Figure 4.41 was used for these measurements.

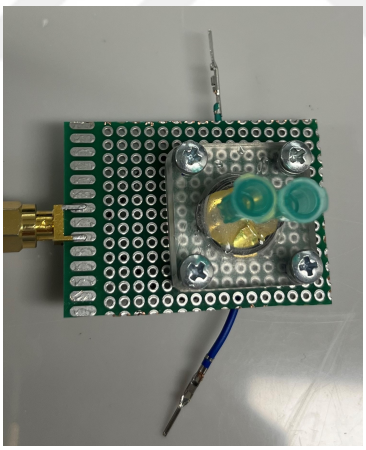

Figure 4.41. Flow Cell.

Measurements were taken 5 times with the designed system when the open QCM was in air, water, and water with 2 different concentrations of glycerol. Designed system's sweep frequency range narrowed to 78.1 kHz in order to shorten the sweep time for these measurements. Sweep's start frequency is 50.078144 MHz and stop frequency is 50.156250 MHz. Sweep time is 1 minute 20 seconds. Impedance analyzer measurements were also taken for all these measurements. Table 4.3 shows the properties of impedance analyzer measurements.

Table 4.3. Properties of impedance analyzer measurements.

When QCM was	Center Frequency(MHz)	Window Size(Hz)	Number of Points
In the air	50.000000	500000	1000
In the water	50.000000	500000	1000
In the 100 ml water after 1 ml glycerol was added	50.100000	500000	1000
In the 100 ml water after 3 ml glycerol was added	50.100000	500000	1000

After measuring the open QCM in the air, two cables are connected to the flow cell. The other side of these cables is in a becker to transport the liquid. Also, a peristaltic pump is used to drop the liquid on the open QCM every two seconds. Figure 4.42 shows the set-up when measuring the open QCM in water, 100 ml water with added 1 ml glycerol, and 100 ml water with added 3 ml glycerol. Table 4.4 shows the impedance analyzer measurement results. (See Appendix G for each measurement graph.)

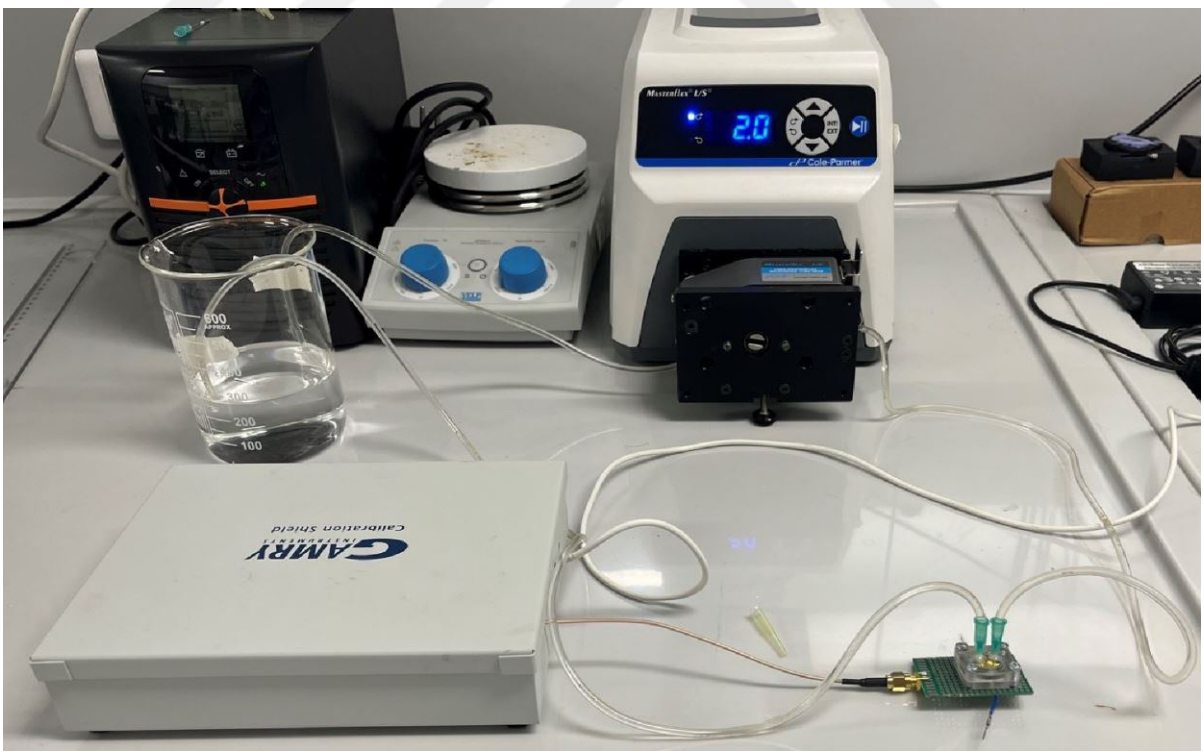

Figure 4.42. Measurement set-up.

Table 4.4. Impedance analyzer measurements results.

When QCM was	**Resonance Frequency(MHz)**
In the air	50.137400
In the water	50.133400
In the 100 ml water after 1 ml glycerol was added	50.133300
In the 100 ml water after 3 ml glycerol was added	50.133300

The designed system measurement results are shown in Figures 4.43, 4.44, 4.45, and 4.46 (See Appendix H for detailed measurement results.).

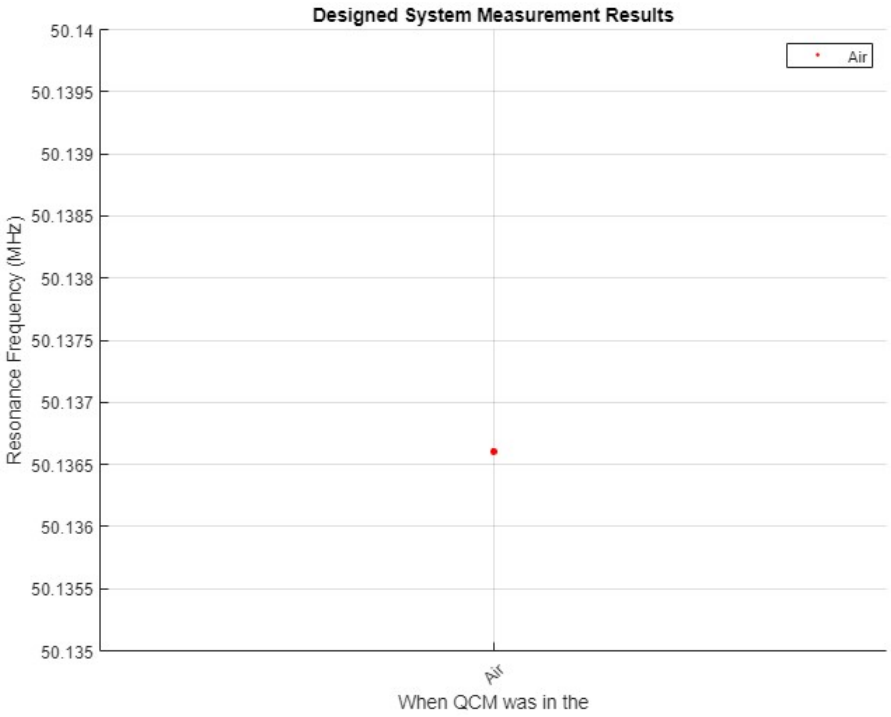

Figure 4.43. Designed system measurement results when QCM was in the air-resonance frequency.

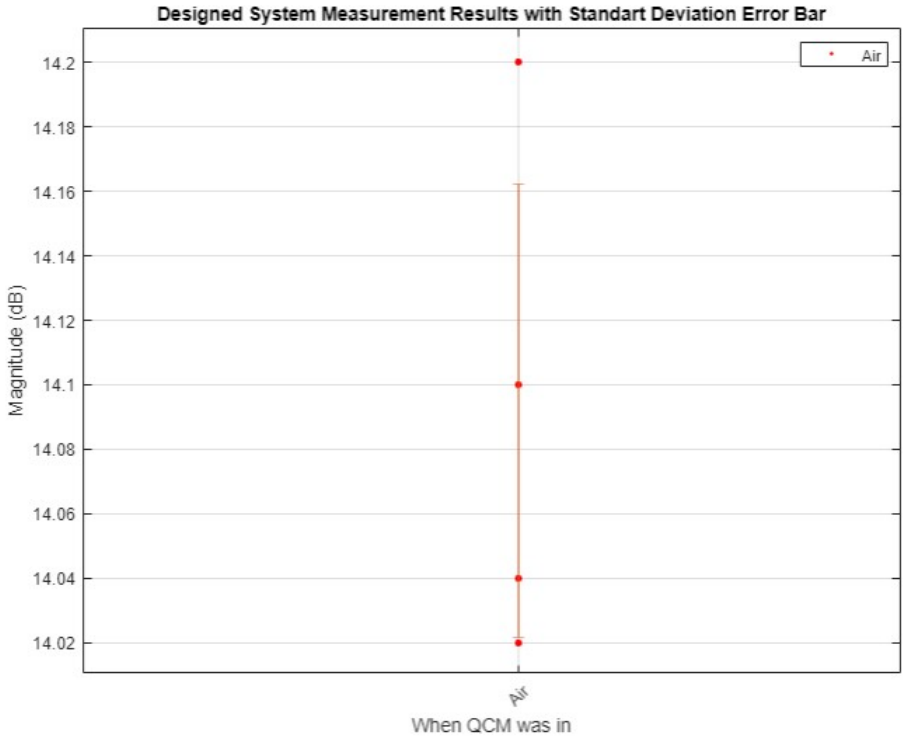

Figure 4.44. Designed system measurement results when QCM was in the air - dip magnitude.

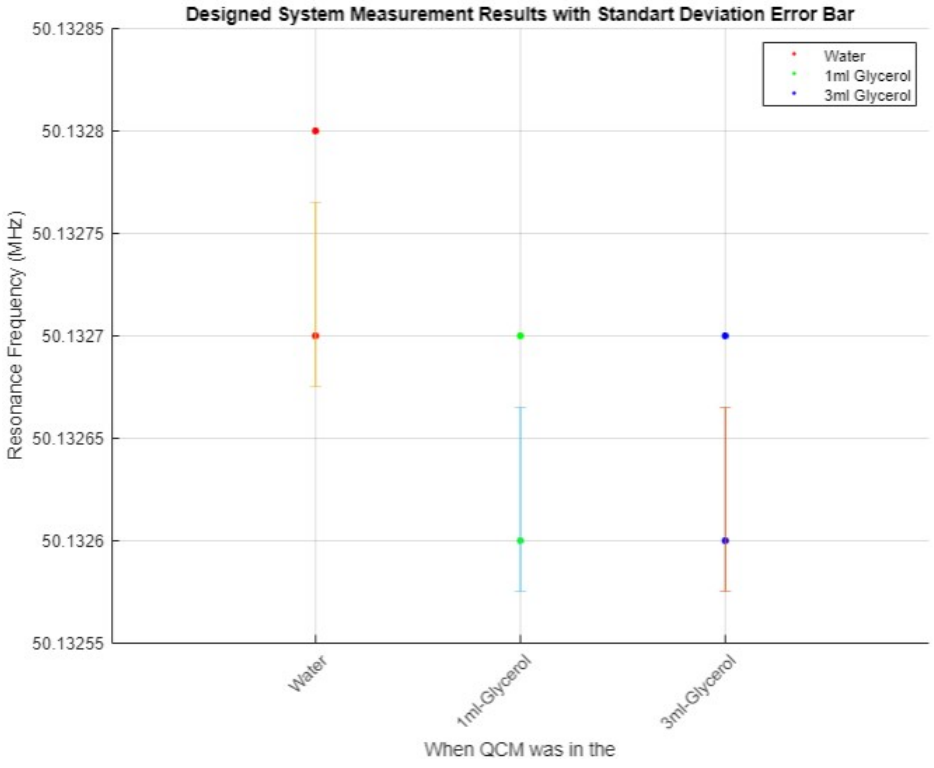

Figure 4.45. Designed system measurement results - resonance frequency.

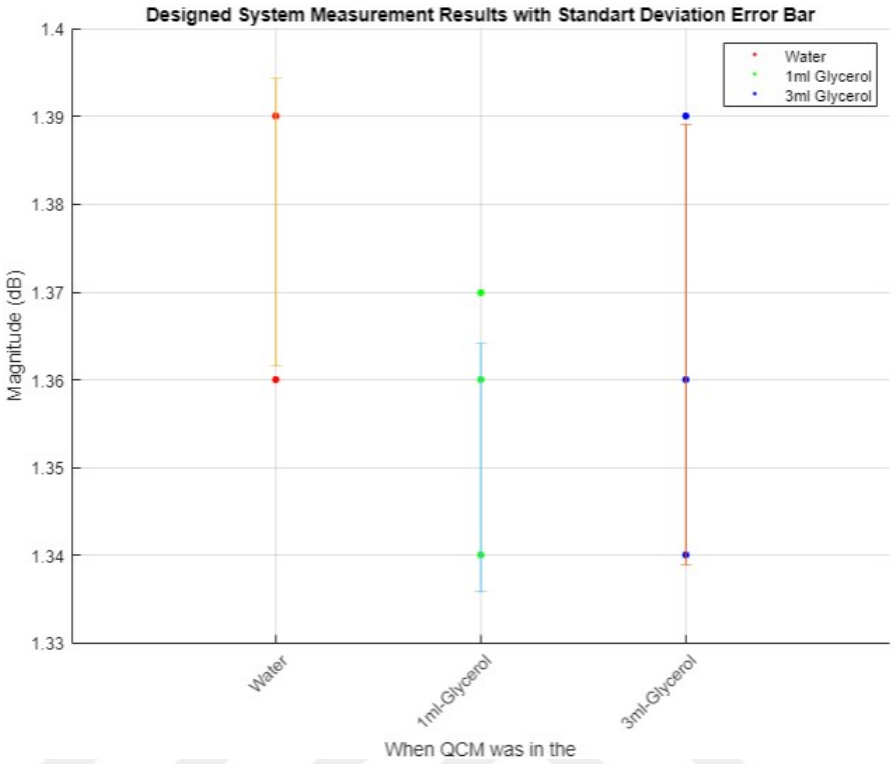

Figure 4.46. Designed system measurement results - dip magnitude.

Table 4.5. Frequency shift according to air.

	Impedance Analyzer	**Designed System**
Resonance Frequency in the air	50.137400	50.136600
Resonance Frequency in water	50.133400	50.132700
Frequency Shift	4 kHz	3.9 kHz

Table 4.6. Frequency shift according to water.

	Impedance Analyzer	**Designed System**
Resonance Frequency in water	50.133400	50.132700
Resonance Frequency in water after 1ml glycerol added	50.133300	50.132600
Resonance Frequency in water after 3ml glycerol added	50.133300	50.132600
Frequency Shift	100 Hz	100 Hz

Tables 4.5 and 4.6 show the frequency shifts for each condition. The resonance frequency values in the tables are median of 5 measurements back to back for designed system.As can be seen from the measurement results designed system success-

fully measured the resonance frequency of the open QCM in air and in water even though different quantities of glycerol were added to the water. Also, it can be seen from the results of these measurements that the designed system measurement results are reliable, repeatable, and not based on chance.

5. ALTERNATIVE SYSTEM DESIGN

After having conducted the board measurements described in Chapter 4, a decision was made to develop an alternative system in case the resolution proved to be insufficient when attempting to control the evaluation board of ADF4351 with the Arduino Due board and sweep it across the desired frequency range. This alternative system's Arduino Due code, MATLAB code, and ADF4351 modifications were made by Can Ervakit and Buğra Selim Bulut who were bachelor students while the work was being performed. The idea is to control the reference frequency of the ADF4351 PLL with a Direct Digital Synthesizer (DDS) (AD9850). Thus, this system is a DDS-controlled PLL (DDS-PLL). The block diagram of the DDS-PLL is shown in Figure 5.1.

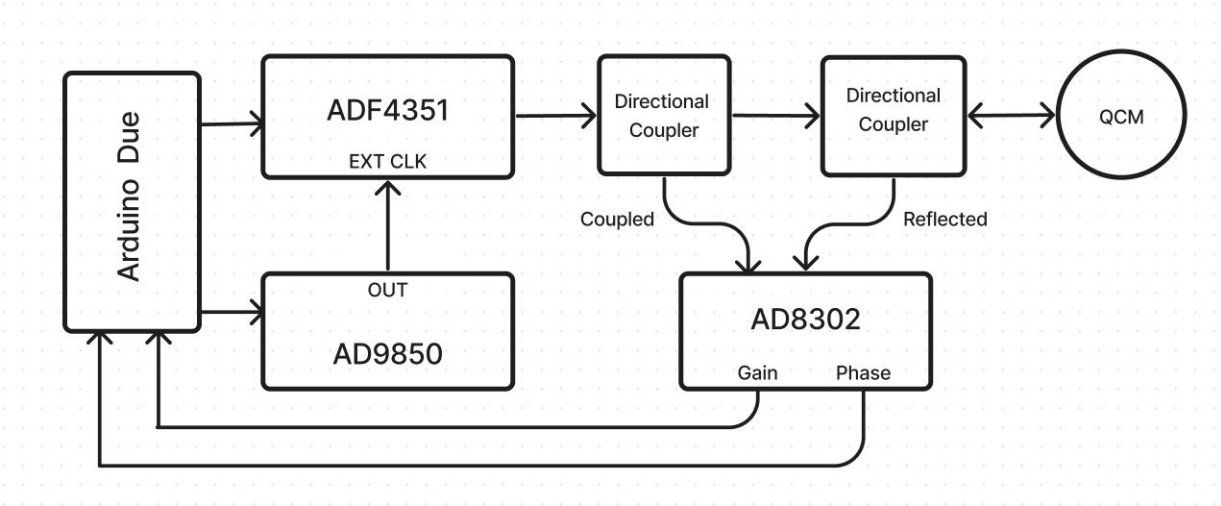

Figure 5.1. Block diagram of alternative system.

5.1. DDS-PLL Components and Methods

The alternative system also uses QCM. AD8302 and couplers are used in the same way as in the previous system. A DDS was used as an external clock for ADF4351, and the ADF4351 was modified so that the board could use the external clock.

5.1.1. DDS (Direct Digital Synthesizer)

Direct digital synthesis is a method of producing an analog waveform that is mostly sine or square-shaped [32]. But a DDS can generate triangular signals as well. A DDS has a phase accumulator, a phase-to-amplitude converter, and a DAC as shown in Figure 5.2 [33].

A DDS produces a sine wave at a specific frequency determined by two variables, the reference clock frequency and the binary number programmed into the frequency register.

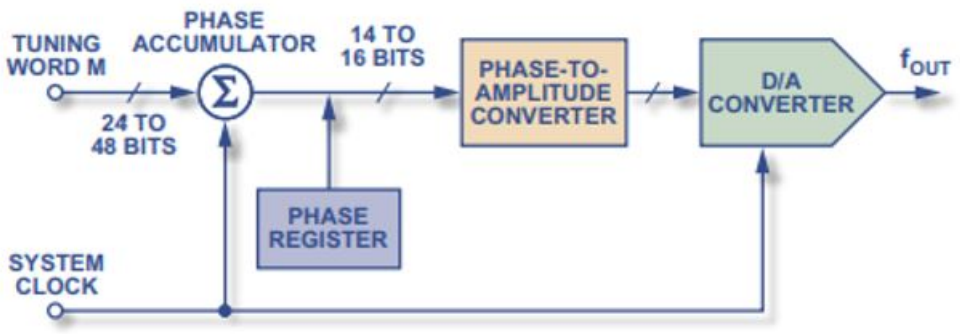

Figure 5.2. Simplified block diagram of the direct digital synthesizer [33].

The primary input to the phase accumulator is a binary number from the frequency register. In the case of a sine look-up table, the phase accumulator determines the phase (angle) address for the look-up table, which then sends the digital value of the amplitude—which corresponds to the sine of that phase angle—to the DAC. The DAC then translates that quantity into a corresponding analog voltage or current value. The phase increment, which is determined by the binary number, is added to the phase accumulator with each clock cycle to produce a fixed-frequency sine wave.

5.1.2. AD9850

The AD 9850 is a digital synthesis waveform generator that can generate sine and square waveforms with high resolution and low phase noise [34]. The internal crystal of the board operates at 125MHz. The output frequency of the AD9850 is around 50 MHz. The circuit architecture of the AD9850 allows to generate output frequencies up to half the reference clock (or 62.5 MHz) and output frequencies can be digitally (asynchronously) changed at a rate of up to 23 million frequency points per second.

In the alternative system, AD9850 is used to generate a frequency, which is applied to the evaluation board of ADF4351 as an external clock.

To control the AD9850 board, an Arduino code is needed. Programming of the AD 9850 is pretty simple since the card is operated by 4 data pins and a 5V power supply (See Figure 5.3).

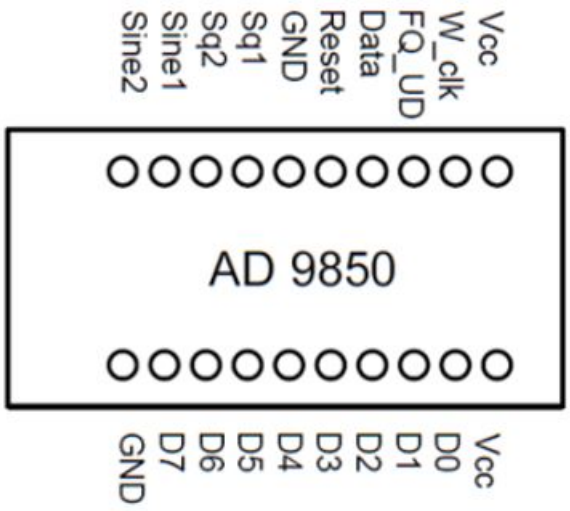

Figure 5.3. Pin diagram of AD9850.

W_{clk} pin is used for data synchronization between Arduino DUE and AD 9850. The data pin is for the initial setup of the AD 9850 and reset is used to return to initial settings. FQ UD pin stands for frequency update and this pin is used to sweep

the output frequency. Sq pins are for square wave output. Two pins have 90° phase difference between them. AD 9850 provides clear square waves up to 1 MHz. After 1 MHz, the waveform starts to change dramatically. For 20 MHz output, it is impossible to use a square wave. Sine pins can produce clear sine waves up to 35 MHz. Since the necessary frequency is 20 MHz, sine1 pin is used.

5.1.3. ADF4351

ADF4351 is a programmable frequency synthesizer that can generate a frequency output from 35 MHz to 4.4 GHz.

ADF 4351 has an internal crystal with 25 MHz operating frequency. It uses this clock to generate frequency. Since it's taught that the resolution would not be sufficient, it is decided to reduce this reference clock's value to have desired resolution. To be able to do that AD9850 is used as an external clock.

Evaluation board of ADF4351 has an external clock input that can be used by simply removing a 0-ohm resistor that connects crystal to the input of VCO. For alternative system, an external clock, which is provided by AD 9850, with 20 MHz frequency is used to run ADF 4351.

5.1.4. Controlling The Alternative System Design with Arduino DUE

The Arduino code in Appendix B is improved to control AD9850 by performing the necessary changes. (See Appendix I for Arduino code of this system, see Appendix J for MATLAB code for this system.) SPI (Serial Peripheral Interface) is used for data transmission and the baud rate is set to 115200 (See Figure 5.4 for connections that are being used in Arduino Due for this system).

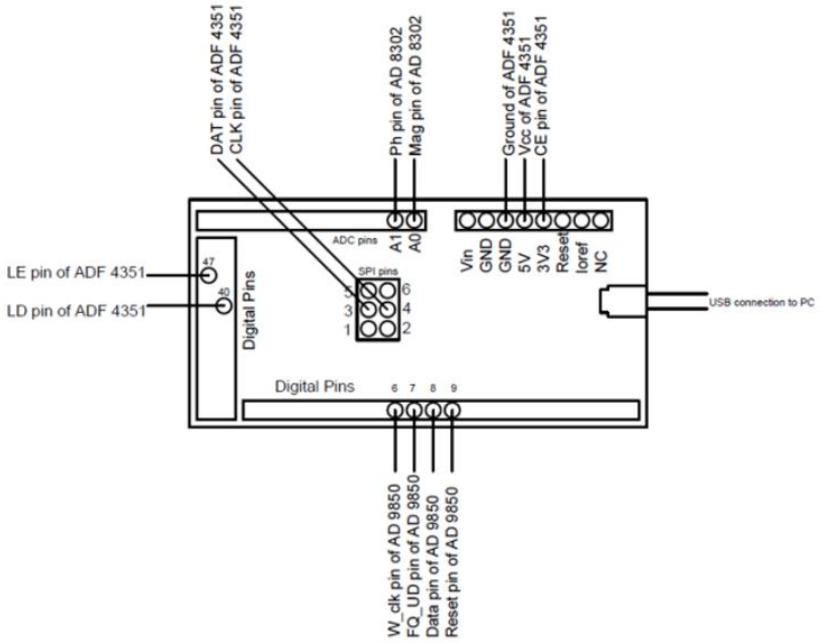

Figure 5.4. Arduino Due connections that are being used in DDS-PLL system.

5.2. Measurements of QCM's with Alternative System Design

This system has a 17.5 Hz resolution. But it can be programmed to increase the value of resolution or decrease the value of resolution down to 2.5 Hz. One measurement took almost 210 s. This value of resolution has been chosen due to the trade-off between resolution and measurement time.

To compare the DDS-PLL system measurement results with the original system design measurement results, the same QCM's as in Chapter 4 have been used in the measurements.

Also, when this system was assembled, different Evaluation Boards for AD8302 and ADF4351 were used. Before doing measurements, each component was tested separately as described in Chapter 4, and proper operation was observed.

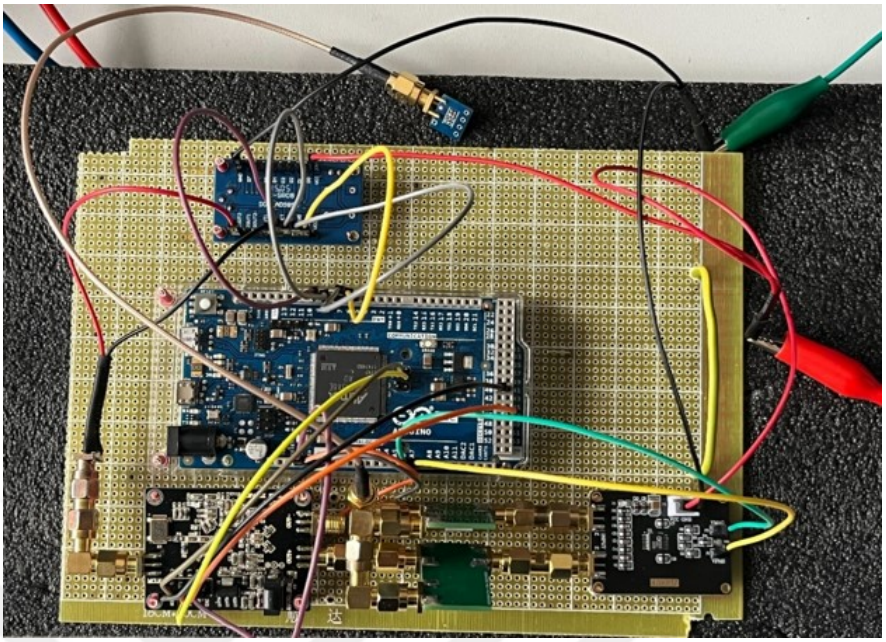

Figure 5.5. Set-up for measurement of alternative system design with packed QCM.

Packed QCM from Figure 4.20 was used. Initially, the set-up for this measurement can be seen in Figure 5.5. The resonance frequency of packed QCM was measured as 49.996100 and its dip magnitude was 12.75 dB as shown in Figure 5.6.

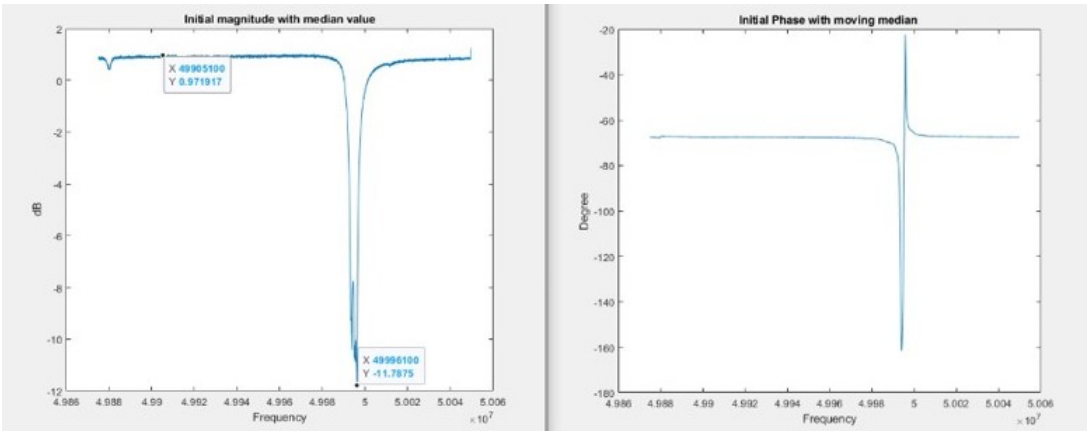

Figure 5.6. Measurement result of alternative system design with packed QCM.

The measurement results for packed QCM with VNA, designed system and alternative system are shown in Table 5.1.

Table 5.1. Measurement results for packed QCM.

	VNA	**Original System**	**DDS-PLL System**
The Resonance Frequency	49.994519 MHz	49.995900 MHz	49.996100 MHz
Dip Magnitude	13.1263 dB	13.8339 dB	12.759417 dB

Then an Open QCM from Figure 4.22 is used for measurements. The measurement set-up is shown in Figure 5.7.

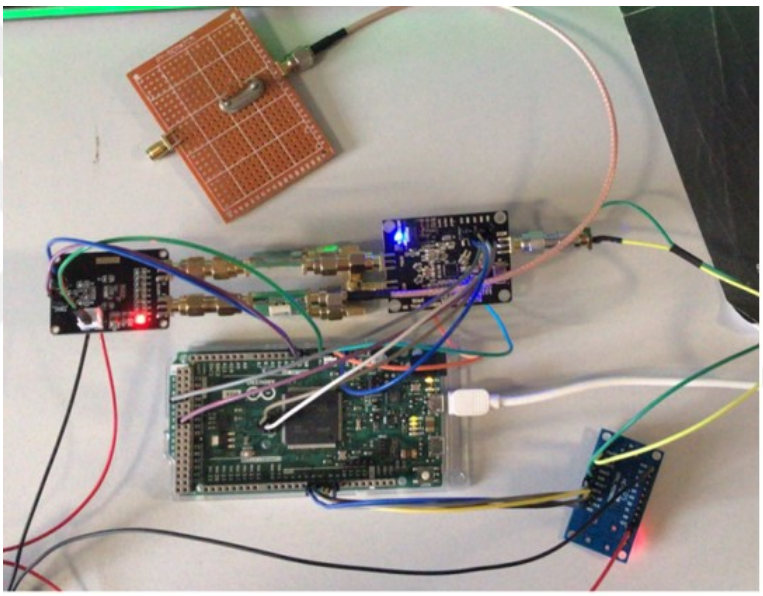

Figure 5.7. Set-up for measurement of alternative system design with an open QCM.

The Open QCM's resonance frequency was measured as 50.149400 MHz, and its dip magnitude was 10.422454 dB with the alternative system design as shown in Figure 5.8. The open QCM measurement results with VNA, designed system, and alternative system are shown in Table 5.2.

Table 5.2. Measurement results for the open QCM.

	VNA	**Original System**	**DDS-PLL System**
The Resonance Frequency	50.142939 MHz	50.14980 MHz	50.14940 MHz
Dip Magnitude	4.81 dB	10.69 dB	10.42 dB

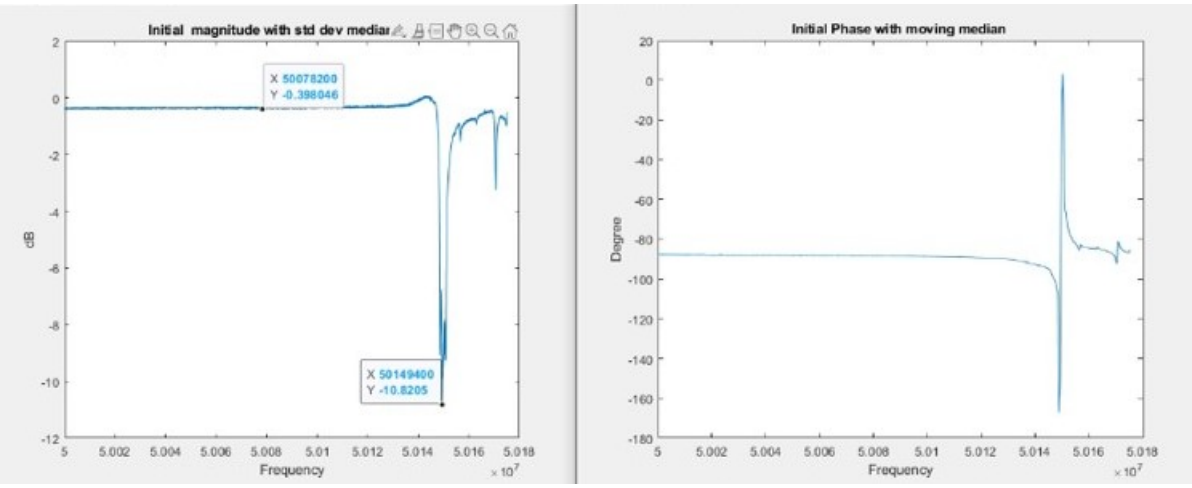

Figure 5.8. Measurement result of alternative system design for an open QCM.

5.2.1. Measurements of an Open QCM with Alternative System Design in Water

After getting reliable results, the resonance frequency of an open QCM and its response when it is in the water was measured.

In order to make a comparison with the measurement results of the QCM, first an open QCM was measured in air, then in water as in Chapter 4. Figure 5.9 shows the result in air and Figure 5.10 shows the result in water.

The Open QCM's resonance frequency was measured as 50.093000 MHz and its dip magnitude was 13.135 dB, as in Figure 5.9, with the alternative system design. The original system design measured this QCM's resonance frequency as 50.093300 MHz and its dip magnitude as 13.4313 dB (See Figure 4.37). This is a different QCM from the previous one. Thus, it has a different resonance frequency and a different dip magnitude. Unfortunately, this QCM was also broken, thus VNA measurements could not be performed.

As can be seen from the results (Figures 5.9 and 5.10), the alternative system design successfully measured the resonance frequency of the QCM when it is in water. It was expected to observe a decrease in the resonance frequency since the QCM has

a different behavior in liquid. Results show that the frequency shift was 7.6 KHz. The resonance frequency of the QCM was measured as 50.085700 MHz and its dip magnitude was 1.548 dB.

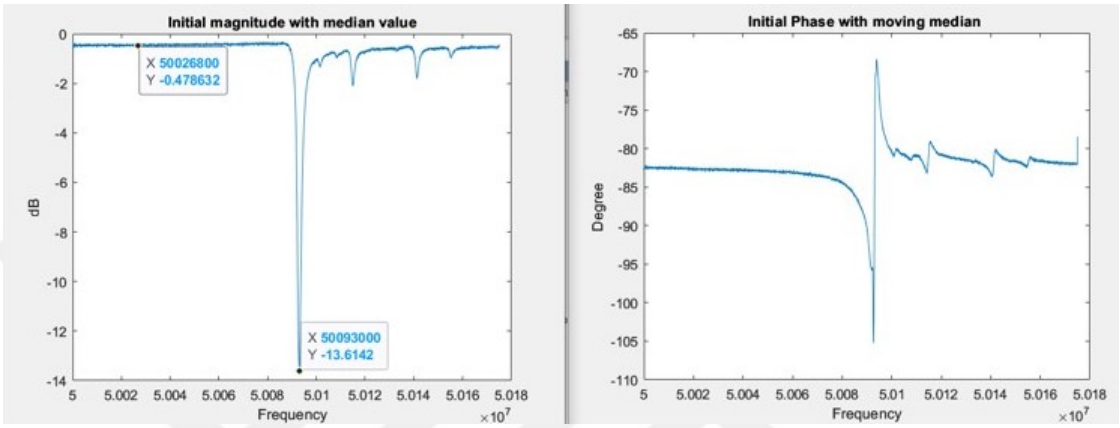

Figure 5.9. Measurement result of alternative system design with an open QCM in the air.

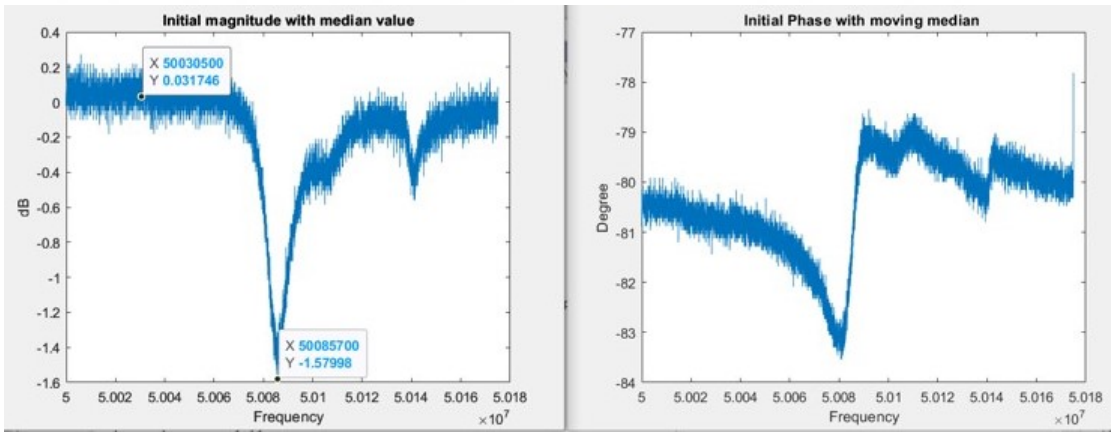

Figure 5.10. Measurement result of alternative system design with an open QCM when it is in the water.

Table 5.3. Measurement results for the open QCM in the water.

	Original System	**DDS-PLL System**
The Resonance Frequency	50.085500 MHz	50.085700 MHz
Dip Magnitude	0.80506 dB	1.548 dB
The Frequency Shift	7.8 kHz	7.6 kHz

The DDS-PLL system design had a better result when the QCM was in water. It can be due to the slightly lower resolution (17.5 Hz) versus the original system.

5.2.2. Alternative System Measurements using an Open QCM in a Flow Cell

After confirming that the alternative system can measure the behavior of the QCM in liquid, an open QCM in a Flow cell was measured without water and with water. Then, the results were compared with each other. Figure 4.38 depicts an open QCM in the Flow Cell after adding water.

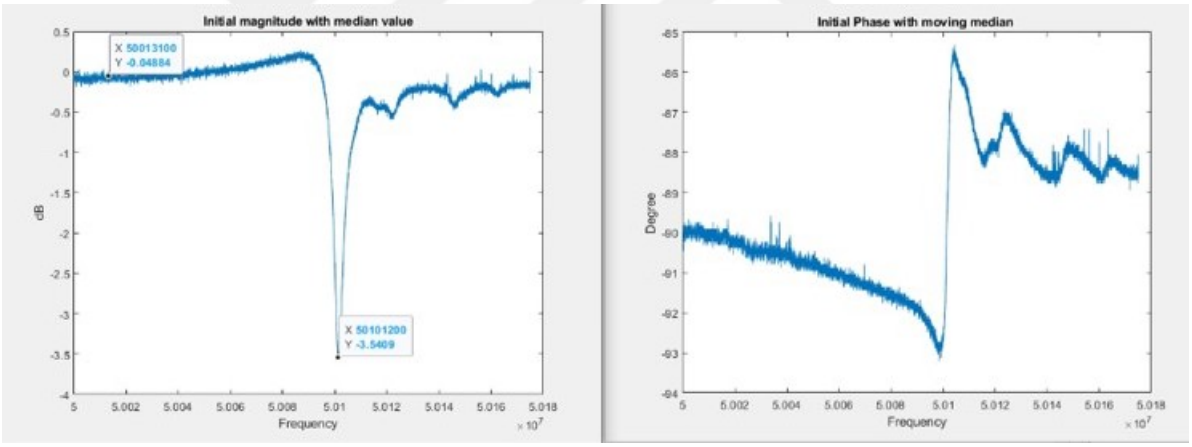

Figure 5.11. Alternative system design measurement results for an open QCM in flow cell before water was added.

Without adding any water to the flow cell, the open QCM was measured with VNA and both of the designed systems. As can be seen from Table 5.4, they are remarkably similar for resonance frequency.

It can be observed that the measured resonance frequencies are almost the same, but the magnitudes are different. The reason could be resolution differences between the systems, or it can be related to matching.

Table 5.4. Measurement results for the open QCM in a flow cell.

	VNA	**Original System**	**DDS-PLL System**
The Resonance Frequency	50.101200 MHz	50.101400 MHz	50.101200 MHz
Dip Magnitude	4.19 dB	3.19 dB	3.49 dB
Resolution	40 Hz	19 Hz	17 Hz

After a comparison of these measurement results, water was added to the flow cell, a few drops of water were in the flow cell as shown in Figure 4.38, and measurements were repeated.

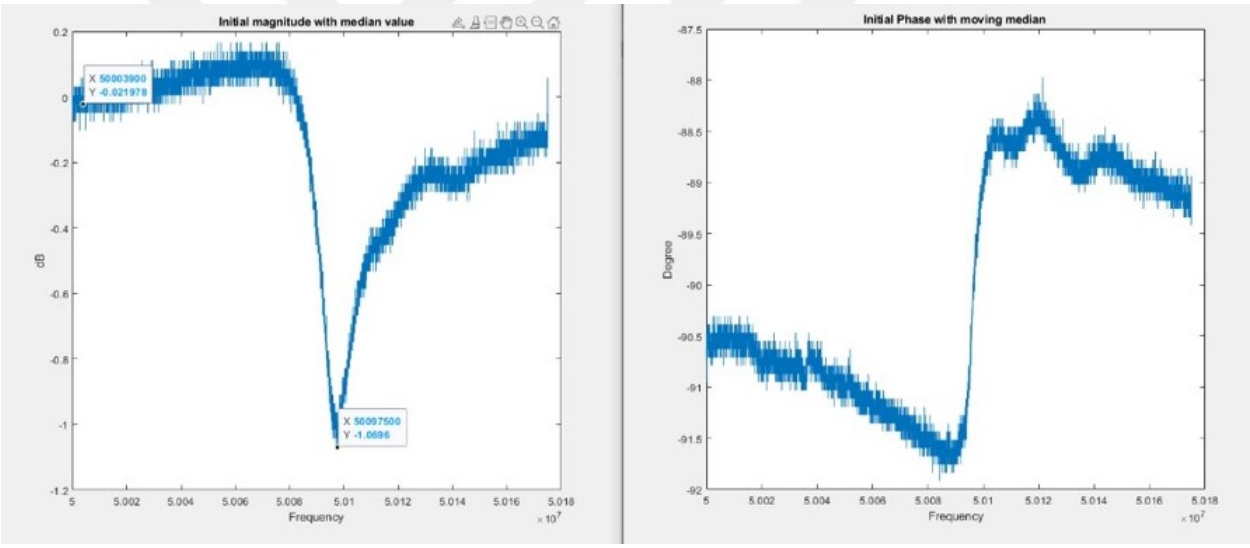

Figure 5.12. Alternative system design measurement results for an open QCM in flow cell after water was added.

As can be seen from Table 5.5, after adding water to the flow cell the resonance frequency of the QCM shifted.

Table 5.5. Measurement results for the open QCM in a flow cell after water added.

	VNA	**Original System**	**DDS-PLL System**
Resonance Frequency	50.100620 MHz	50.100400 MHz	50.09750 MHz
Dip Magnitude	1.9583 dB	1.61 dB	1.0476 dB
Frequency Shift	680 Hz	1 kHz	3.7 kHz

5.2.3. Measurements of Alternative System and Impedance Analyzer using an Open QCM in a Flow Cell

After verifying that the DDS-PLL system can measure QCM's behavior in air and in water, a preliminary measurement was made to verify the system again when two sugar cubes were added to 100 ml of water. At the end of this measurement, the DDS-PLL system is verified and another measurement was performed at Acıbadem University using an Impedance Analyzer. The flow cell in Figure 4.41 was used for these measurements.

Measurements were taken 5 times with the DDS-PLL system when the open QCM was in air, water, and water with 2 different concentrations of glycerol. The DDS-PLL system's sweep frequency range was narrowed to 87.5 kHz in order to shorten the sweep time for these measurements. Sweep's start frequency is 50.062512 MHz and stop frequency is 50.150084 MHz. Sweep time is 1 minute 40 seconds. Impedance analyzer measurements were also taken for all these measurements. The properties of impedance analyzer measurements and the results of these measurements are the same in Tables 4.3 and 4.4.

The same set-up was used in Figure 4.42 for measuring the open QCM in water, 100 ml water with added 1 ml glycerol, and 100 ml water with added 3 ml glycerol.

The DDS-PLL system measurement results are shown in Figures 5.13, 5.14,5.15, and 5.16 (See Appendix K for detailed measurement results).

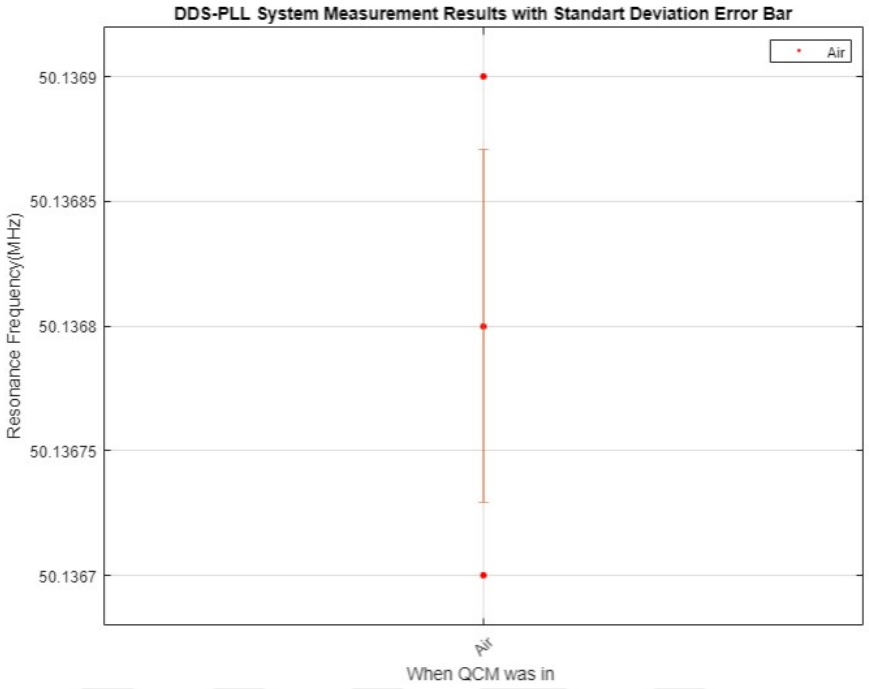

Figure 5.13. DDS-PLL system measurement results when QCM was in the air-resonance frequency.

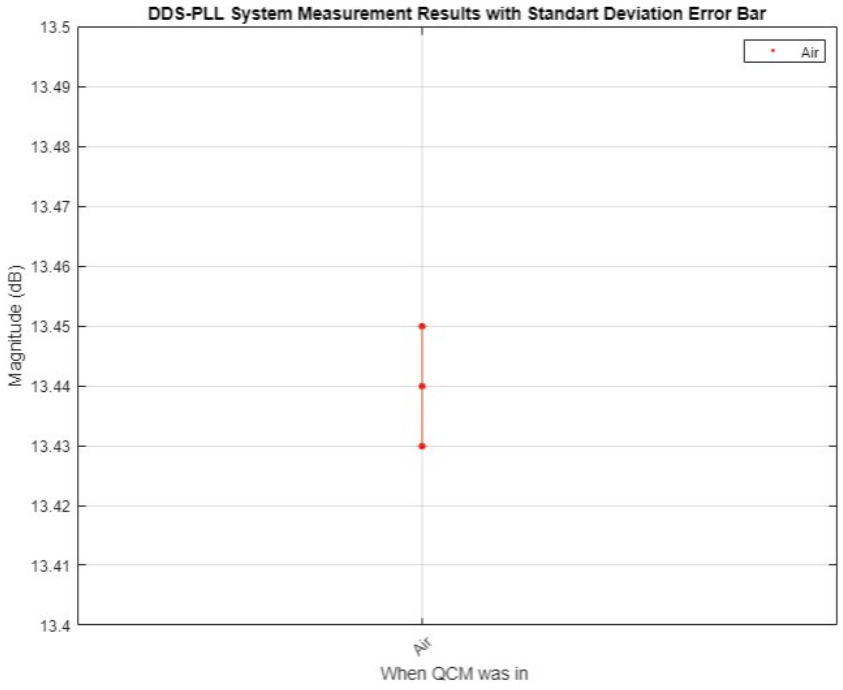

Figure 5.14. DDS-PLL system measurement results when QCM was in the air - dip magnitude.

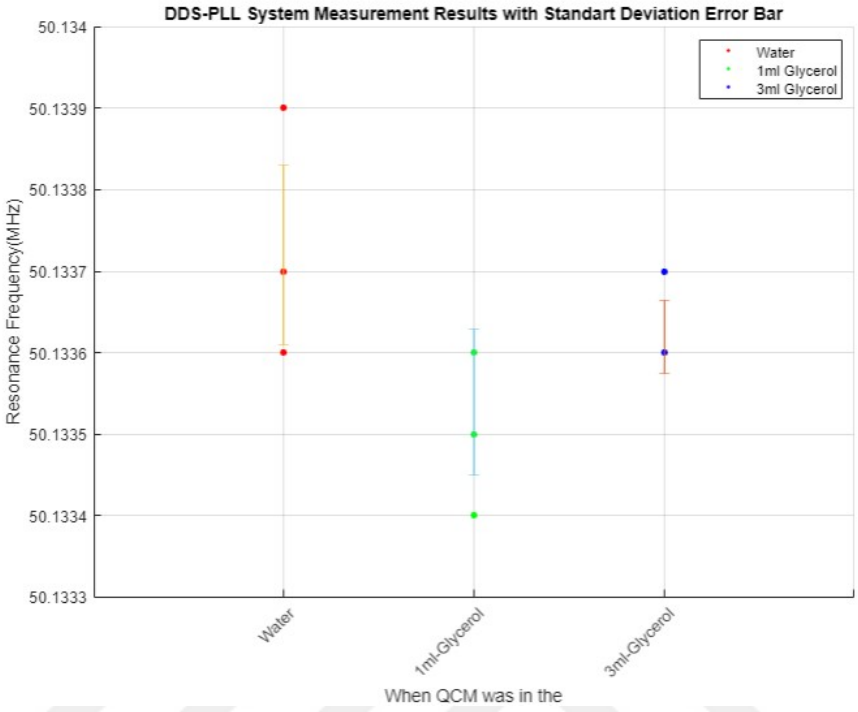

Figure 5.15. DDS-PLL system measurement results - resonance frequency.

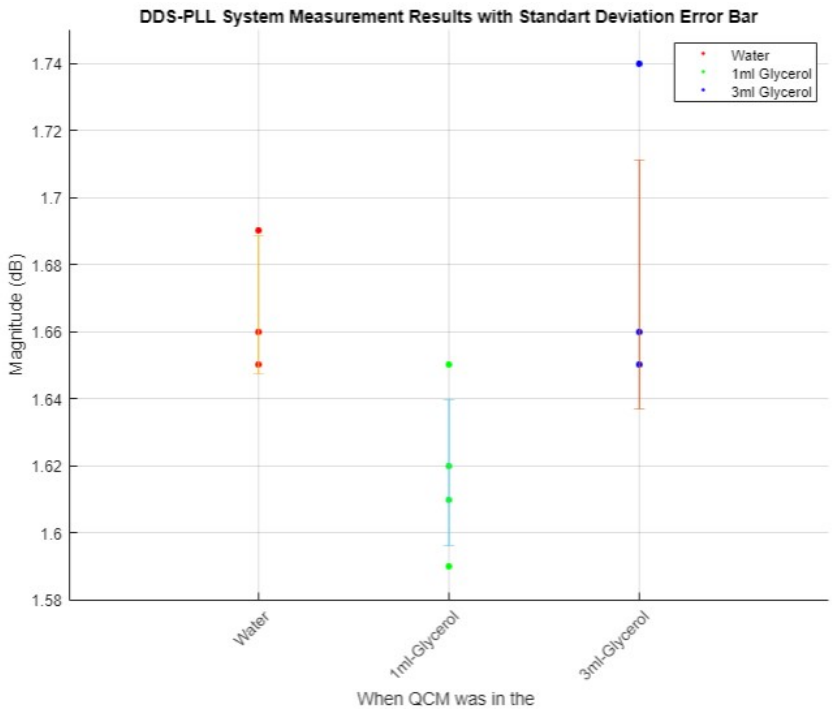

Figure 5.16. DDS-PLL system measurement results - dip magnitude.

Table 5.6. Frequency shift according to air.

	Impedance Analyzer	**Designed System**	**DDS-PLL System**
Resonance Frequency in the air	50.137400	50.136600	50.136800
Resonance Frequency in water	50.133400	50.132700	50.133700
Frequency Shift	4 kHz	3.9 kHz	3.1 kHz

Table 5.7. Frequency shift according to water.

	Impedance Analyzer	**Designed System**	**DDS-PLL System**
Resonance Frequency in water	50.133400	50.132700	50.133700
Resonance Frequency in water after 1ml glycerol added	50.133300	50.132600	50.133600
Resonance Frequency in water after 3ml glycerol added	50.133300	50.132600	50.133600
Frequency Shift	100 Hz	100 Hz	100 Hz

Tables 5.6 and 5.7 shows the frequency shifts for each condition. The resonance frequency values in the tables are median of 5 measurements back to back for designed system and DDS-PLL system. As can be seen from the measurement results DDS-PLL system successfully measured the resonance frequency of the open QCM in air and in water even though different quantities of glycerol were added to the water. Also, it can be seen from the results of these measurements that the DDS-PLL system measurement results are reliable, repeatable, and not based on chance.

6. CONCLUSION

QCM is a well-known acoustic transducer that is used commonly in sensor applications. In this work, QCM's history, fundamentals, theory and measurement methods, the designed system, and its components are explained in detail. Five different open QCM's were used, and open QCM measurements were conducted with two different systems, VNA and Impedance Analyzer.

In this thesis, a compact VNA operating at the frequency range of 35 MHz - 4.4 GHz with a resolution of 19 Hz was designed using discrete components. As can be seen from the measurement results,it was successful in measuring the resonance frequency of the QCM and its dip magnitude both in air and in water and these measurements are reliable and repeatable.

Also, it is explained an alternative system design (DDS-PLL System) that is compact, operates in the same frequency range and has a resolution down to 2.5 Hz.As can be seen from the measurement results, this system measured successfully the resonance frequency of the QCM and its dip magnitude both in air and in water.

Due to time schedule constraints, further tests and developments of the designed system could not be performed, yet in the future work, to develop the designed system to be wireless and electrodeless an RF amplifier, an attenuator, and a switch can be added. The next step should be to design an antenna for this system. After all these steps, the system should be calibrated to have a baseline for the measurements. Then measurements of the whole designed system should be done to verify its operation. For the final step, a PCB design of the verified system should be made. Figure 6.1 shows the schematic of the system design for wireless and electrodeless QCM based biosensor.

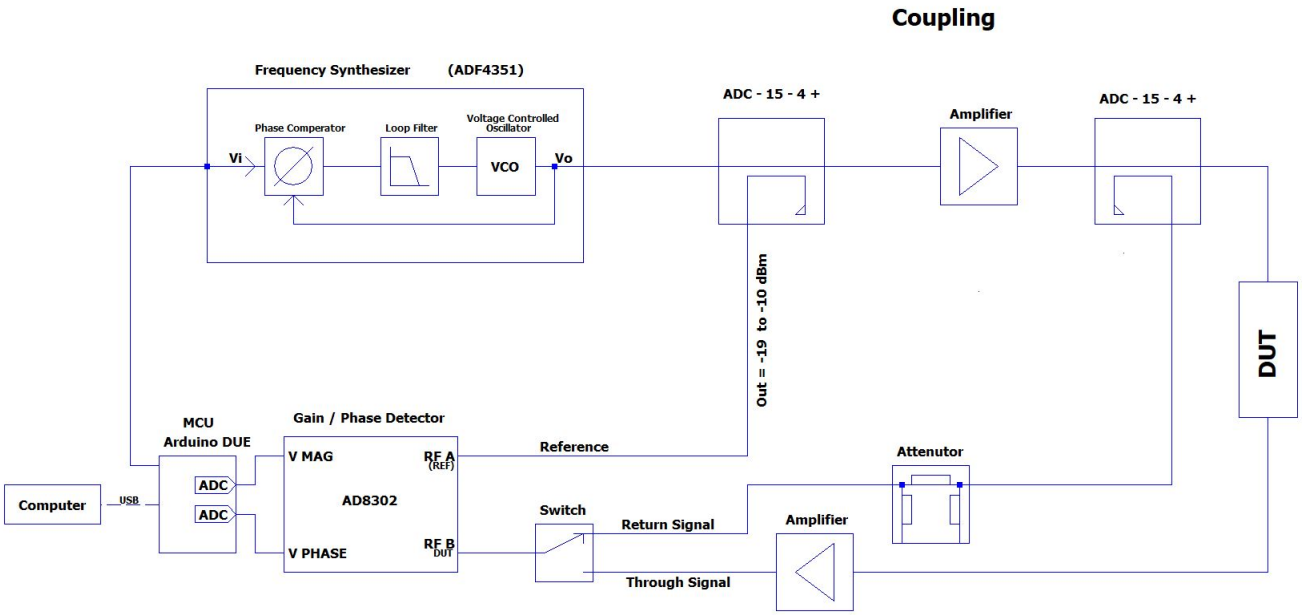

Figure 6.1. Schematic of system design for wireless and electrodeless QCM based biosensor.

REFERENCES

1. Mehrotra, P., "Biosensors and Their Applications–A Review", *Journal of Oral Biology and Craniofacial Research*, Vol. 6, No. 2, pp. 153–159, 2016.

2. Heineman, W. R. and W. B. Jensen, "Leland C. Clark Jr.(1918–2005)", *Biosensors and Bioelectronics*, Vol. 21, No. 8, pp. 1403–1404, 2006.

3. Nikhil, B., J. Pawan, F. Nello and E. Pedro, "Introduction to Biosensors", *Essays in Biochemistry*, Vol. 60, No. 1, pp. 1–8, 2016.

4. Afzal, A., A. Mujahid, R. Schirhagl, S. Z. Bajwa, U. Latif and S. Feroz, "Gravimetric Viral Diagnostics: QCM Based Biosensors for Early Detection of Viruses", *Chemosensors*, Vol. 5, No. 1, p. 7, 2017.

5. Mannelli, I., M. Minunni, S. Tombelli and M. Mascini, "Quartz Crystal Microbalance (QCM) Affinity Biosensor for Genetically Modified Organisms (GMOs) detection", *Biosensors and Bioelectronics*, Vol. 18, No. 2-3, pp. 129–140, 2003.

6. Serra, P. A., *Biosensors: Emerging Materials and Applications*, BoD–Books on Demand, Rijeka, 2011.

7. Sauerbrey, G., "The Use of Quartz Oscillators for Weighing Thin Layers and for Microweighing", *Zeitschrift für Physik*, Vol. 155, pp. 206–222, 1959.

8. Na Songkhla, S. and T. Nakamoto, "Overview of Quartz Crystal Microbalance Behavior Analysis and Measurement", *Chemosensors*, Vol. 9, No. 12, p. 350, 2021.

9. Cady, W. G., *Piezoelectricity: Volume Two: An Introduction to the Theory and Applications of Electromechanical Phenomena in Crystals*, Courier Dover Publications, New York, 2018.

10. Ward, M. D. and D. A. Buttry, "In Situ Interfacial Mass Detection With Piezoelectric Transducers", *Science*, Vol. 249, No. 4972, pp. 1000–1007, 1990.

11. Van der Werff, M., Y. Yuan, E. Hirst, P. Xu, H. Chen and J. Bronlund, "Quartz Crystal Microbalance Induced Bond Rupture Sensing for Medical Diagnostics", *Sensors Journal, IEEE*, Vol. 7, pp. 762 – 769, 06 2007.

12. IQD, "A Short Primer on AT-cut Quartz Crystals", `https://www.iqdfrequencyproducts.com/blog/2015/06/29/a-short-primer-on-at-cut-quartz-crystals/`, accessed on June 8, 2023.

13. Ward, M. D. and E. J. Delawski, "Radial Mass Sensitivity of The Quartz Crystal Microbalance in Liquid Media", *Analytical Chemistry*, Vol. 63, No. 9, pp. 886–890, 1991.

14. Huang, X., Q. Bai, J. Hu and D. Hou, "A Practical Model of Quartz Crystal Microbalance in Actual Applications", *Sensors*, Vol. 17, No. 8, p. 1785, 2017.

15. Sauerbrey, G., "The Use of Quartz Oscillators for Weighing Thin Layers and for Microweighing", *Zeitschrift für Physik*, Vol. 155, No. 2, pp. 206–222, 1959.

16. Nano Science Instruments, "Quartz Crystal Microbalance (QCM)", `https://www.nanoscience.com/techniques/quartz-crystal-microbalance/`, accessed on July 12, 2023.

17. Kanazawa, K. K. and J. G. Gordon, "Frequency of A Quartz Microbalance in Contact with Liquid", *Analytical Chemistry*, Vol. 57, No. 8, pp. 1770–1771, 1985.

18. Kanazawa, K. K. and J. G. Gordon II, "The Oscillation Frequency of A Quartz Resonator in Contact with Liquid", *Analytica Chimica Acta*, Vol. 175, pp. 99–105, 1985.

19. Barnes, C., "Development of Quartz Crystal Oscillators for Under-Liquid Sensing",

Sensors and Actuators A: Physical, Vol. 29, No. 1, pp. 59–69, 1991.

20. Satoh, T., R. I. Ruslan, S. Gotoh and T. Akitsu, "Double-Resonance Quartz Crystal Oscillator and Excitation of A Resonator Immersed in Liquid Media", *IEEE Transactions on Ultrasonics, Ferroelectrics, and Frequency Control*, Vol. 58, No. 4, pp. 788–797, 2011.

21. Ruslan, R. I. B., T. Satoh and T. Akitsu, "Voltage-Controlled Double-Resonance Quartz Oscillator Using Variable-Capacitance Diode", *IEEE Transactions on Ultrasonics, Ferroelectrics, and Frequency Control*, Vol. 59, No. 4, pp. 738–745, 2012.

22. Rodahl, M. and B. Kasemo, "Frequency and Dissipation-Factor Responses To Localized Liquid Deposits on a QCM Electrode", *Sensors and Actuators B: Chemical*, Vol. 37, No. 1-2, pp. 111–116, 1996.

23. Shoaib, N., *Vector Network Analyzer (VNA) Measurements and Uncertainty Assessment*, Springer, Berlin, 2016.

24. National Instruments, "Introduction to Network Analyzer Measurements Fundamentals and Background", `https://download.ni.com/evaluation/rf/Introduction-to-Network-Analyzer-Measurements.pdf`, accessed on June 6, 2023.

25. KEYSIGHT, "Network Analysis", `https://www.keysight.com/us/en/solutions/measurement-fundamentals/network-analysis.html`, accessed on June 5, 2023.

26. Analog Devices, "Wideband Synthesizer with Integrated VCO", `https://www.analog.com/media/en/technical-documentation/data-sheets/adf4351.pdf`, accessed on June 10, 2023.

27. Analog Devices, "LF–2.7 GHz RF/IF Gain and Phase Detector", `https://www.analog.com/media/en/technical-documentation/data-sheets/AD8302.pdf`, accessed on June 10, 2023.

28. Analog Devices, "Evaluation Board for the ADF4351 Fractional-N PLL Frequency Synthesizer", https://www.analog.com/media/en/technical-documentation/user-guides/UG-435.pdf, accessed on June 12, 2023.

29. Mini Circuits, "Directional Coupler", https://www.minicircuits.com/pdfs/ADC-15-4+.pdf, accessed on June 12, 2023.

30. Wikipedia, "Impedance Analyzer", https://en.wikipedia.org/wiki/Impedance-analyzer, accessed on August 12, 2023.

31. KEYSIGHT, "E4990A Impedance Analyzer", https://www.keysight.com/us/en/assets/7018-04255/brochures/5991-3888.pdf, accessed on August 12, 2023.

32. Vankka, J., *Direct Digital Synthesizers: Theory, Design, and Applications*, M.S. Thesis, Helsinki University of Technology, 2000.

33. Analog Dialogue, "All About Direct Digital Synthesis", https://www.analog.com/media/en/analog-dialogue/volume-38/number-3/articles/all-about-direct-digital-synthesis.pdf, accessed on June 6, 2023.

34. Analog Devices, "CMOS, 125 MHz Complete DDS Synthesizer", https://www.analog.com/media/en/technical-documentation/data-sheets/AD9850.pdf, accessed on June 12, 2023.

APPENDIX A: REGISTER MAPS OF ADF4351

REGISTER 0

RESERVED	16-BIT INTEGER VALUE (INT)																12-BIT FRACTIONAL VALUE (FRAC)												CONTROL BITS		
DB31	DB30	DB29	DB28	DB27	DB26	DB25	DB24	DB23	DB22	DB21	DB20	DB19	DB18	DB17	DB16	DB15	DB14	DB13	DB12	DB11	DB10	DB9	DB8	DB7	DB6	DB5	DB4	DB3	DB2	DB1	DB0
0	N16	N15	N14	N13	N12	N11	N10	N9	N8	N7	N6	N5	N4	N3	N2	N1	F12	F11	F10	F9	F8	F7	F6	F5	F4	F3	F2	F1	C3(0)	C2(0)	C1(0)

REGISTER 1

RESERVED			PHASE ADJUST	PRESCALER	12-BIT PHASE VALUE (PHASE) DBR[1]												12-BIT MODULUS VALUE (MOD) DBR[1]												CONTROL BITS		
DB31	DB30	DB29	DB28	DB27	DB26	DB25	DB24	DB23	DB22	DB21	DB20	DB19	DB18	DB17	DB16	DB15	DB14	DB13	DB12	DB11	DB10	DB9	DB8	DB7	DB6	DB5	DB4	DB3	DB2	DB1	DB0
0	0	0	PH1	PR1	P12	P11	P10	P9	P8	P7	P6	P5	P4	P3	P2	P1	M12	M11	M10	M9	M8	M7	M6	M5	M4	M3	M2	M1	C3(0)	C2(0)	C1(1)

REGISTER 2

RESERVED	LOW NOISE AND LOW SPUR MODES		MUXOUT			REFERENCE DOUBLER DBR[1]	RDIV2 DBR[1]	10-BIT R COUNTER DBR[1]									DOUBLE BUFFER	CHARGE PUMP CURRENT SETTING DBR[1]				LDF	LDP	PD POLARITY	POWER-DOWN	CP THREE-STATE	COUNTER RESET	CONTROL BITS		
DB31	DB30	DB29	DB28	DB27	DB26	DB25	DB24	DB23	DB22	DB21	DB20	DB19	DB18	DB17	DB16	DB15	DB14	DB13	DB12	DB11	DB10	DB9	DB8	DB7	DB6	DB5	DB4	DB3	DB2	DB1	DB0
0	L2	L1	M3	M2	M1	RD2	RD1	R10	R9	R8	R7	R6	R5	R4	R3	R2	R1	D1	CP4	CP3	CP2	CP1	U6	U5	U4	U3	U2	U1	C3(0)	C2(1)	C1(0)

REGISTER 3

RESERVED								BAND SELECT CLOCK MODE	ABP	CHARGE CANCEL	RESERVED		CSR	RESERVED	CLK DIV MODE		12-BIT CLOCK DIVIDER VALUE											CONTROL BITS		
DB31	DB30	DB29	DB28	DB27	DB26	DB25	DB24	DB23	DB22	DB21	DB20	DB19	DB18	DB17	DB16	DB15	DB14	DB13	DB12	DB11	DB10	DB9	DB8	DB7	DB6	DB5	DB4	DB3	DB2	DB1	DB0
0	0	0	0	0	0	0	0	F4	F3	F2	0	0	F1	0	C2	C1	D12	D11	D10	D9	D8	D7	D6	D5	D4	D3	D2	D1	C3(0)	C2(1)	C1(1)

REGISTER 4

RESERVED								FEEDBACK SELECT	DBB[2] RF DIVIDER SELECT			8-BIT BAND SELECT CLOCK DIVIDER VALUE								VCO POWER-DOWN	MTLD	AUX OUTPUT SELECT	AUX OUTPUT ENABLE	AUX OUTPUT POWER		RF OUTPUT ENABLE	OUTPUT POWER		CONTROL BITS		
DB31	DB30	DB29	DB28	DB27	DB26	DB25	DB24	DB23	DB22	DB21	DB20	DB19	DB18	DB17	DB16	DB15	DB14	DB13	DB12	DB11	DB10	DB9	DB8	DB7	DB6	DB5	DB4	DB3	DB2	DB1	DB0
0	0	0	0	0	0	0	0	D13	D12	D11	D10	BS8	BS7	BS6	BS5	BS4	BS3	BS2	BS1	D9	D8	D7	D6	D5	D4	D3	D2	D1	C3(1)	C2(0)	C1(0)

REGISTER 5

RESERVED								LD PIN MODE		RESERVED	RESERVED		RESERVED																CONTROL BITS		
DB31	DB30	DB29	DB28	DB27	DB26	DB25	DB24	DB23	DB22	DB21	DB20	DB19	DB18	DB17	DB16	DB15	DB14	DB13	DB12	DB11	DB10	DB9	DB8	DB7	DB6	DB5	DB4	DB3	DB2	DB1	DB0
0	0	0	0	0	0	0	0	D15	D14	0	1	1	0	0	0	0	0	0	0	0	0	0	0	0	0	0	0	0	C3(1)	C2(0)	C1(1)

[1]DBR = DOUBLE-BUFFERED REGISTER—BUFFERED BY THE WRITE TO REGISTER 0.
[2]DBB = DOUBLE-BUFFERED BITS—BUFFERED BY THE WRITE TO REGISTER 0, IF AND ONLY IF DB13 OF REGISTER 2 IS HIGH.

09800-023

Figure A.1. Register maps.

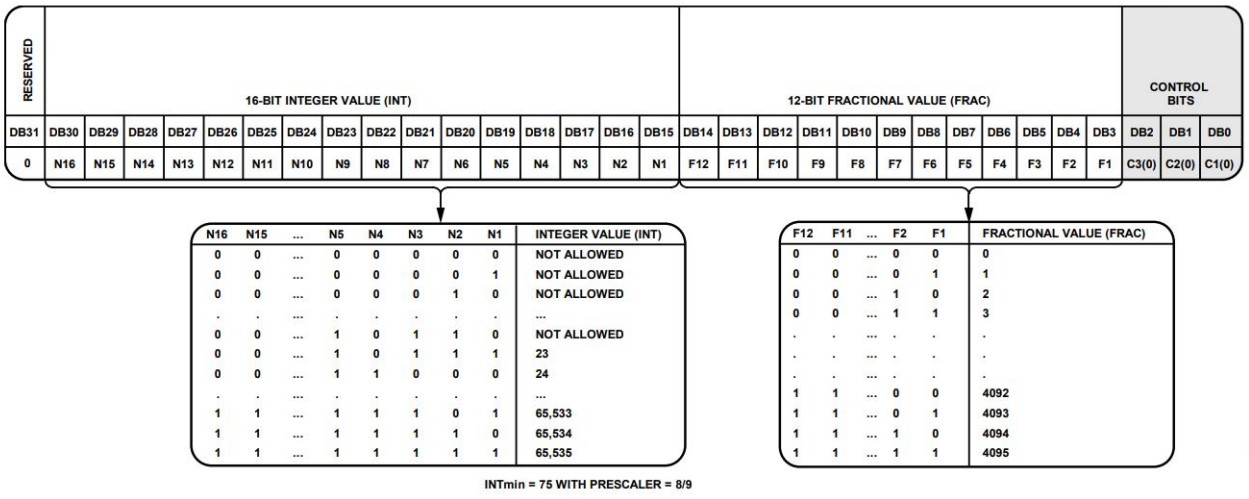

Figure A.2. Register 0.

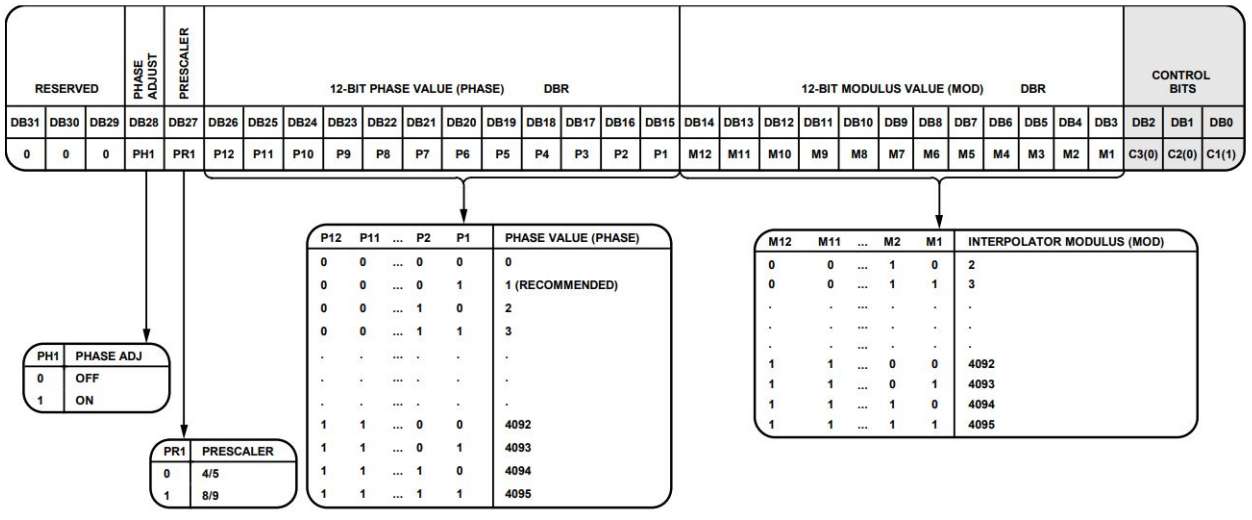

Figure A.3. Register 1.

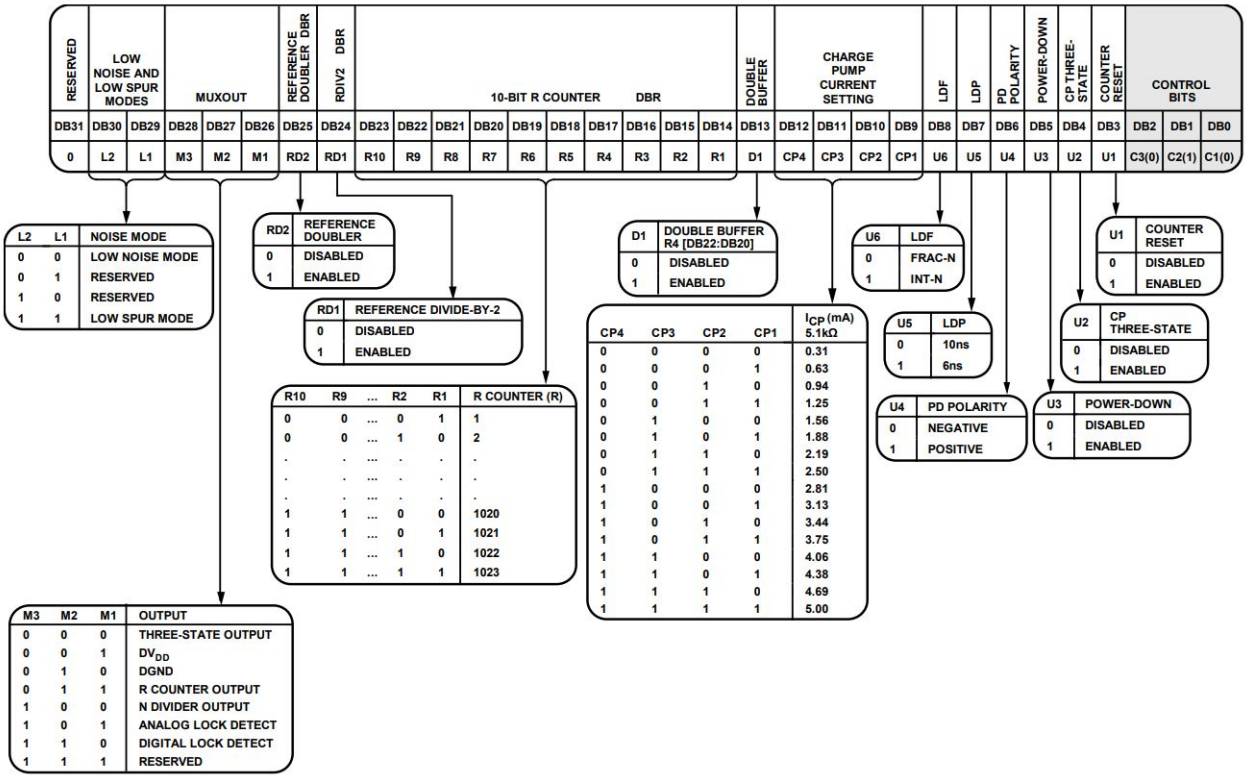

Figure A.4. Register 2.

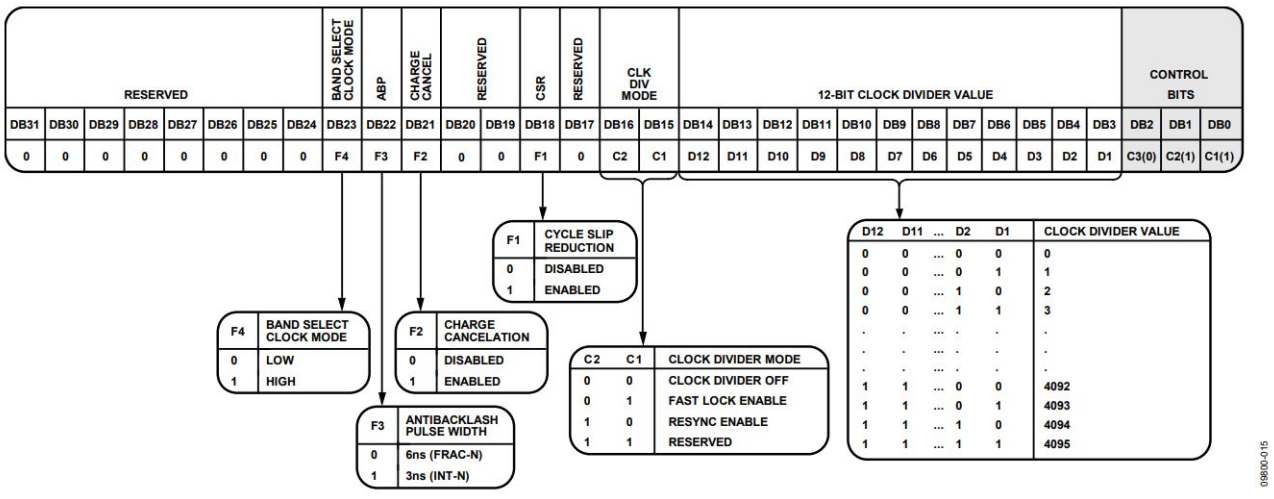

Figure A.5. Register 3.

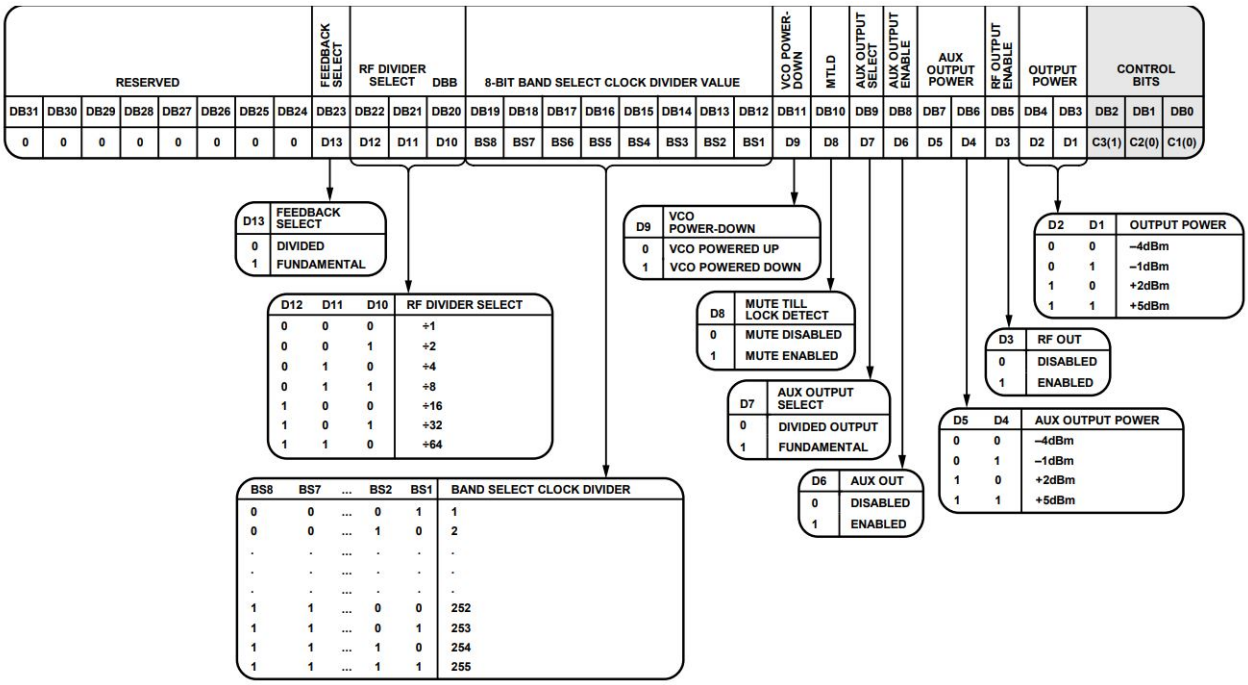

Figure A.6. Register 4.

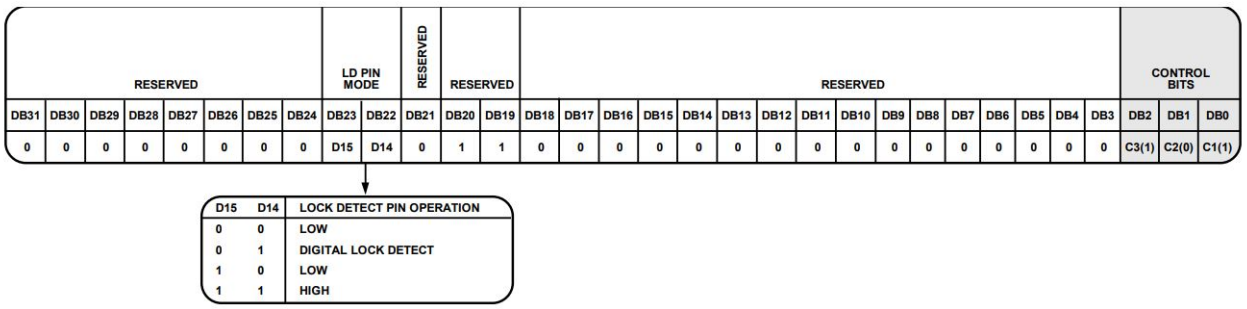

Figure A.7. Register 5.

APPENDIX B: ARDUINO DUE CODE

```
#include <SPI.h>

// de SQ3SWF 2019

#define SHL(x,y) ((uint32_t)1<<y)*x

#define REF_CLK 25000000
uint8_t slave_select_pin = 47;
int input_pin = 40;
int AD8302_Mag_in = A2 ;   //  Variable to select appropriate channel of ADC corresponding to A0
int AD8302_Pha_in = A3 ;  //  Variable to select appropriate channel of ADC corresponding to A1
int val0=0;
int val1=0;
int val2=0;
unsigned long time_now=0;
unsigned long time_now2=0;
unsigned long a=0;
unsigned long long frequency =49999000;

// Register 0:
uint16_t INT=0;
uint16_t INT2=0;

uint16_t FRAC=0;

// Register 1:
uint8_t phase_adj=0;
uint8_t prescaler = 0;
uint16_t phase = 1;
uint16_t MOD = 4095;

// Register 2:
uint8_t low_noise_spur=3;
uint8_t muxout=6;
uint8_t ref_doubler=1;
uint8_t rdiv2 = 0;
uint16_t r_counter = 10;
uint8_t dbl_buf;
uint8_t charge_pump_current = 0b111;
uint8_t ldf=1; uint8_t ldp=0;
uint8_t pd_polarity = 1;
uint8_t powerdown;
uint8_t cp_three_state;
uint8_t counter_reset;

// Register 3:
uint8_t band_mode_clksel=1;
uint8_t abp;
uint8_t chg_cancel=0;
uint8_t csr=0;
uint8_t clkdiv_mode=0;
uint16_t clock_divider = 150;

```

```
// Register 4:
uint8_t feedback_sel =1;
uint8_t rf_div_sel = 2;   // 0 = /1, 1=/2, 2=/4 ...
uint8_t band_select_clkdiv = 50;
uint8_t vco_pwrdown = 0;
uint8_t mtld = 1;
uint8_t aux_outsel = 0;
uint8_t aux_outena;
uint8_t aux_pwr;
uint8_t rf_ena =1 ; // 0 - output disabled
uint8_t out_pwr = 3; // 0 - min, 3 - max

// Register 5:
uint8_t ld_pinmode = 1;

uint32_t reg[6] = {0,0,0,0,0,0};

uint32_t pfd_freq = (REF_CLK*(1.0+ref_doubler))/(r_counter*((1.0+rdiv2)));

void prepare_registers() {

  if(frequency >= 2200000000) rf_div_sel = 0;
  if(frequency < 2200000000) rf_div_sel = 1;
  if(frequency < 1100000000) rf_div_sel = 2;
  if(frequency < 550000000) rf_div_sel = 3;
  if(frequency < 275000000) rf_div_sel = 4;
  if(frequency < 137500000) rf_div_sel = 5;
  if(frequency < 68750000) rf_div_sel = 6;

  INT = (frequency*(1<<rf_div_sel))/pfd_freq;
  INT2= INT + 1 ;


  reg[1] = SHL(phase_adj, 28)  | SHL(prescaler, 27)  | SHL(phase, 15)  | SHL(MOD, 3) | 0b001;
  reg[2] = SHL(low_noise_spur, 29) | SHL(muxout, 26) | SHL(ref_doubler, 25) | SHL(rdiv2, 24) | SHL(r_counter, 14) \
           | SHL(dbl_buf, 13) | SHL(charge_pump_current, 9) | SHL(ldf, 8) | SHL(ldp, 7) | SHL(pd_polarity, 6) \
           | SHL(powerdown, 5) | SHL(cp_three_state, 4) | SHL(counter_reset, 3) | 0b010;
  reg[3] = SHL(band_mode_clksel, 23) | SHL(abp, 22) | SHL(chg_cancel, 21) | SHL(csr, 18) | SHL(clkdiv_mode, 15) \
           | SHL(clock_divider, 3) | 0b011;
  reg[4] = SHL(feedback_sel, 23) | SHL(rf_div_sel, 20) | SHL(band_select_clkdiv, 12) | SHL(vco_pwrdown, 9) \
           | SHL(mtld, 10) | SHL(aux_outsel, 9) | SHL(aux_outena, 8) | SHL(aux_pwr, 6) | SHL(rf_ena, 5) | SHL(out_pwr, 3) | 0b100;
  reg[5] = SHL(ld_pinmode, 22) | SHL(0b11, 19) | 0b101;

}
void sweepfrequency(){
  val0=digitalRead(input_pin);
  if (val0=HIGH){

   reg[0] = SHL(INT, 15) | SHL(FRAC, 3) | 0b000;


  for (int i=1; i<=MOD;i++){
    delayMicroseconds(1);
    FRAC=i;
    reg[0]=SHL(INT, 15) | SHL(FRAC, 3);

   digitalWrite(slave_select_pin, LOW);
   delayMicroseconds(1);

   /*
   SPI.transfer((uint8_t)(reg[0] >> 24));
   SPI.transfer((uint8_t)(reg[0] >> 16));
   SPI.transfer((uint8_t)(reg[0] >> 8));
   SPI.transfer((uint8_t)(reg[0]));
   */

   prepare_registers();
   updateAllRegisters();

   digitalWrite(slave_select_pin, HIGH);
   delayMicroseconds(1);

  //READ-AD8302
  for (int i=1; i<12;i++){
   val1=analogRead(AD8302_Mag_in );
   val2=analogRead(AD8302_Pha_in );
```

```
 float voltageA0 = val1 ;
 float voltageA1 = val2 ;
 float frac1=FRAC;
 float mod1=MOD;
 float s=frac1/mod1;

uint32_t rf_out_freq=((INT+(s))*(pfd_freq/pow(2,rf_div_sel)));

Serial.print("\n ");Serial.print(voltageA0);
Serial.print(" "); Serial.print(voltageA1);
 //Serial.print(" \t \t Time"); Serial.println(time_now2 - time_now );
Serial.print(" ");Serial.print(rf_out_freq);
}

 }


 reg[0] = SHL(INT2, 15) | SHL(FRAC, 3) | 0b000;

 for (int i=1; i<=MOD;i++){
   delayMicroseconds(1);
   FRAC=i;
   reg[0]=SHL(INT2, 15) | SHL(FRAC, 3);

 digitalWrite(slave_select_pin, LOW);
 delayMicroseconds(1);

 /*
 SPI.transfer((uint8_t)(reg[0] >> 24));
 SPI.transfer((uint8_t)(reg[0] >> 16));
 SPI.transfer((uint8_t)(reg[0] >> 8));
 SPI.transfer((uint8_t)(reg[0]));
 */
 prepare_registers();
 updateAllRegisters();

 digitalWrite(slave_select_pin, HIGH);
 delayMicroseconds(1);

//READ-AD8302
 for (int i=1; i<12;i++){
 val1=analogRead(AD8302_Mag_in );
 val2=analogRead(AD8302_Pha_in );

 float voltageA0 = val1 ;
 float voltageA1 = val2 ;
  float frac1=FRAC;
 float mod1=MOD;
 float s=frac1/mod1;

uint32_t rf_out_freq=((INT2+(s))*(pfd_freq/pow(2,rf_div_sel)));
```

```
183
184   Serial.print("\n "); Serial.print(voltageA0);
185   Serial.print(" "); Serial.print(voltageA1);
186   //Serial.print(" \t \t Time"); Serial.println(time_now2 - time_now );
187   Serial.print(" ");Serial.print(rf_out_freq);
188   }
189
190
191   }
192
193
194
195   }
196
197 }
198 void sendRegisterToAdf(uint16_t reg_id) {
199
200   digitalWrite(slave_select_pin, LOW);
201   delayMicroseconds(1);
202   SPI.transfer((uint8_t)(reg[reg_id] >> 24));
203   SPI.transfer((uint8_t)(reg[reg_id] >> 16));
204   SPI.transfer((uint8_t)(reg[reg_id] >> 8));
205   SPI.transfer((uint8_t)(reg[reg_id]));
206
207   digitalWrite(slave_select_pin, HIGH);
208   delayMicroseconds(1);
209    digitalWrite(slave_select_pin, LOW);
210
211  }
212
213 void updateAllRegisters() {
214   for(int i=5; i>=0; i--) {
215     sendRegisterToAdf(i);
216   }
217
218  }
219
220 void setup() {
221   pinMode (input_pin,INPUT);
222   pinMode (slave_select_pin, OUTPUT);
223   digitalWrite(slave_select_pin, LOW);
224
225   SPI.setDataMode(SPI_MODE0);
226   SPI.setBitOrder(MSBFIRST);
227   SPI.setClockDivider(SPI_CLOCK_DIV128);
228   SPI.begin();
229
230   Serial.begin(115200);
231
232   delayMicroseconds(1);
233
234   prepare_registers();
235   updateAllRegisters();
236
237  //ADC -> ADC_MR |= 0x80;
238  // ADC -> ADC_CR = 2;
239  // ADC -> ADC_CHER = (1<<AD8302_Mag_in) | (1<<AD8302_Pha_in);
240
241   analogReadResolution(12);
242   //ADC -> ADC_CHER = 0x80;
243
244   //readAD8302 ();
245   time_now = millis();
246 for (int a = 0; a<50000; a++){
247   //READ-AD8302
248   val1=analogRead(AD8302_Mag_in );
249
250 }
251 time_now2 = millis();
252
253 }
254
255 char key, cwmode=0;
256
257
258 void loop() {
259  /*
260   prepare_registers();
261   updateAllRegisters();
262   */
263   sweepfrequency();
264
265 }
```

APPENDIX C: DETAILED ANALYSIS OF ADF435'S LOOP FILTER USING ADISIMPLL

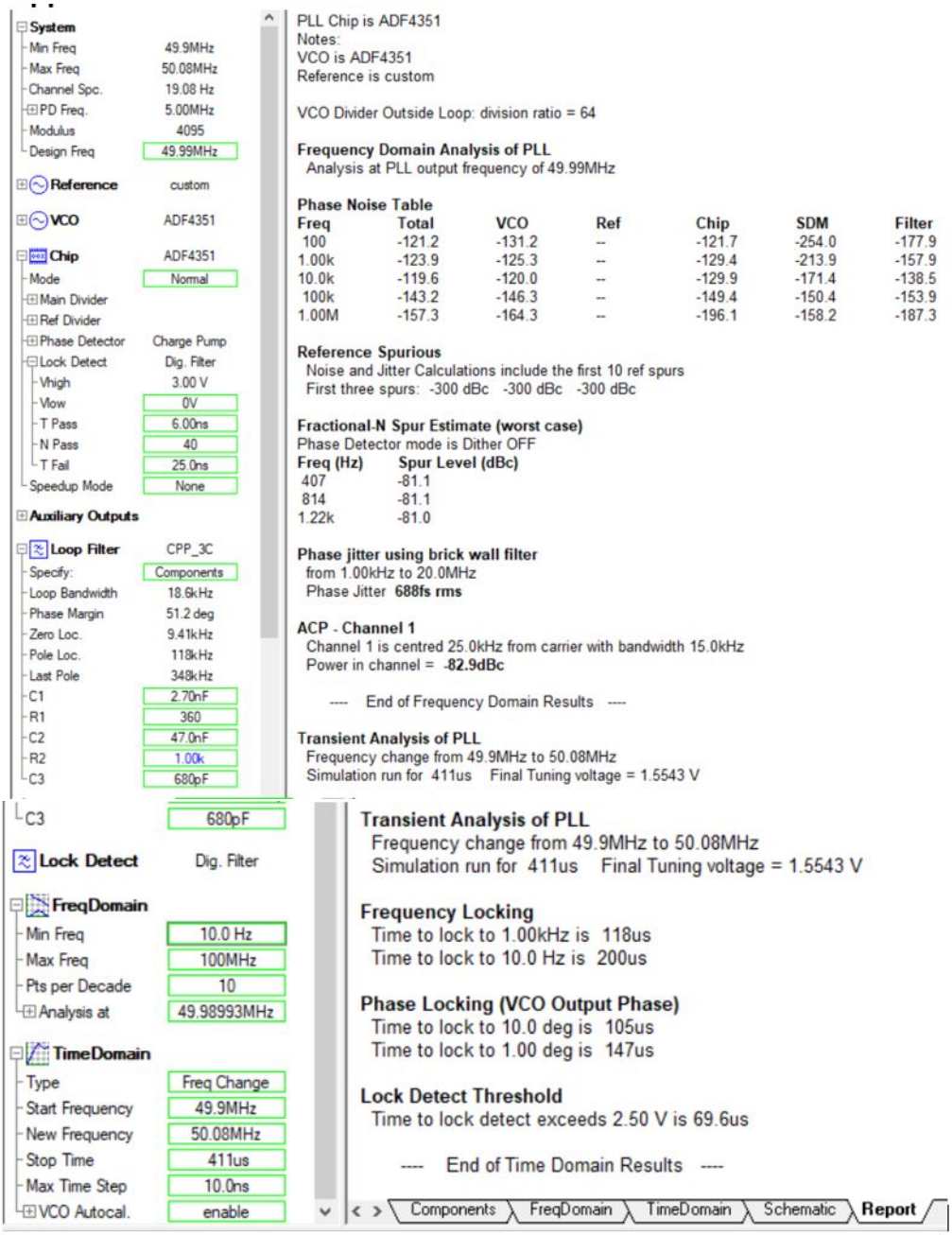

Figure C.1. Detailed Analysis Of ADF435's Loop Filter Using ADISIMPLL

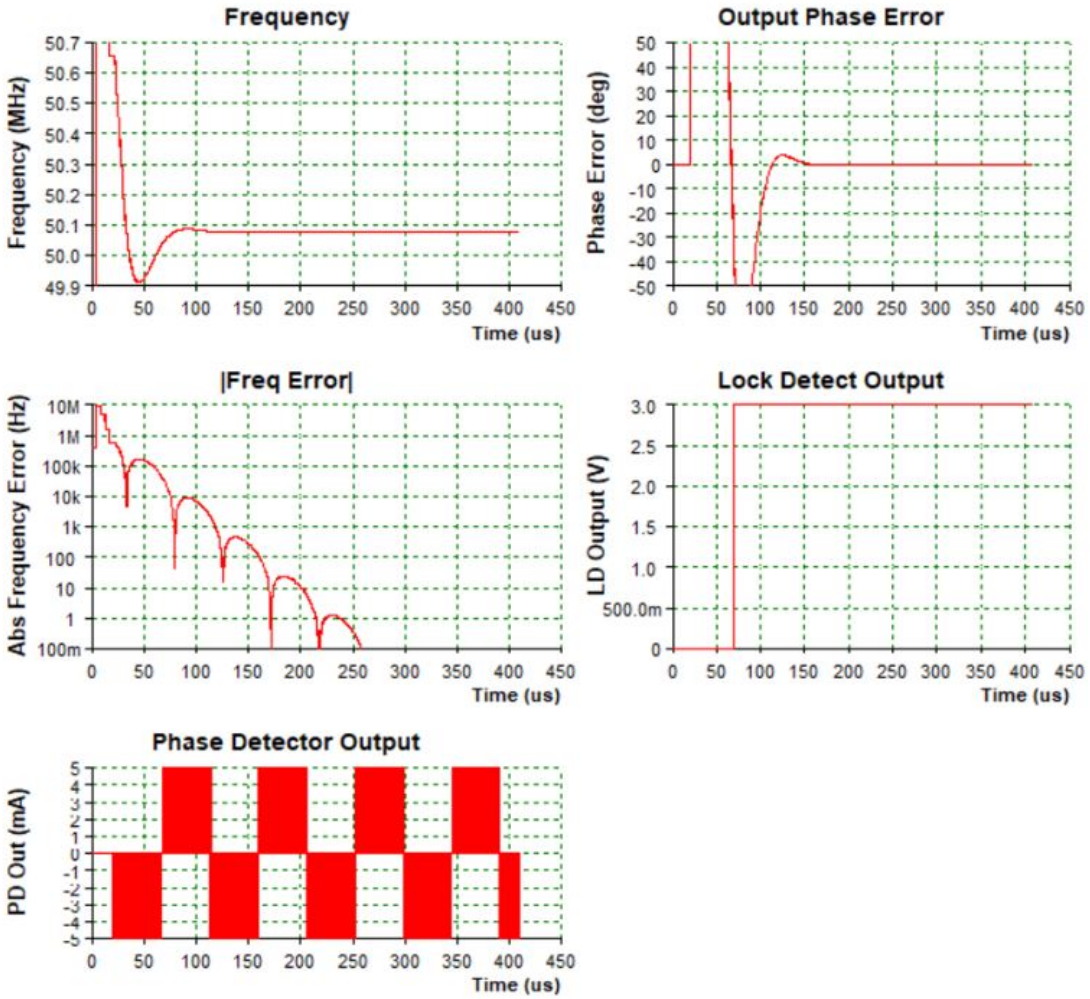

Figure C.2. ADF435's Loop Filter Analysis Graphs

APPENDIX D: MATLAB CODE

Matlab Code that reads the data and draws it into two different graphs or just one graph.

```
clc;
close all;
clear all;

textread 20.03.2023.txt
Mag=((ans*1000)-930)/30
plot (Mag)
grid on
title("Magnitude")
xlabel('Measurement Index')
ylabel('dB')

%textread 20.03.2023.txt
%Phase=((Ph*1000)-1800)/10
%plot (Phase)
%grid on
%title("Phase")
%xlabel('Measurement Index')
%ylabel('Degree')
```

APPENDIX E: MATLAB CODE

MATLAB Code that reads the data and draws it two different graphs as Magnitude and Phase.

```
clc;
close all;
clear all;


textread Mag-2-20.01.2023.txt
Mag=ans
s=8190
x=Mag(1:s+1)
a=Mag(s:2*s)
b=Mag(2*s:3*s)
c=Mag(3*s:4*s)
d=Mag(4*s:5*s)
e=Mag(5*s:6*s)
f=Mag(6*s:7*s)
g=Mag(7*s:8*s)
h=Mag(8*s:9*s)
m=Mag(9*s:10*s)
plot (x)
hold on
plot (a)
hold on
plot (b)
hold on
plot (c)
hold on
plot (d)
hold on
plot (e)
hold on
plot (f)
hold on
plot (g)
hold on
plot (h)
hold on
plot (m)
grid on
title("Magnitude")
xlabel('Measurement Index')
ylabel('Voltage[V]')

figure
l=(x+a+b+c+d+e+f+g+h+m)/10
k=((l*1000)-900)/30
plot (k)
grid on
title("Avarage of 10 Magnitude Sweep")
ylabel('dB')
xlabel('Measurement Index')

```

```
figure
textread Phase-2-20.01.2023.txt
Phase=ans
x=Mag(1:s+1)
a=Mag(s:2*s)
b=Mag(2*s:3*s)
c=Mag(3*s:4*s)
d=Mag(4*s:5*s)
e=Mag(5*s:6*s)
f=Mag(6*s:7*s)
g=Mag(7*s:8*s)
h=Mag(8*s:9*s)
m=Mag(9*s:10*s)
plot (x)
hold on
plot (a)
hold on
plot (b)
hold on
plot (c)
hold on
plot (d)
hold on
plot (e)
hold on
plot (f)
hold on
plot (g)
hold on
plot (h)
hold on
plot (m)
grid on
title("Phase")
xlabel('Measurement Index')
ylabel('Voltage[V]')

figure
l=(x+a+b+c+d+e+f+g+h+m)/10
k=((l*1000)-1800)/10
plot (k)
grid on
title("Avarage of 10 Phase Sweep")
ylabel('Degree')
xlabel('Measurement Index')
```

APPENDIX F: MATLAB CODE

```
clc;
close all;
clear all;

M = readmatrix('02.05.2023.txt')

Mag=M(1:90090,1);
Phase=M(1:90090,2);
Frequency=M(1:90090,3);

a=1;
b=1;
d=1;
n=11;
c=b*n;
K=[];
L=[];
N=[];

for b=1:8190
    S=M(a:c,1);
    Z=M(a:c,2);
    V=M(a:c,3);
    F=median(S);
    P=median(Z);
    H=mean(V);
    K=[K,F];
    L=[L,P];
    N=[N,H];
    b=b+1;
    c=b*n;
    a=a+11;
end

Mg=K*(3.3/4095);
Ph=L*(3.3/4095);
Mag=((Mg*1000)-930)/30;
Phase=((Ph*1000)-1800)/10;
plot(N,Mag);
title("Magnitude")
xlabel('Frequency')
ylabel('dB')
figure
plot(N,Phase);
title("Phase")
xlabel('Frequency')
ylabel('Degree')
```

APPENDIX G: IMPEDANCE ANALYZER MEASUREMENT RESULTS

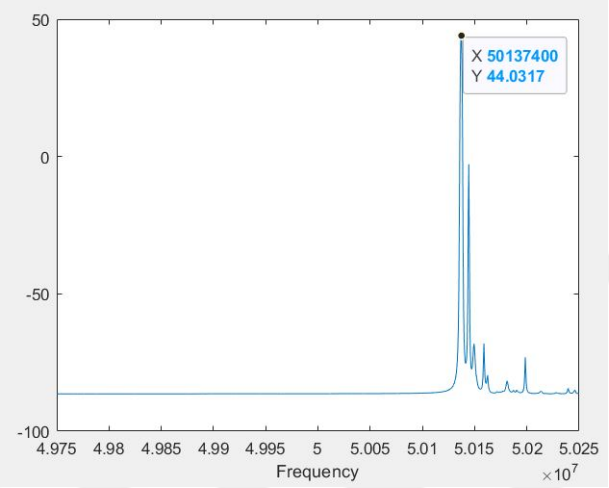

Figure G.1. Impedance analyzer measurement results when open QCM was in the air.

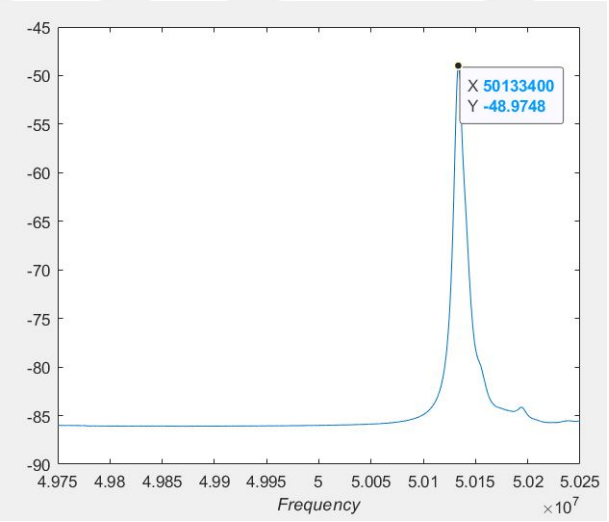

Figure G.2. Impedance analyzer measurement results when open QCM was in water.

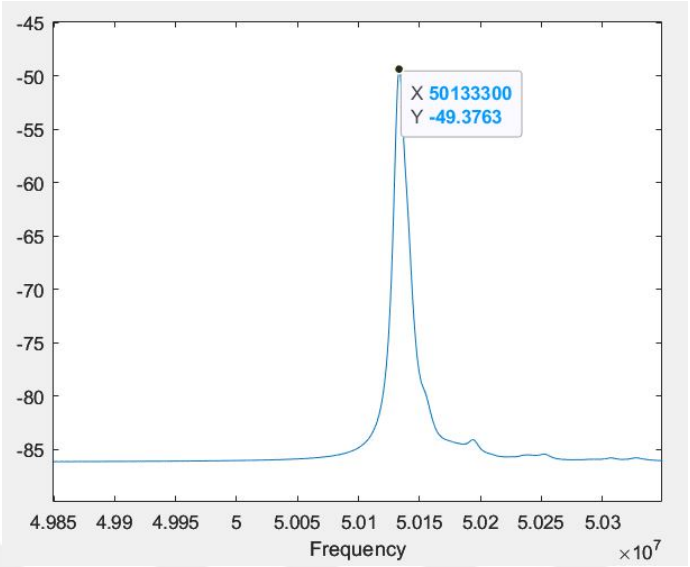

Figure G.3. Impedance analyzer measurement results when open QCM was in 100 ml water after 1ml glycerol was added.

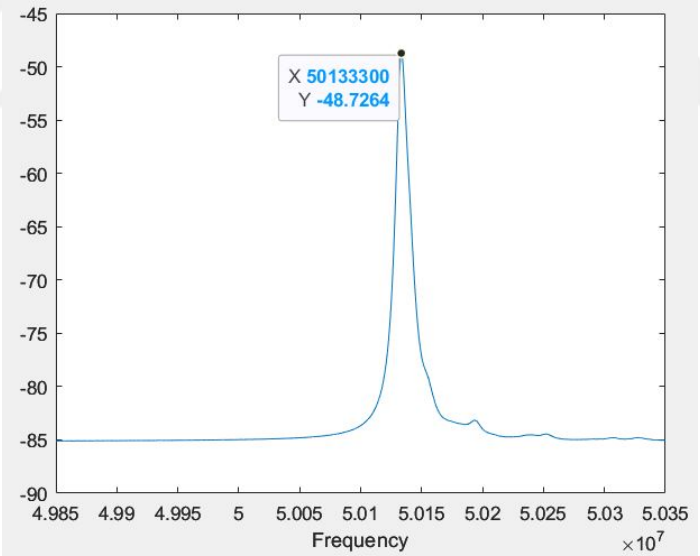

Figure G.4. Impedance analyzer measurement results when open QCM was in 100 ml water after 3ml glycerol was added.

APPENDIX H: DESIGNED SYSTEM MEASUREMENT RESULTS

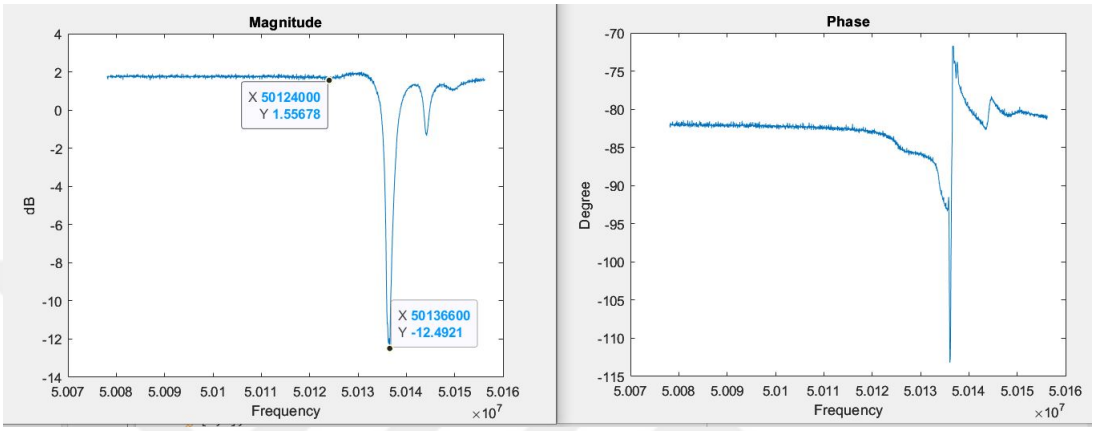

Figure H.1. Designed system measurement results-1 when open QCM was in the air.

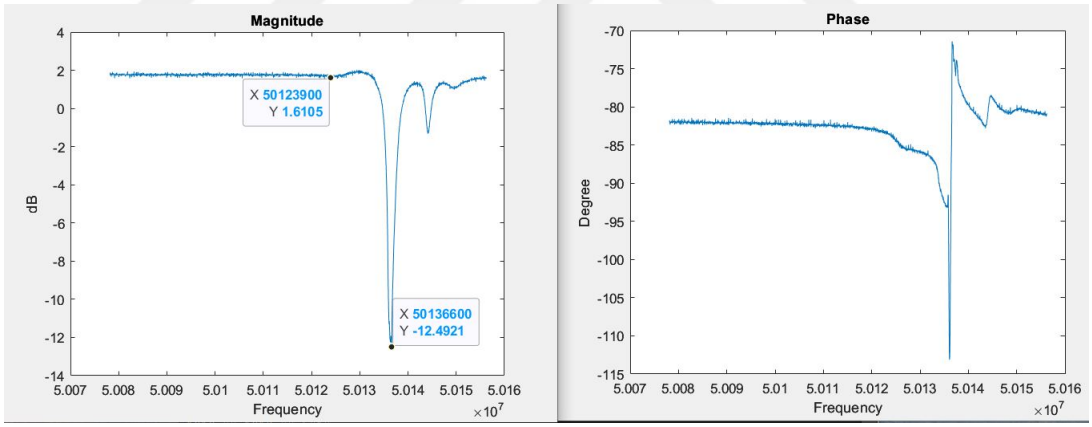

Figure H.2. Designed system measurement results-2 when open QCM was in the air.

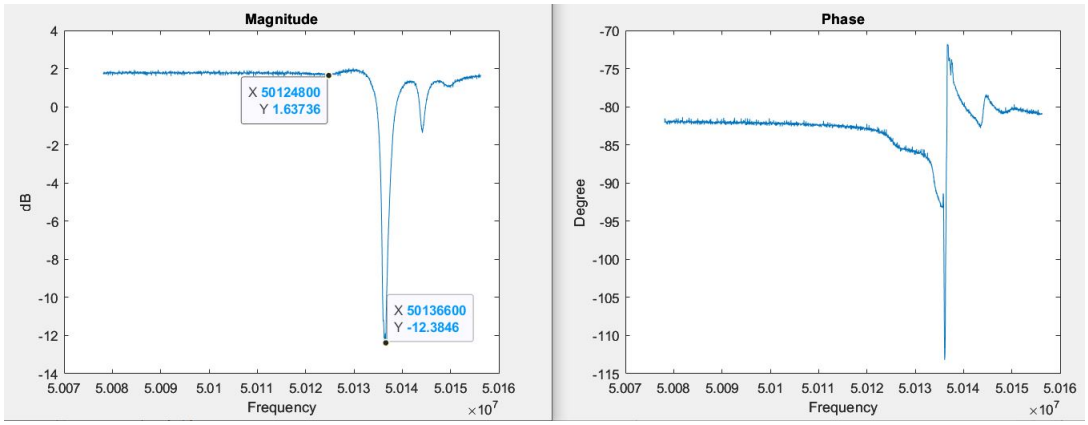

Figure H.3. Designed system measurement results-3 when open QCM was in the air.

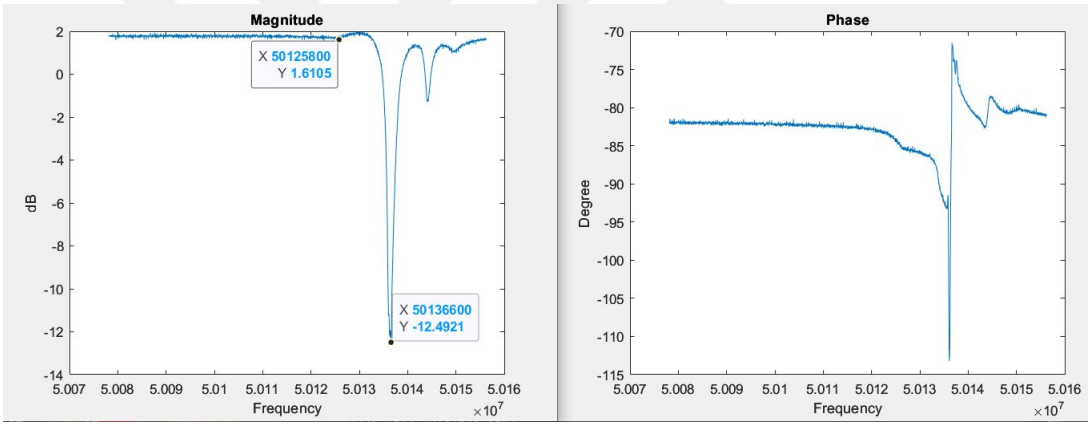

Figure H.4. Designed system measurement results-4 when open QCM was in the air.

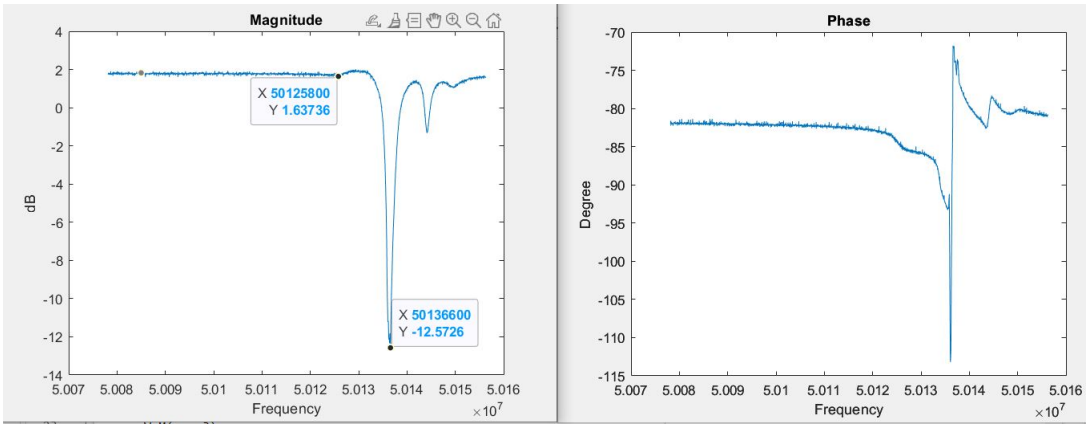

Figure H.5. Designed system measurement results-5 when open QCM was in the air.

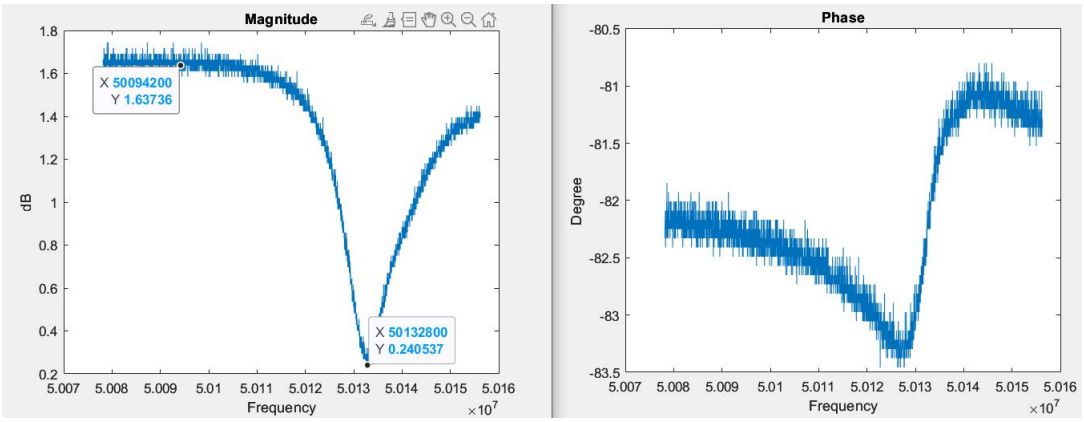

Figure H.6. Designed system measurement results-1 when open QCM was in water.

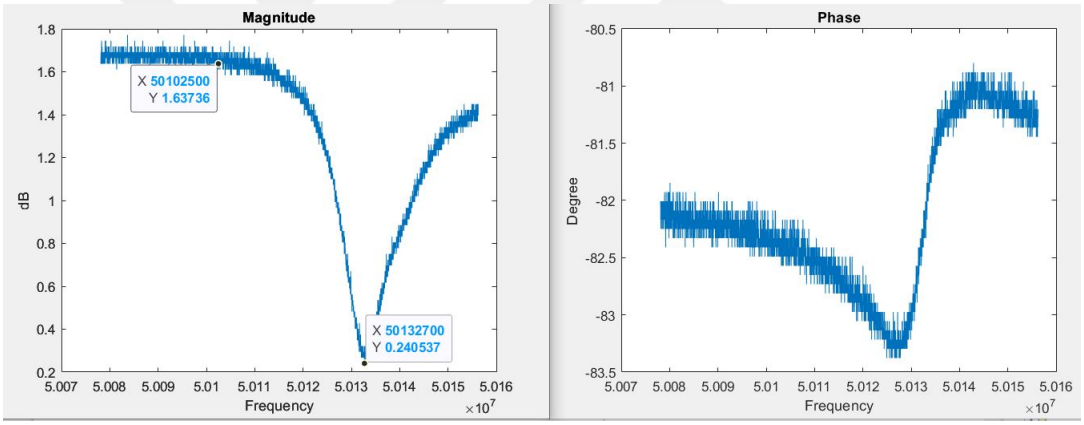

Figure H.7. Designed system measurement results-2 when open QCM was in water.

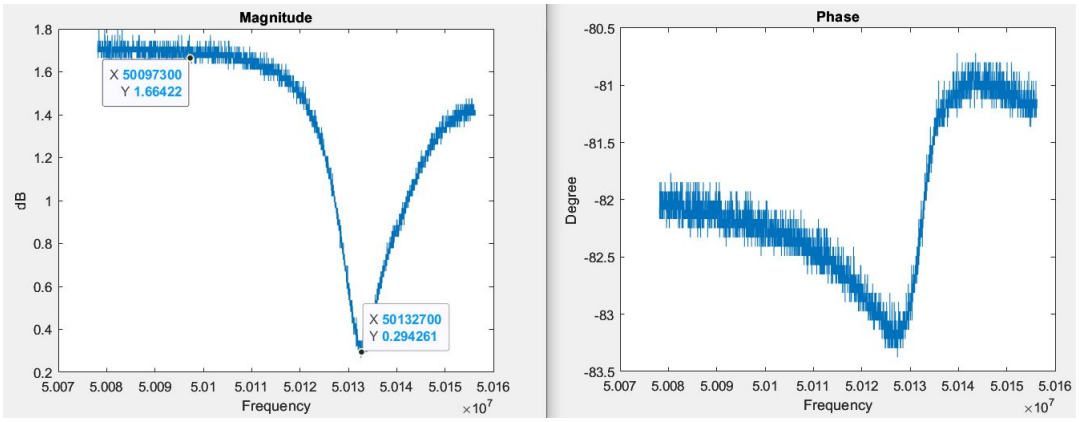

Figure H.8. Designed system measurement results-3 when open QCM was in water.

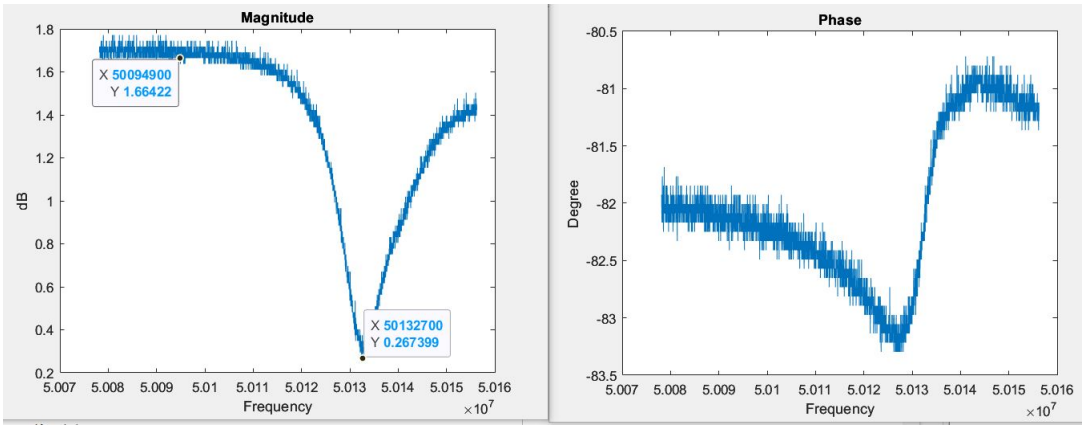

Figure H.9. Designed system measurement results-4 when open QCM was in water.

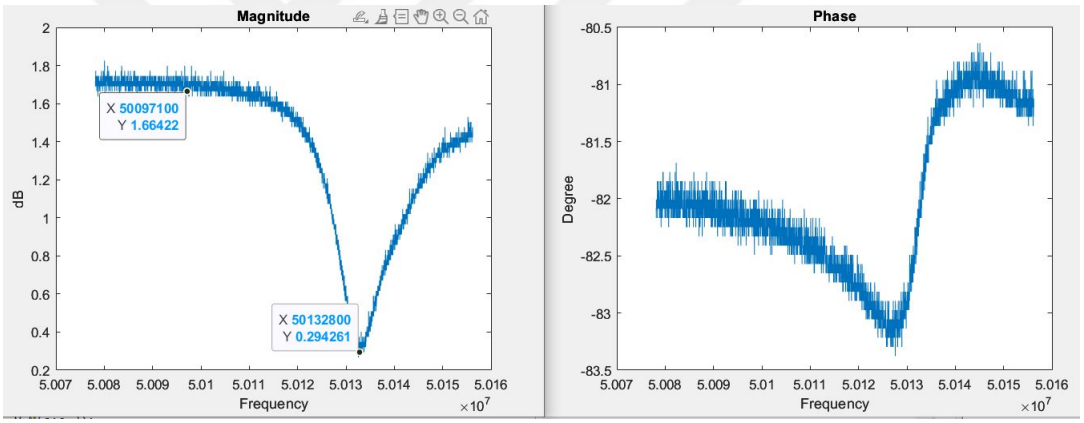

Figure H.10. Designed system measurement results-5 when open QCM was in water.

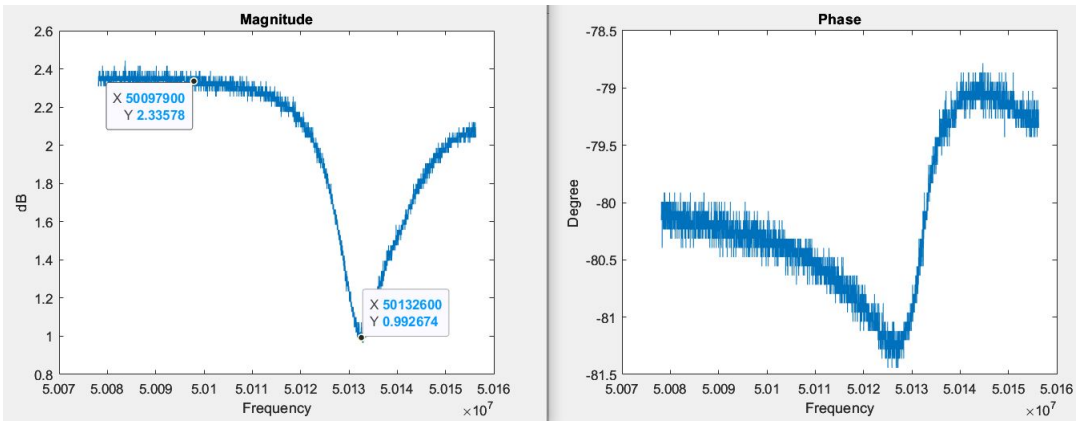

Figure H.11. Designed system measurement results-1 when open QCM was in 100 ml water after 1ml glycerol was added.

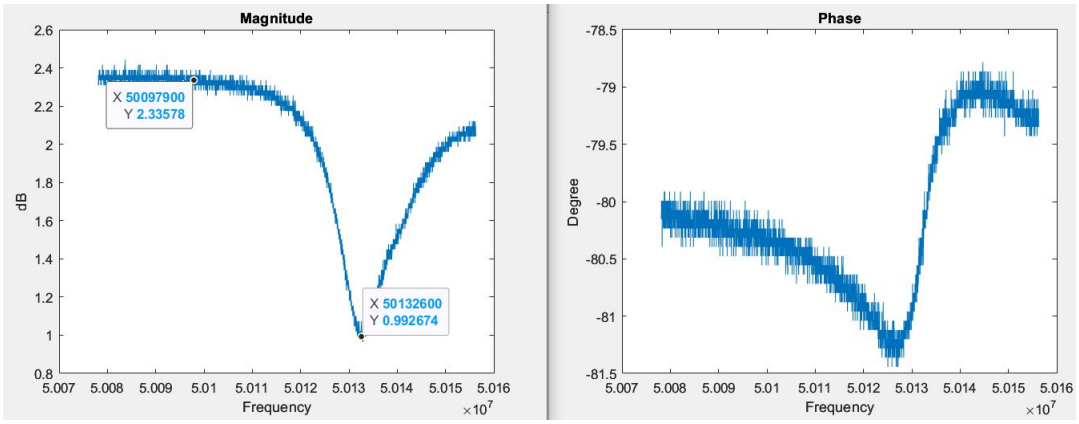

Figure H.12. Designed system measurement results-2 when open QCM was in 100 ml water after 1ml glycerol was added.

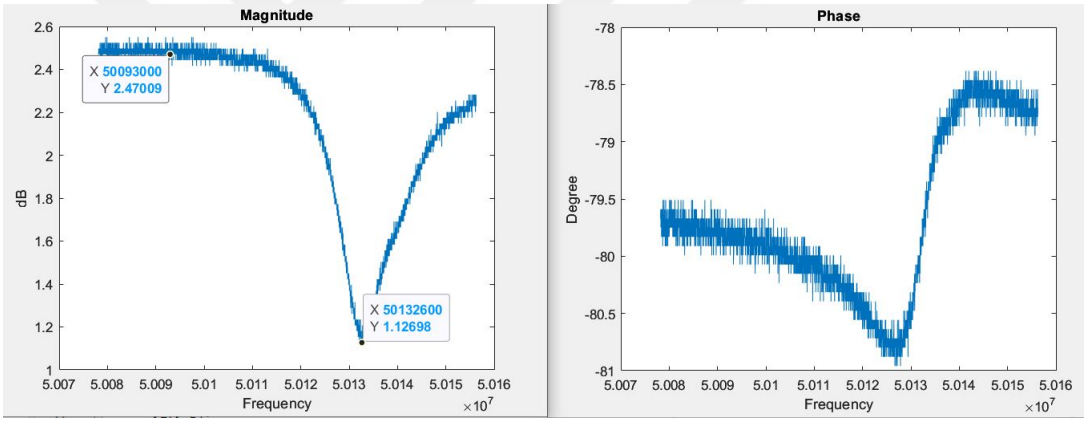

Figure H.13. Designed system measurement results-3 when open QCM was in 100 ml water after 1ml glycerol was added.

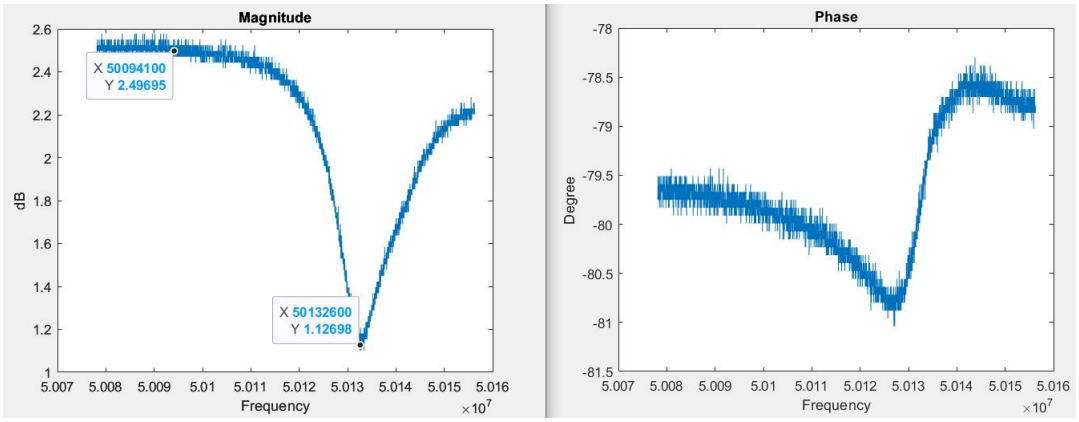

Figure H.14. Designed system measurement results-4 when open QCM was in 100 ml water after 1ml glycerol was added.

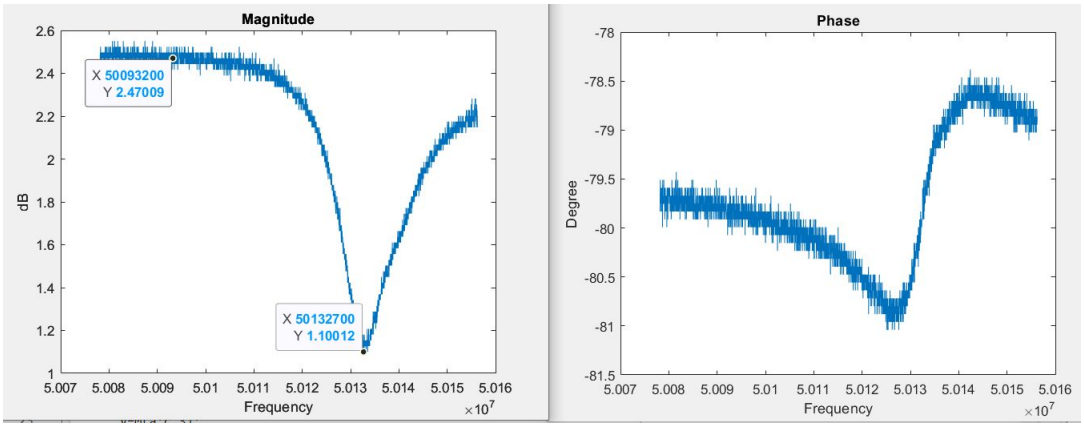

Figure H.15. Designed system measurement results-5 when open QCM was in 100 ml water after 1ml glycerol was added.

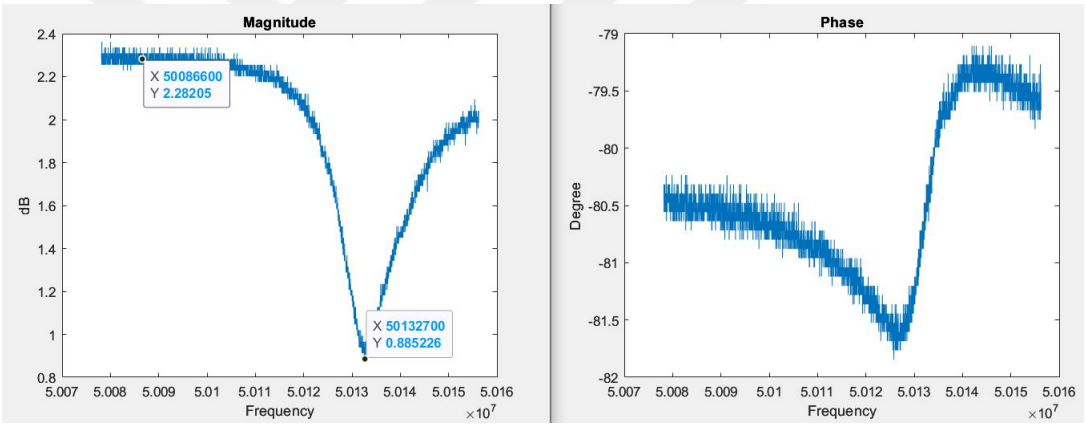

Figure H.16. Designed system measurement results-1 when open QCM was in 100 ml water after 3ml glycerol was added.

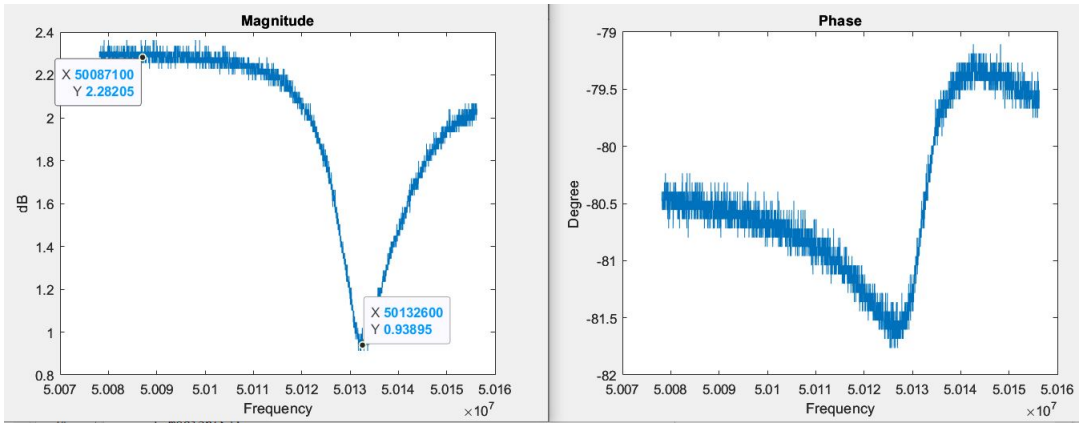

Figure H.17. Designed system measurement results-2 when open QCM was in 100 ml water after 3ml glycerol was added.

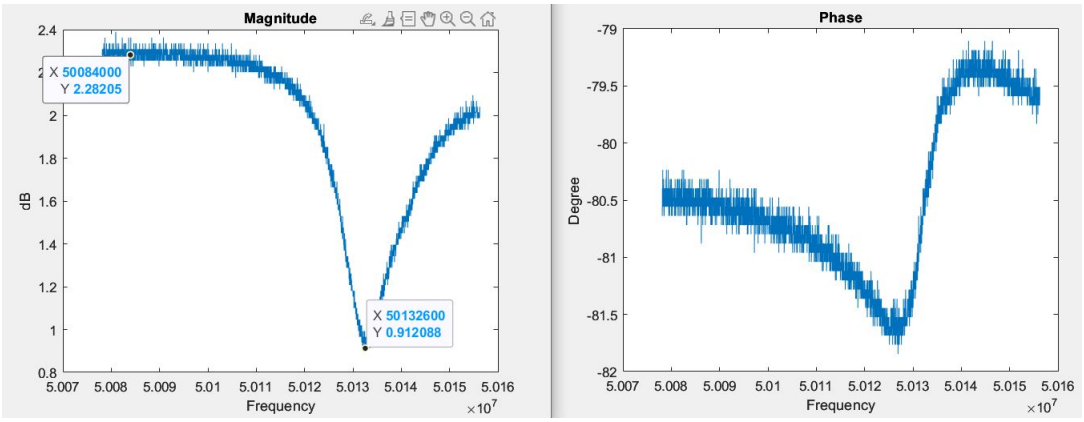

Figure H.18. Designed system measurement results-3 when open QCM was in 100 ml water after 3ml glycerol was added.

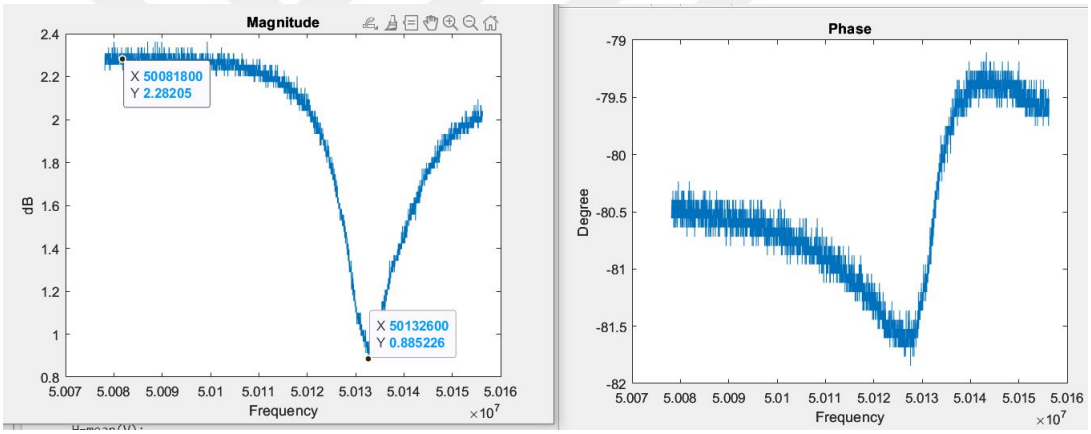

Figure H.19. Designed system measurement results-4 when open QCM was in 100 ml water after 3ml glycerol was added.

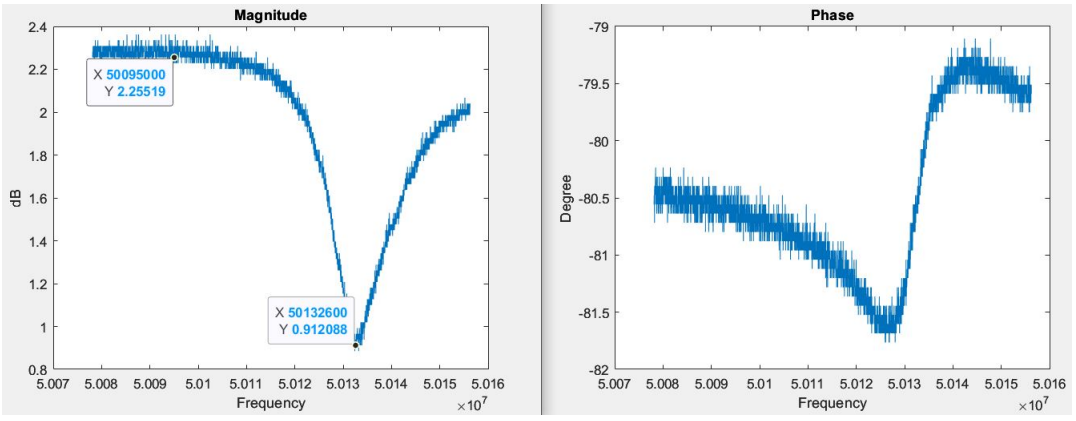

Figure H.20. Designed system measurement results-5 when open QCM was in 100 ml water after 3ml glycerol was added.

APPENDIX I: ARDUINO DUE CODE FOR DDS-PLL SYSTEM

```
#include <SPI.h>
#include <Arduino.h>

#define SHL(x,y) ((uint32_t)1<<y)*x

#define REF_CLK 20000000

////////////////////////////////////
class AD9850{
  public:
  AD9850();

  void begin(int w_clk, int fq_ud, int data, int reset);
  void setfreq(double f, uint8_t p);
  void down();
  void up();
  void calibrate(double TrimFreq);

  private:
  int W_CLK;int FQ_UD;
  int DATA;int RESET;
  uint32_t deltaphase;
  uint8_t phase1;
  void update();
  void begin_priv();
  void pulse(int pin);
  double calibFreq;
};

AD9850 DDS;

AD9850::AD9850() {
}

void AD9850::begin(int w_clk, int fq_ud, int data, int reset) {
  W_CLK = w_clk;FQ_UD = fq_ud;DATA = data;RESET = reset;deltaphase = 0;phase1 = 0;calibFreq = 125000000;
  begin_priv();
}

void AD9850::begin_priv() {
  pinMode(W_CLK, OUTPUT);
  pinMode(FQ_UD, OUTPUT);
  pinMode(DATA, OUTPUT);
  pinMode(RESET, OUTPUT);

  pulse(RESET);
  pulse(W_CLK);
  pulse(FQ_UD);
}

void AD9850::update() {
  for (int i=0; i<4; i++, deltaphase>>=8) {
    shiftOut(DATA, W_CLK, LSBFIRST, deltaphase & 0xFF);
  }
  shiftOut(DATA, W_CLK, LSBFIRST, phase1 & 0xFF);pulse(FQ_UD);
}

void AD9850::setfreq(double f, uint8_t p) {
  deltaphase = f * 4294967296.0 / calibFreq;phase1 = p << 3;update();
}

void AD9850::down() {
```

```
  pulse(FQ_UD);shiftOut(DATA, W_CLK, LSBFIRST, 0x04);pulse(FQ_UD);
}

void AD9850::up() {
  update();
}

void AD9850::calibrate(double TrimFreq) {
  calibFreq = TrimFreq;
}

void AD9850::pulse(int pin) {
  digitalWrite(pin, HIGH);digitalWrite(pin, LOW);
}

////////////////////////////////////////////////////

uint8_t slave_select_pin = 47;
int input_pin = 40;
int val=0;
//unsigned long long frequency = 50000000;
//unsigned long long frequency = 60000000;
unsigned long long frequency = 49990000;
unsigned long long frequency4 = 20000000;
////

int AD8302_Mag_in = A6 ;   //  Variable to select appropriate channel of ADC corresponding to A0
int AD8302_Pha_in = A7 ;  //  Variable to select appropriate channel of ADC corresponding to A1
int val1=0;
int val2=0;

////

// Register 0:
uint16_t INT=0;uint16_t FRAC=0;

// Register 1:
uint8_t phase_adj=0;uint8_t prescaler = 0;uint16_t phase = 1;uint16_t MOD = 4095;

// Register 2:
uint8_t low_noise_spur=3;uint8_t muxout=6;
uint8_t ref_doubler=1;uint8_t rdiv2 = 0;
uint16_t r_counter = 10;uint8_t dbl_buf;
uint8_t charge_pump_current = 0b111;
uint8_t ldf=0; uint8_t ldp=0;uint8_t pd_polarity = 1;
uint8_t powerdown;uint8_t cp_three_state;uint8_t counter_reset;

// Register 3:
uint8_t band_mode_clksel=1;uint8_t abp=0;
uint8_t chg_cancel=0;uint8_t csr=0;
uint8_t clkdiv_mode=0;uint16_t clock_divider = 150;

// Register 4:
uint8_t feedback_sel =1;uint8_t rf_div_sel = 2;
uint8_t band_select_clkdiv = 50;
uint8_t vco_pwrdown = 0;
uint8_t mtld = 1;uint8_t aux_outsel = 0;
uint8_t aux_outena;uint8_t aux_pwr;
uint8_t rf_ena =1 ;uint8_t out_pwr = 3;

// Register 5:
uint8_t ld_pinmode = 1;

```

```
uint32_t reg[6] = {0,0,0,0,0,0};

uint32_t pfd_freq = (REF_CLK*(1.0+ref_doubler))/(r_counter*((1.0+rdiv2)));

void prepare_registers() {

  if(frequency >= 2200000000) rf_div_sel = 0;
  if(frequency < 2200000000) rf_div_sel = 1;
  if(frequency < 1100000000) rf_div_sel = 2;
  if(frequency < 550000000) rf_div_sel = 3;
  if(frequency < 275000000) rf_div_sel = 4;
  if(frequency < 137500000) rf_div_sel = 5;
  if(frequency < 68750000) rf_div_sel = 6;

  INT = (frequency*(1<<rf_div_sel))/pfd_freq;

  reg[0] = SHL(INT, 15) | SHL(FRAC, 3) | 0b000;
  reg[1] = SHL(phase_adj, 28)  | SHL(prescaler, 27)  | SHL(phase, 15)  | SHL(MOD, 3) | 0b001;
  reg[2] = SHL(low_noise_spur, 29) | SHL(muxout, 26) | SHL(ref_doubler, 25) | SHL(rdiv2, 24) | SHL(r_counter, 14) \
         | SHL(dbl_buf, 13) | SHL(charge_pump_current, 9) | SHL(ldf, 8) | SHL(ldp, 7) | SHL(pd_polarity, 6) \
         | SHL(powerdown, 5) | SHL(cp_three_state, 4) | SHL(counter_reset, 3) | 0b010;
  reg[3] = SHL(band_mode_clksel, 23) | SHL(abp, 22) | SHL(chg_cancel, 21) | SHL(csr, 18) | SHL(clkdiv_mode, 15) \
         | SHL(clock_divider, 3) | 0b011;
  reg[4] = SHL(feedback_sel, 23) | SHL(rf_div_sel, 20) | SHL(band_select_clkdiv, 12) | SHL(vco_pwrdown, 9) \
         | SHL(mtld, 10) | SHL(aux_outsel, 9) | SHL(aux_outena, 8) | SHL(aux_pwr, 6) | SHL(rf_ena, 5) | SHL(out_pwr, 3) | 0b100;
  reg[5] = SHL(ld_pinmode, 22) | SHL(0b11, 19) | 0b101;
}

void sweepfrequency(){
  val=digitalRead(input_pin);
  if (val=HIGH){
    for (int i=1; i<=MOD;i++){
      delayMicroseconds(1);
      FRAC=i;
      reg[0]=SHL(INT, 15) | SHL(FRAC, 3);
      digitalWrite(slave_select_pin, LOW);
      delayMicroseconds(1);
      prepare_registers();
      updateAllRegisters();
      digitalWrite(slave_select_pin, HIGH);
      delayMicroseconds(1);
    }
  }
}

void sendRegisterToAdf(uint16_t reg_id) {
  digitalWrite(slave_select_pin, LOW);
  delayMicroseconds(1);
  SPI.transfer((uint8_t)(reg[reg_id] >> 24));
  SPI.transfer((uint8_t)(reg[reg_id] >> 16));
  SPI.transfer((uint8_t)(reg[reg_id] >> 8));
  SPI.transfer((uint8_t)(reg[reg_id]));
  digitalWrite(slave_select_pin, HIGH);
  delayMicroseconds(1);
  digitalWrite(slave_select_pin, LOW);
}

void updateAllRegisters() {
  for(int i=5; i>=0; i--) {
    sendRegisterToAdf(i);
  }
}
```

```
188
189  void setup() {
190    DDS.begin(6, 7, 8, 9);
191    int phase2 = 0;DDS.setfreq(frequency4, phase2);
192    pinMode (input_pin,INPUT);
193    pinMode (slave_select_pin, OUTPUT);
194    digitalWrite(slave_select_pin, LOW);
195    SPI.setDataMode(SPI_MODE0);
196    SPI.setBitOrder(MSBFIRST);
197    SPI.setClockDivider(SPI_CLOCK_DIV128);
198    SPI.begin();
199    Serial.begin(115200);
200    delayMicroseconds(1);
201    prepare_registers();
202    updateAllRegisters();
203    analogReadResolution(12);
204  }
205
206  char key, cwmode=0;
207
208  void loop() {
209    DDS.calibrate(124999000);
210    Serial.begin(115200);
211
212    int i=0;
213    int increase = 7;
214    for(i=0;i<10000;i++){
215      double frequency3 = 20000000 + i*increase;
216      int phase2 = 0;
217      DDS.setfreq(frequency3, phase2);
218      delayMicroseconds(100);
219  int j=0;
220
221  float frac1=FRAC;
222  float mod1=MOD;
223  float s=frac1/mod1;
224  pfd_freq = ((REF_CLK+i*increase)*(1.0+ref_doubler))/(r_counter*((1.0+rdiv2)));
225  uint32_t rf_out_freq=((INT+(s))*(pfd_freq/pow(2,rf_div_sel)));
226
227  for(j=0;j<11;j++){
228    val1=analogRead(AD8302_Mag_in);
229    val2=analogRead(AD8302_Pha_in);
230    Serial.print(val1);Serial.print(" ");Serial.print(val2);Serial.print(" ");Serial.print(rf_out_freq);Serial.print(" ");Serial.print(i);Serial.print("\n");
231  }
232  }
233  }
234
```

APPENDIX J: MATLAB CODE FOR DDS-PLL SYSTEM

```
clc;
close all;
clear all;

M_wrong = readmatrix('12.08.2023-bcd.txt');

sze = size(M_wrong);
x_size = sze(1);
y_size = sze(2);

start_point = 1;

while( (M_wrong(start_point,y_size) ~= 0) && (M_wrong(start_point,4) ~= 0))
    start_point = start_point+1;
end

M = M_wrong(start_point:x_size,:);

mag = M(12:110000,1);
ph = M(12:110000,2);
fre = M(12:110000,3);

for i=1:9999
    freq(i)=fre(1+(i-1)*11);
end

ind1 = 1;
ind2 = 1;
count1 = 0;
count2 = 0;
avg_mag = 0;
avg_ph = 0;
tot_mag = 0;
tot_ph = 0;

for j=1:9999
    temp_mag = mag( ((j-1)*11+1):j*11 );
    temp_ph = ph( ((j-1)*11+1):j*11 );
    sorted_temp_mag = sort(temp_mag);
    sorted_temp_ph = sort(temp_ph);
    new_mag( ((j-1)*11+1):j*11 ) = sorted_temp_mag;
    new_ph( ((j-1)*11+1):j*11 ) = sorted_temp_ph;
end

for j=0:9998
    st_dv_mag = std( mag( (j*11+1):((j+1)*11) ) );
    st_dv_ph = std( ph( (j*11+1):((j+1)*11) ) );

    for i=1:11
        avg_mag = avg_mag + mag(j*11 + i);
        avg_ph = avg_ph + ph(j*11 + i);
    end

```

```
    avg_mag = avg_mag/11;
    avg_ph = avg_ph/11;

    for i=1:11
        if (mag(j*11 + i) < avg_mag + st_dv_mag) && (mag(j*11 + i) > avg_mag - st_dv_mag)
            std_mag(ind1) = mag(j*11 + i);
            ind1 = ind1 + 1;
            tot_mag = tot_mag + mag(j*11 + i);
            count1 = count1 + 1;

        end
        if (ph(j*11 + i) < avg_ph + st_dv_ph) && (ph(j*11 + i) > avg_ph - st_dv_ph)
            std_ph(ind2) = ph(j*11 + i);
            ind2 = ind2 + 1;
            tot_ph = tot_ph + ph(j*11 + i);
            count2 = count2 + 1;
        end
    end

    med_mag_std(j+1) = median(std_mag)*3.3/4095;
    med_ph_std(j+1) = median(std_ph)*3.3/4095;

    avg_mag_std(j+1) = (tot_mag/count1)*3.3/4095;
    avg_ph_std(j+1) = (tot_ph/count2)*3.3/4095;

    avg_mag = 0;
    avg_ph = 0;
    tot_mag = 0;
    tot_ph = 0;
    count1 = 0;
    count2 = 0;
    ind1 = 1;
    ind2 = 1;
end

for i=1:9999
    med_mag(i) = new_mag( ((2*i-1)*11+1)/2 );
    med_ph(i) = new_ph( ((2*i-1)*11+1)/2 );
end

med_mag = med_mag*3.3/4095;
med_ph = med_ph*3.3/4095;

med_mag_std = (med_mag_std*1000-900)/30;
avg_mag_std = (avg_mag_std*1000-900)/30;
med_mag = (med_mag*1000-900)/30;

med_ph_std = (med_ph_std*1000-1800)/10;
avg_ph_std = (avg_ph_std*1000-1800)/10;
med_ph = (med_ph*1000-1800)/10;

mean_mag_movmedian = movmedian(med_mag,7);


plot(freq,(med_mag/2.5));
xlabel('Frequency');ylabel('dB');title('Initial magnitude with median value');
figure;
plot(freq,avg_mag_std);
xlabel('Frequency');ylabel('dB');title('Initial magnitude with std dev average ')
figure;
plot(freq,med_mag_std);
xlabel('Frequency');ylabel('dB');title('Initial  magnitude with  median value ');
figure;
plot(freq,med_ph);
xlabel('Frequency');ylabel('Degree');title('Initial Phase with moving median ');
```

APPENDIX K: DDS-PLL SYSTEM MEASUREMENT RESULTS

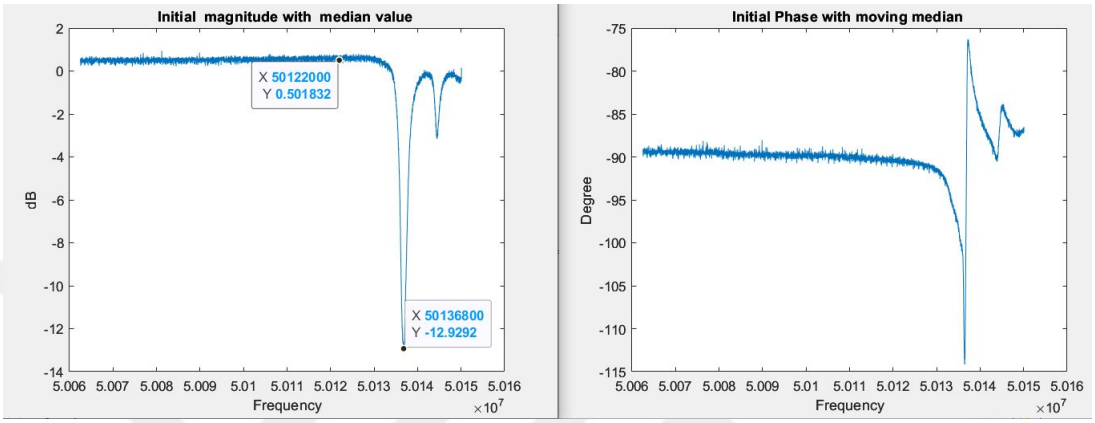

Figure K.1. DDS-PLL system measurement results-1 when open QCM was in the air.

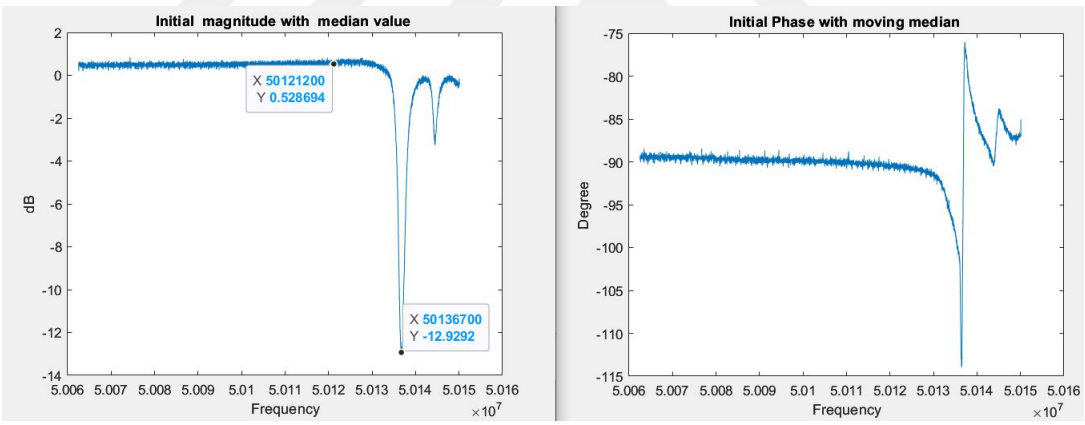

Figure K.2. DDS-PLL system measurement results-2 when open QCM was in the air.

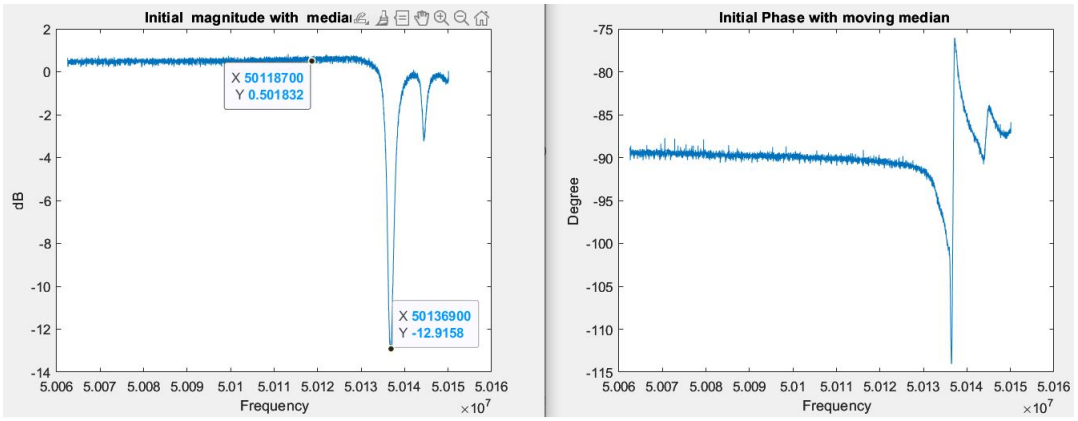

Figure K.3. DDS-PLL system measurement results-3 when open QCM was in the air.

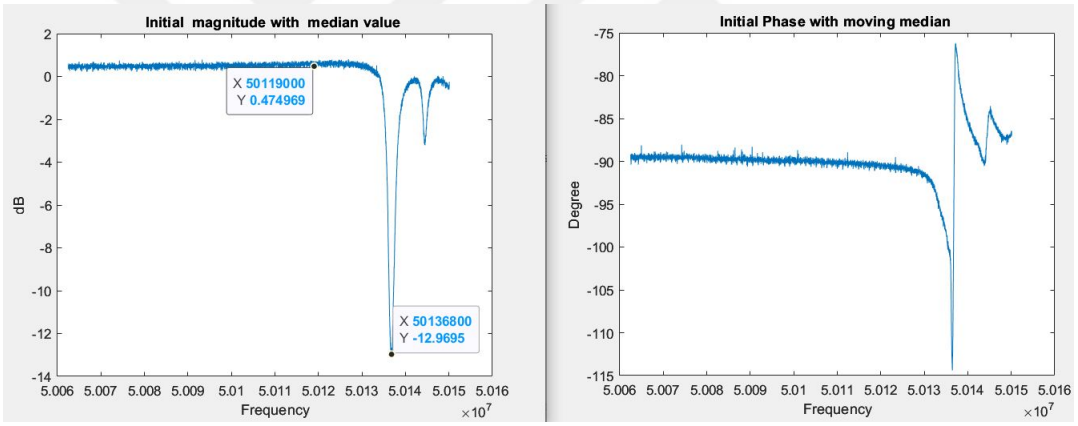

Figure K.4. DDS-PLL system measurement results-4 when open QCM was in the air.

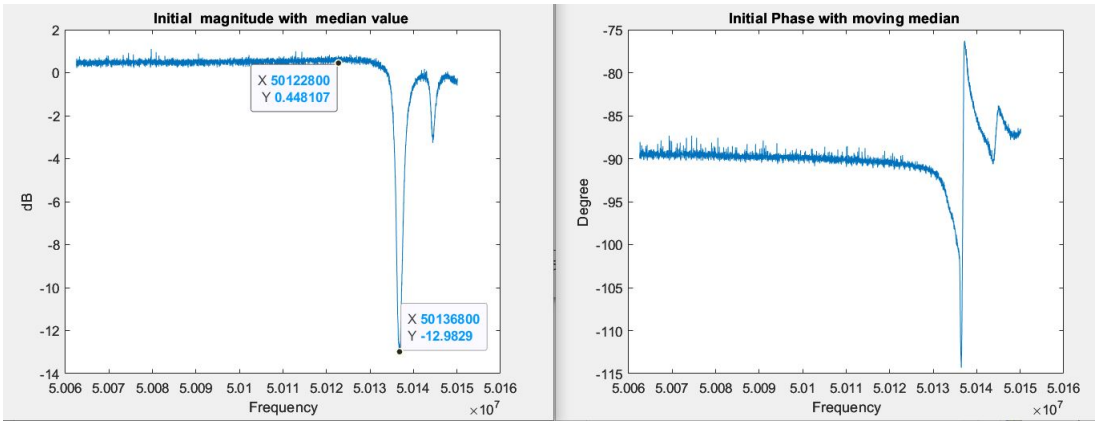

Figure K.5. DDS-PLL system measurement results-5 when open QCM was in the air.

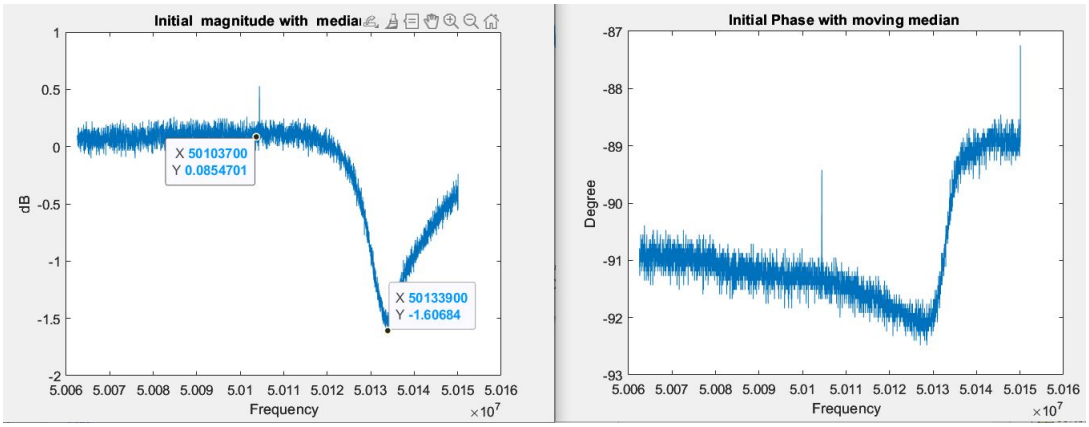

Figure K.6. DDS-PLL system measurement results-1 when open QCM was in water.

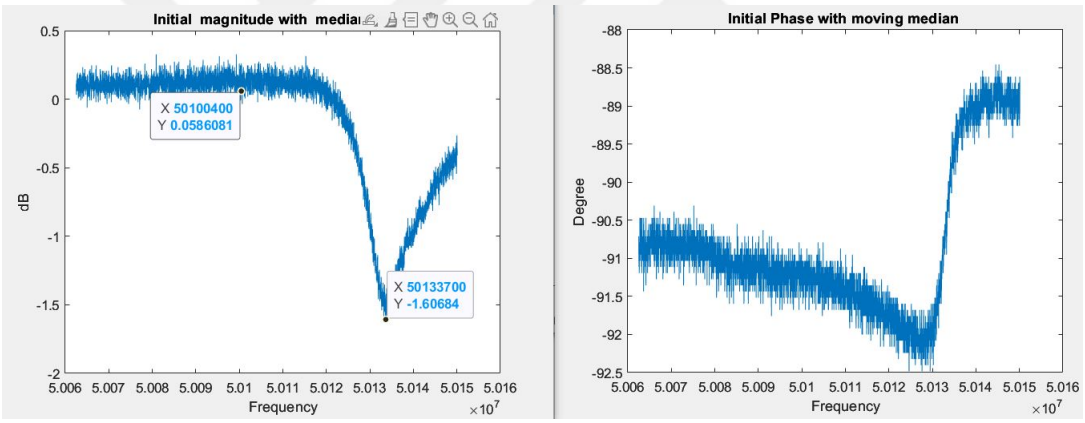

Figure K.7. DDS-PLL system measurement results-2 when open QCM was in water.

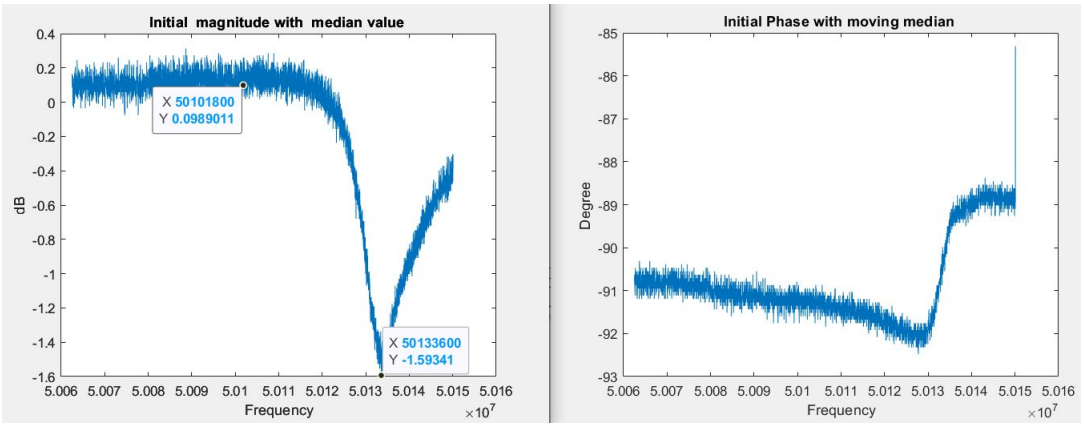

Figure K.8. DDS-PLL system measurement results-3 when open QCM was in water.

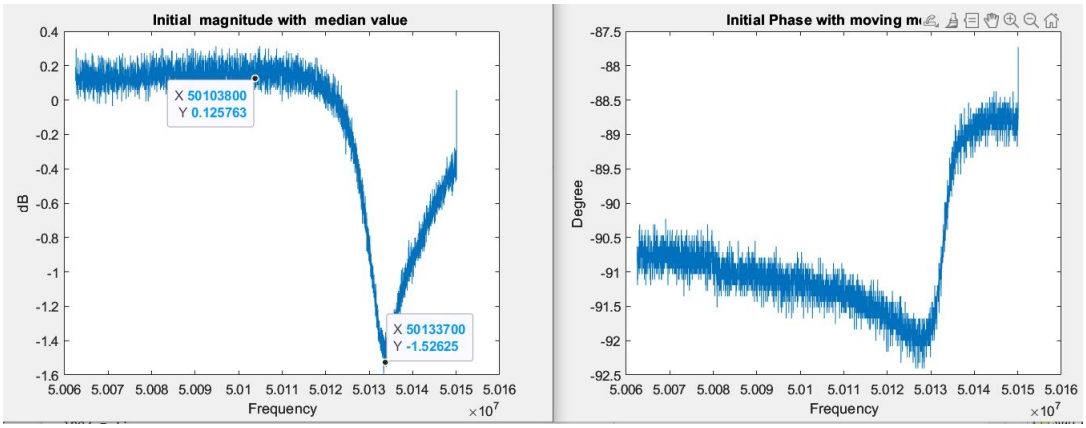

Figure K.9. DDS-PLL system measurement results-4 when open QCM was in water.

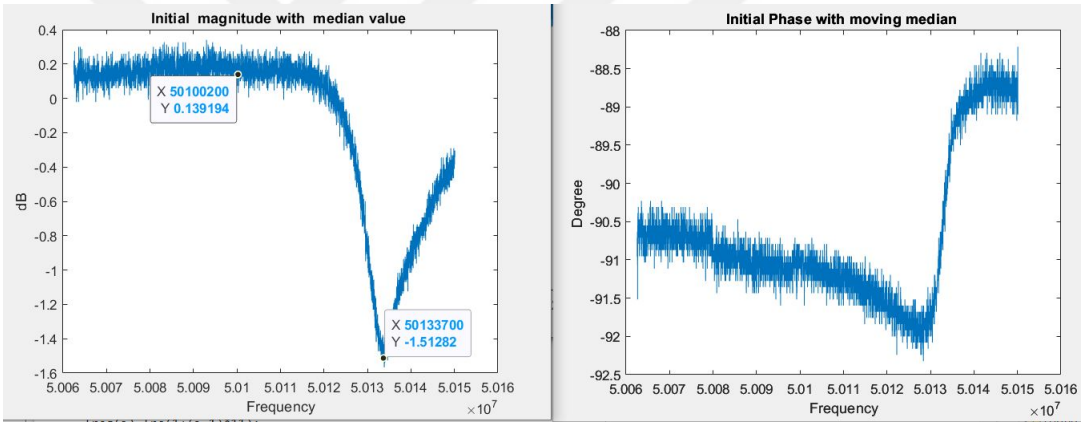

Figure K.10. DDS-PLL system measurement results-5 when open QCM was in water.

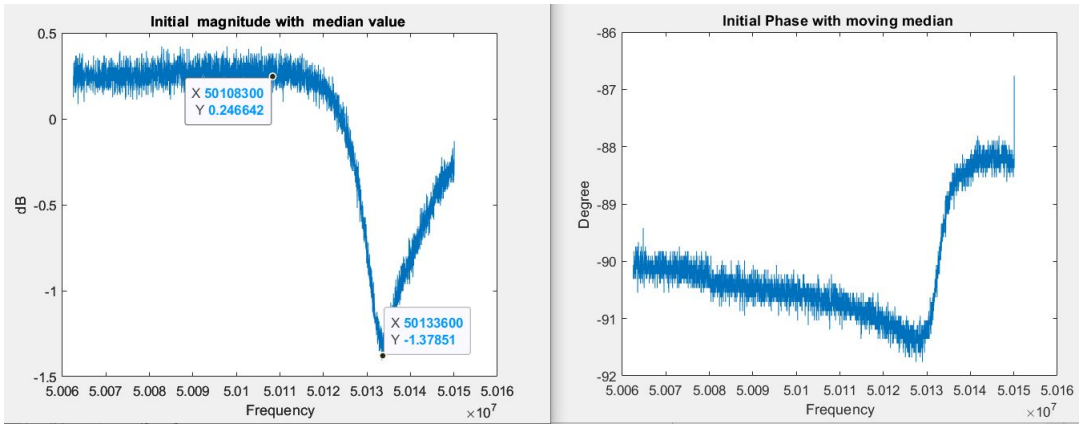

Figure K.11. DDS-PLL system measurement results-1 when open QCM was in 100 ml water after 1ml glycerol was added.

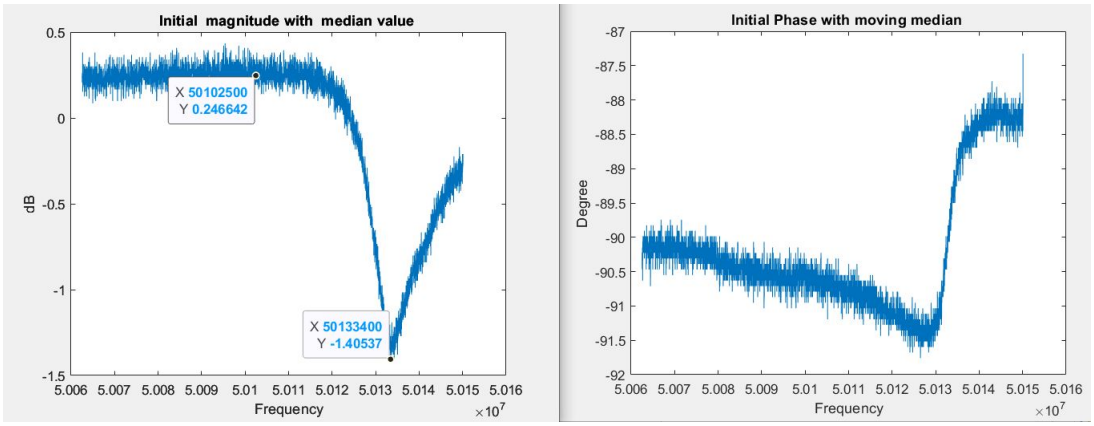

Figure K.12. DDS-PLL system measurement results-2 when open QCM was in 100 ml water after 1ml glycerol was added.

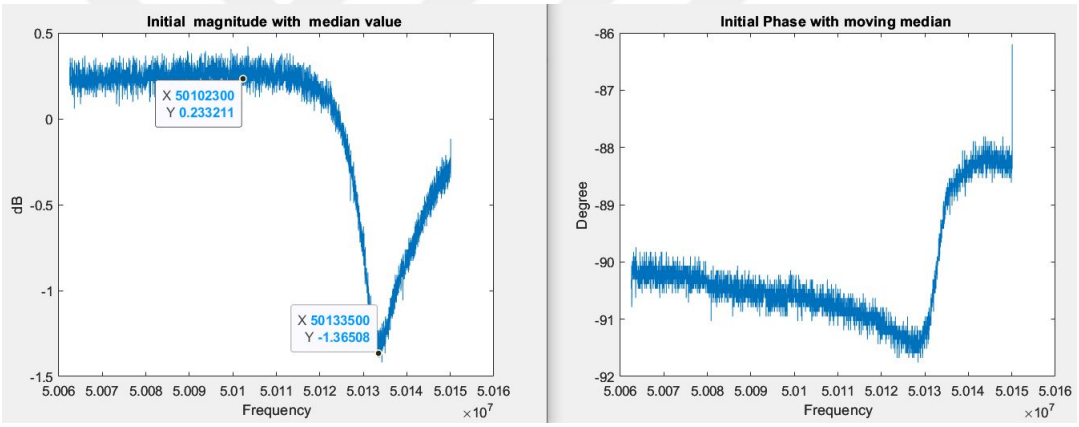

Figure K.13. DDS-PLL system measurement results-3 when open QCM was in 100 ml water after 1ml glycerol was added.

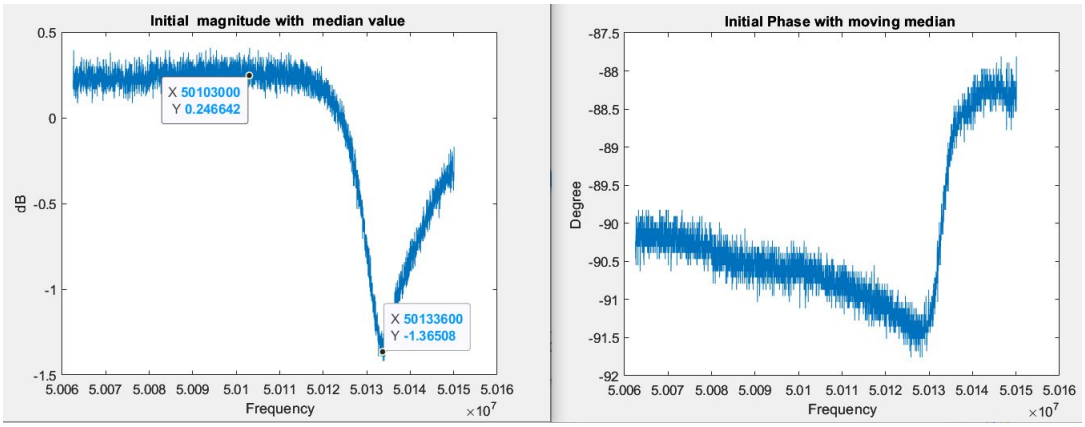

Figure K.14. DDS-PLL system measurement results-4 when open QCM was in 100 ml water after 1ml glycerol was added.

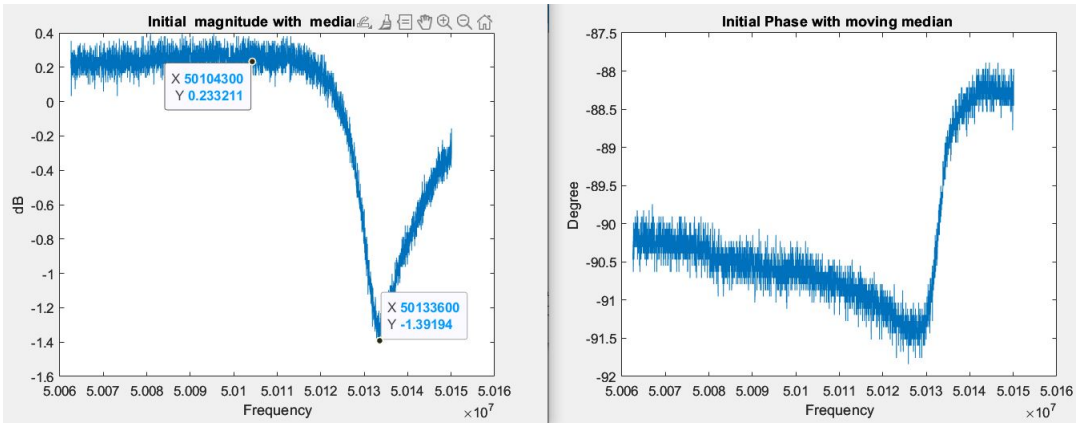

Figure K.15. DDS-PLL system measurement results-5 when open QCM was in 100 ml water after 1ml glycerol was added.

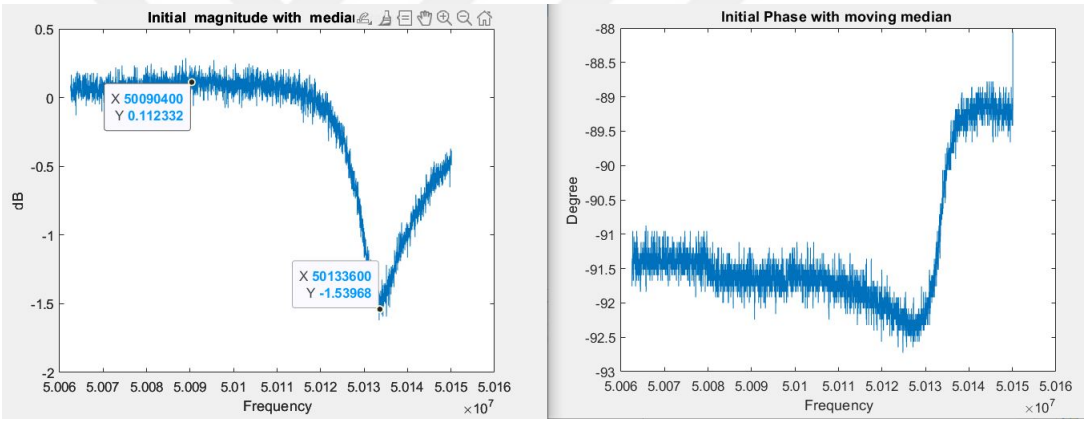

Figure K.16. DDS-PLL system measurement results-1 when open QCM was in 100 ml water after 3ml glycerol was added.

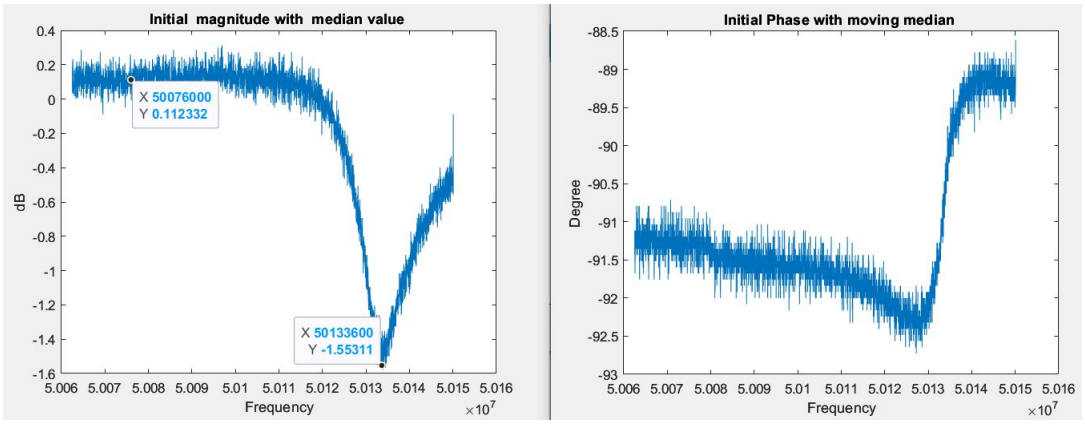

Figure K.17. DDS-PLL system measurement results-2 when open QCM was in 100 ml water after 3ml glycerol was added.

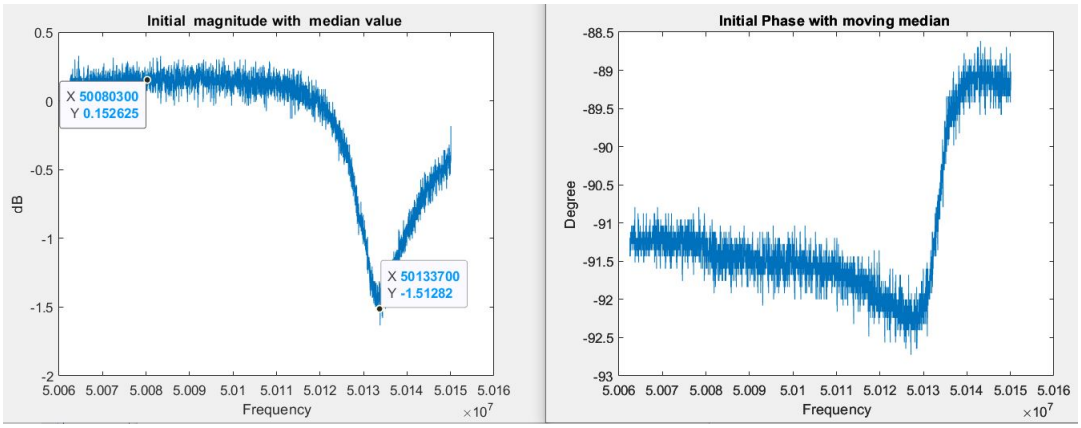

Figure K.18. DDS-PLL system measurement results-3 when open QCM was in 100 ml water after 3ml glycerol was added.

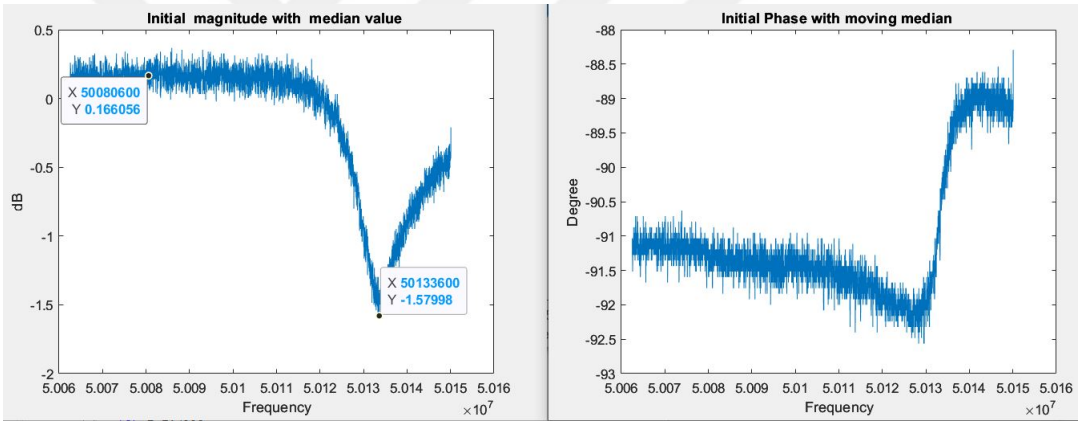

Figure K.19. DDS-PLL system measurement results-4 when open QCM was in 100 ml water after 3ml glycerol was added.

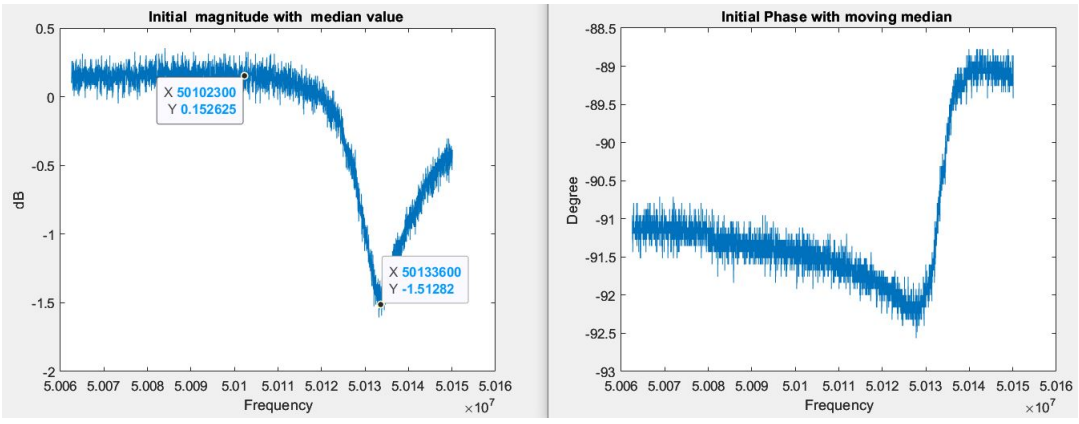

Figure K.20. DDS-PLL system measurement results-5 when open QCM was in 100 ml water after 3ml glycerol was added.